National Library of Canada
Acquisitions and Bibliographic Services Branch
395 Wellington Street
Ottawa, Ontario
K1A 0N4

Bibliothèque nationale du Canada
Direction des acquisitions et des services bibliographiques
395, rue Wellington
Ottawa (Ontario)
K1A 0N4

Your file Votre référence

Our file Notre référence

NOTICE

The quality of this microform is heavily dependent upon the quality of the original thesis submitted for microfilming. Every effort has been made to ensure the highest quality of reproduction possible.

If pages are missing, contact the university which granted the degree.

Some pages may have indistinct print especially if the original pages were typed with a poor typewriter ribbon or if the university sent us an inferior photocopy.

Reproduction in full or in part of this microform is governed by the Canadian Copyright Act, R.S.C. 1970, c. C-30, and subsequent amendments.

AVIS

La qualité de cette microforme dépend grandement de la qualité de la thèse soumise au microfilmage. Nous avons tout fait pour assurer une qualité supérieure de reproduction.

S'il manque des pages, veuillez communiquer avec l'université qui a conféré le grade.

La qualité d'impression de certaines pages peut laisser à désirer, surtout si les pages originales ont été dactylographiées à l'aide d'un ruban usé ou si l'université nous a fait parvenir une photocopie de qualité inférieure.

La reproduction, même partielle, de cette microforme est soumise à la Loi canadienne sur le droit d'auteur, SRC 1970, c. C-30, et ses amendements subséquents.

Canada

Parametric Study of a Tuning Scheme for the Design of Friction Damped Braced Frames

Luciano Martin

A Thesis

in

The Department

of

Civil Engineering

Presented in Partial Fulfilment of the Requirements

for the Degree of Master of Applied Science at

Concordia University

Montreal, Quebec, Canada

April 1994

ISBN 0-315-90808-4

Canada

ABSTRACT

PARAMETRIC STUDY OF A TUNING SCHEME FOR THE DESIGN OF FRICTION DAMPED BRACED FRAMES

LUCIANO MARTIN

This thesis addressed the question of plan-wise slip load and stiffness distribution of friction damper equipped braces in an effort to refine the procedure currently employed in design.

Initially, single storey, stiffness eccentric models having stiffness ratios, KB / KF, of three and ten were subjected to an ensemble of earthquakes over a range of slip load and static stiffness eccentricities (e_{pb} and e_s) such that $-e_s < e_{pb} < e_s$ and $0 < e_s < 1.2$. The results demonstrated that as e_{pb} shifted to the flexible side of the structures, maximum displacements and peak ductility demands were reduced. Maximum improvements over the current design approach were obtained when $e_{pb} = -e_s$, although for ease of applicability in design, $e_{pb} = 0$ provided excellent results.

Based on these results, a 3-D inelastic analysis of a five storey, reinforced concrete structure having an eccentricity of $0.35D_n$ and equipped with friction bracing was also presented. Comparisons were made between the current design approach and the suggested design ($e_{pb} = 0$). Friction bracing designed with $e_{pb} = 0$ was shown to reduce top storey displacements, deck rotations, and peak ductility demands by approximately 20 percent of the current design value. Results obtained for the multi-storey structure correlated well with those of the single storey models and revealed the existence of an upper limit for the KB / KF ratio that may be applied in design. Modification of the brace stiffness distribution was shown to be ineffective as cases with $e_{pb} = 0$ and $e_{sb} = 0$ produced similar results to those having $e_{pb} = 0$ and $e_{sb} \approx e_{sf}$.

The research demonstrated that in addition to RB / RF and KB / KF, the design of friction bracing must also consider the slip load eccentricity, be it practical, $e_{pb} = 0$, or theoretical, $e_{pb} = -e_{sf}$.

ACKNOWLEDGEMENTS

It is my humble opinion that there are only two requirements for success and happiness. First, one must have the ability to positively influence the lives of those he encounters. Second, one must also be enriched by the presence of those around him. I cannot for certain claim the former, but I am proud to say that I have experienced the latter. As such, I would like to take the opportunity to thank all those who have had a positive influence on my work and stay at Concordia. First and foremost, thanks to my family and friends for their patience, understanding, and continuous presence. Heartfelt thanks go out to Miguel, Sachin, Aniruddha, Peter, Mas, and Marco for their insight, encouragement, Unix 'lizardry', inspiration and ability to keep me sane. Thanks also to the guys in the 'Cage' for showing me that, contrary to popular belief, innovation and dedication in engineering is alive and well at Concordia. Acknowledgements must also go out to the Natural Science and Engineering Research Council of Canada and Concordia University, without whose financial rewards (scholarships and instructorships) and facilities this thesis would never have happened. Finally, thanks to my supervisor, Dr. O. A. Pekau, for his leadership and guidance.

TABLE OF CONTENTS

PAGE

TABLE OF CONTENTS

PAGE

TABLE OF CONTENTS

PAGE

LIST OF FIGURES

LIST OF FIGURES

LIST OF FIGURES

LIST OF FIGURES

LIST OF FIGURES

LIST OF FIGURES

LIST OF TABLES

NOTATIONS

a, a_1, a_2	distance from center of mass to resisting elements oriented along Y-axis
A	area used for braces
AD	designation for structure having braces implemented according to the alternative design approach with $e_{pb} = 0$ and $e_{sb} = 0$
CD	designation for structure having braces implemented according to current design practice
CM	center of mass of floor under consideration
CR	center of strength for arrangement of resisting elements
CS	center of stiffness of floor under consideration
d	distance from center of mass to resisting elements oriented along X-axis
D	plan dimension parallel to excitation
D_n	plan dimension perpendicular to excitation
e_p	strength eccentricity of combined system
e_{pb}	slip load eccentricity of braces
e_{pf}	strength eccentricity of unbraced frame
e_{pb}^*	normalized slip load eccentricity of braces
e_{pf}^*	normalized strength eccentricity of unbraced frame
e_s	stiffness eccentricity of combined system
e_{sb}	stiffness eccentricity of braces
e_{sf}	stiffness eccentricity of unbraced frame
e_s^*	normalized eccentricity of combined system
e_{sb}^*	normalized stiffness eccentricity of braces
e_{sf}^*	normalized stiffness eccentricity of unbraced frame
FDBF	friction damped braced frame
k_{iy}	stiffness of individual resisting element

KB	lateral stiffness of brace
KF	lateral stiffness of unbraced frame
m	mass of structure
MRF	moment resisting frame
RB_{yi}	yield load of single resisting element
RB	resistance of brace
RF	resistance of unbraced frame
SD	designation for structure having braces implemented according to the suggested design approach with $e_{pb} = 0$
T	period of structure
γ	relative torsional stiffness
μ	member ductility demand
ρ	radius of gyration about the center of mass
$\omega_{y,\theta}$	uncoupled lateral and torsional frequencies
$\omega_{1,2}$	coupled natural frequencies of the system
Ω_o	uncoupled torsional-lateral frequency ratio

CHAPTER 1

INTRODUCTION

In recent years a novel approach to aseismic design of braced frames has been introduced which consists of the incorporation of friction damping devices in tension-compression cross-braces to help absorb the excess energy input of severe earthquake excitations [1]. The concept of the friction damping device arose from the recognition that costs related to the repair and rehabilitation of buildings and their non-structural components in the aftermath of an earthquake could be prohibitive.

The introduction of friction damped braced frames (FDBF) as a means of controlling structure response to seismic excitations has spawned much work dealing with the development of a tuning process that would ensure maximum energy dissipation while minimizing lateral and torsional displacements. Until now, however, research has concentrated on determining optimum ratios of stiffness and strength between the friction damped braces and the unbraced frames [2, 3]. Little consideration has been given to the plan-wise distribution of strength and stiffness between the device-equipped resisting braces.

It is the intent of this thesis to address the question of plan-wise slip load and stiffness distribution in an effort to determine a method for redistributing these properties that would be easy to apply while ensuring a further reduction in the lateral and torsional displacements expected.

The research presented herein consists of four phases: the first phase looks at the effects of slip load distribution on the displacements and ductility demands of a single storey model structure with two degrees of freedom; the second phase briefly addresses the issue of stiffness distribution between the resisting braces once a practical slip load distribution has been set; and the third phase examines the effect of the new slip load distribution on the amount of energy that the reconfigured braces will be expected to

dissipate. The fourth and final phase consists of a case study of a multi-storey, three dimensional structure equipped with the reconfigured braces and can be construed as an application of the results obtained from the one storey analysis.

Phase I evaluates previous models used [3,4] and their ability to provide responses over a full range of slip load distributions. A suitable model is then chosen, and maximum displacements and ductility demands are obtained for a full range of eccentricities and an ensemble of earthquakes, namely, the artificial Newmark-Blume-Kapur earthquake, the 1940 El Centro N-S excitation, the 1977 Bucharest N-S excitation, and the 1952 Taft S69E excitation. Comparisons are also made with the results of other researchers to determine potential benefits of slip load redistribution. Particular attention is given to two classes of structures: those having the center of strength of the unbraced structure coincident with the center of mass, and those having the center of strength of the unbraced structure coincident with the center of stiffness of the unbraced structure.

Phase II applies the practical slip load distribution obtained from Phase I to obtain the maximum displacements and ductility demands for a full range of brace stiffness distributions. As in Phase I, attention is given to the strength symmetric and strength eccentric structures.

Phase III uses the findings of the previous phases to report the amount of energy that will be imparted to the structures considered as well as the amount of energy that the braces will be expected to dissipate.

The final phase, Phase IV, extends the findings obtained to a multi-storey concrete building representing an initial design of the Concordia University Library. A case study of the five storey portion of this building is presented and attention is focused on the ability of the new brace configuration to further reduce the response of the structure to severe earthquake loading.

A brief review of the literature serving as a basis for this research is presented below. Other relevant literature is given at appropriate points in each of the chapters.

1.1 LITERATURE REVIEW

Since the introduction of friction dampers by Pall and Marsh in 1982 [1], many studies have been carried out to determine their effectiveness in both symmetric and asymmetric structures. Collectively, these studies have shown that in order to optimize structure performance, tuning of the friction damped braces must be done according to both the stiffness and the slip load of the braces. The initial research carried out by Baktash demonstrated that maximum energy dissipation would occur when the slip load of the friction device was equal to the resistance of the unbraced frame in which it was to be installed [2]. This analysis, however, was simplified by considering uniquely symmetric structures requiring the analysis of only one friction damped braced frame (FDBF).

Demonstrating the effectiveness of FDBF in controlling the seismic response of asymmetric structures, Pekau and Guimond showed that the ratio of brace stiffness to unbraced frame stiffness must also be considered in the design of FDBF [3]. They established that an optimum design required this ratio to exceed seven. These conclusions were based on results obtained through the use of a one storey structure supported by two identical FDBF. Eccentricity was created by moving the FDBF so that the center of stiffness of the structure, lying halfway between the two FDBF, no longer coincided with the center of mass of the deck.

Considering only the unbraced single storey structure, Goel and Chopra [4], as well as Bruneau and Mahin [5], revealed the importance of selecting the appropriate numerical model when analyzing the response of buildings subjected to coupled lateral-torsional motions. They showed that while there existed an interchangeability between stiffness eccentric and mass eccentric models when analyzing the linear elastic behavior of asymmetric systems, the models' differences in plan-wise distribution of strength and stiffness variably influenced their behavior in the inelastic range. Neither study, however,

considered the effect of introducing friction damped braces into the systems.

Since there is little research that deals specifically with the behavior of structures equipped with FDBF, much of the foundation of the current work is based on the behavior of unbraced structures. As such, the idea for a potential method of optimization of the slip load and stiffness distribution is drawn from the works of Ayala, Garcia, and Escobar [6], Tso and Ying [7], and Sadek and Tso [8]. These researchers were studying strength distribution between resisting frames as a means of modifying those sections of the Mexico building code pertaining to earthquake resistant design. Their studies showed that structures having strength eccentricity negative that of the stiffness eccentricity actually responded better under seismic loading than structures having their strength eccentricity limited to the positive range only. They further suggested that future modifications of the code should consider taking advantage of this phenomenon.

1.2 PHASE I: SLIP LOAD DISTRIBUTION IN 1-STOREY STRUCTURE

The research of Baktash and Guimond [2, 3] helped establish the structural limits of KB / KF and RB / RF, and in Chapter 3 an attempt is made at determining how these limits may be imposed within the structure. The single storey models investigated are assigned global values of RB / RF = 1.0 and KB / KF = 10, and two types of models are investigated, namely, strength symmetric and strength eccentric models. Strength symmetric models are so designated because they have $e_{pf} = 0$, while strength eccentric models are those having $e_{pf} = e_s$. In determining the optimum distribution of slip load, the total required slip load of the structure is first concentrated on the stiff side of the model, then for each successive analysis, the slip load of the flexible side is increased and that of the stiff side is reduced while RB / RF is maintained at a constant value equal to one. The distribution of slip load between resisting frames is characterized by its eccentricity, e_{pb}, which is expected to vary between $-e_s$ and e_s.

The results obtained reflect those obtained by Ayala, Garcia, and Escobar [6] and Tso and Ying [7] for unbraced single storey structures. That is, the optimum responses occur when $e_{pb} < 0$.

Recognizing that there are some fundamental behavioral differences between mass eccentric and stiffness eccentric models as explained by Goel and Chopra [4], some effort is dedicated to demonstrate the limitations and performances of each model so as to produce results that may be generalized. The results obtained will demonstrate that the optimum slip load distribution is one in which $e_{pb} = -e_s$, although for practical design purposes, slip loads may be distributed according to $e_{pb} = 0$ Both these distributions show a significant reduction in ductility demands and maximum edge displacements.

1.3 PHASE II: INVESTIGATION OF STIFFNESS DISTRIBUTION

Chapter 3 also investigates the influence of the stiffness distribution of the braces on the overall response of the single storey model. Setting the slip load distribution such that $e_{pb} = 0$, the stiffness eccentricity of the braces is gradually redistributed from one brace to the other, as was the slip load in Phase I, and the responses and ductility demands are obtained. It is acknowledged that modifying the stiffness distribution of the braces in a system having KB / KF = 10 will greatly affect the overall eccentricity of the structure and some effort is made to address the impact of modifying e_{sb} on e_s^*. The results obtained will demonstrate that for the models considered $e_{sb}^* = -e_{sf}^* / 2$ gives the optimum response, although this response is less than 10 percent lower than $e_{sb}^* = 0$. Improvements are reported in terms of reduced displacements and ductility demands. In the latter case, the demands of the system are reduced to a level near that of the elastic response, which represents a significant reduction when compared to the ductility demands of the unbraced symmetric case. However, given the relation between e_{sb} and e_s^*, it is expected that for smaller KB / KF ratios, the effect of e_{sb} on e_s^* will be somewhat attenuated.

1.4 PHASE III: ENERGY ABSORPTION

The final part of Chapter 3 looks at the effect of the redistribution of brace slip loads on the ability of the models to dissipate the inelastic energy as heat in the friction braces. From the results of Phase I, two models are retained. One has $e_{pb} = 0$, and the other has $e_{pb} = -e_s$. The energy dissipated by the braces of these models is compared to that obtained for the case of $e_{pb} = e_s$. This comparison is done for both the strength eccentric and strength symmetric models. For the strength eccentric model, $e_{pb} = e_s$ reveals an inadequate participation of the braces in the dissipation process, as evidenced by high ductility requirements and large displacements. In this case, most of the energy is going straight into the frames, with the braces dissipating only 20 to 50 percent of the input energy. Effective redistribution of the brace properties increases this participation to 60 percent of the energy imparted to the structure. In the case of the strength symmetric model ($e_{pf} = 0$), the magnitude of KB / KF is such that the structure is unaffected by a shift in e_{pf}, and its energy response is the same as that of the strength eccentric model ($e_{pf} = e_s$).

The significance of the latter results is that an increase in energy dissipation by the braces means that less work is expected from the frames. Hence fewer, smaller, plastic excursions are expected and this eventually translates into lower ductility demands and deflections.

1.5 PHASE IV: CASE STUDY OF 5-STOREY STRUCTURE EQUIPPED WITH RECONFIGURED BRACES

The final phase of this work, described in Chapter 4, looks at incorporating the results of Chapter 3 into a computer model representing an early design of the new Concordia University Library Complex. More specifically, a three dimensional inelastic analysis using the computer program DRAIN-Tabs [9] is conducted in order to compare

the effects of the suggested design approaches ($e_{pb} = 0$, $e_{sb} = e_{sf}$ and $e_{pb} = 0$, $e_{sb} = 0$) to that of the current approach ($e_{pb} = e_{sf}$, $e_{sb} = e_{sf}$).

The friction braces used in this building are similar to those used by Guimond [10] and Baktash [2] and consist of tension-compression cross-braces, which are recognized for their post-elastic behavior and for promoting improved ductility [11].

The structure itself consists of a five storey, flat slab, reinforced concrete building that is 36.9 m long and 27.6 m wide, with columns spaced out on a 9 m grid. Because the structure is used as a library, the concentration of books on one side of each floor is considered to cause an eccentricity of $0.35D_n$ for excitations parallel to the X-axis. Resistance to these excitations is provided by 6 frames oriented along the X-axis, while Y-direction excitations are resisted by 5 frames oriented along the Y-axis. Braces are located near the north and south edges of the structure for X-direction excitations, while only one brace located near the east edge directly dissipates energy due to Y-direction excitations.

Preliminary analysis of the structure shows that there exists an upper limit as to what KB / KF ratio may be used in the design of the braces. Although a KB / KF ratio equal to ten, as suggested by the analysis of Chapter 3 and the work of Reference [3], would have been preferred, for the structure chosen, the useful limit is KB / KF = 3.0. A shortened analysis of the type carried out in Chapter 3 is performed to verify that the behavior of the single storey model reflects that obtained for KB / KF = 10.

Results obtained for the multi-storey model with the modified bracing show a reduction of edge displacements, rotations, and ductility demands, especially in those elements located on the vulnerable flexible side, when compared to the same structure equipped with friction braces designed according to current accepted practice. However, inclusion of stiffness redistribution shows no change over simply modifying the slip load distribution, thereby suggesting that in the design of friction damped braced frames, three items govern. They are the optimum value of RB / RF, the optimum value of KB / KF, and the optimum distribution of the slip load between the friction damper equipped braces.

Analysis of the overall results obtained shows that the improved performance of $e_{pb} = 0$ over that of $e_{pb} = e_{sf}$ agrees well with the results obtained for the single storey models.

CHAPTER 2

DESCRIPTION OF SINGLE STOREY MODELS

2.1 INTRODUCTION

The following section describes the structural models that will be used to investigate the effects that redistributing the slip load and stiffness between the friction device equipped braces has on the maximum edge displacements, element ductility demands, and overall energy dissipation. The single storey model is used in the early part of the investigation in order to reduce modelling and computation time. Extension of these results to multi-storey, multi-frame structures has been verified by other researchers and will be treated in a later section[12].

Two types of models are introduced and described: the mass eccentric model used by Guimond [10], and the stiffness eccentric model used by Goel and Chopra [4]. Preliminary analysis performed using the dynamic analysis program DRAIN-2D [13] has revealed that the original model used by Guimond is not versatile enough to explore the entire range of slip load and stiffness distributions available. Therefore, introduction of the stiffness eccentric model is made to overcome this deficiency.

2.2 DESCRIPTION OF THE MASS ECCENTRIC MODEL (Without Braces)

This section describes the basic mass eccentric model used in this study, as well as two of its variants: the strength symmetric model and the strength eccentric model. These variants are considered because most buildings are composed of an amalgamation of various resisting elements (shear walls, moment resisting frames of concrete or steel, etc.), each of which may have different stiffness or strength characteristics which need to be reflected by the models chosen. The braces have been neglected for the time being to

simplify the description, but will be treated in a later section.

The basic structure consists of a rigid rectangular deck of mass m, that is supported by two massless, planar frame elements as depicted in Figure 2.1. The layout is such that the model represents a single storey, monosymmetric structure. The deck has dimensions of $D_n = 3\rho$ and $D = (\sqrt{3})\rho$, where ρ is the mass radius of gyration about the center of mass. The aspect ratio (D_n/D) is thus chosen to be 1.732. Although the responses are likely to be less than if the aspect ratio were below unity [14], the choice of such an aspect ratio is more representative of what may be encountered in practice. Most importantly, however, is the choice of deck dimensions such that the mass radius of gyration satisfies the equation:

$$\rho^2 = (D_n^2 + D^2)/12 \tag{2.1}$$

In addition to being symmetric about the X-axis, lateral movement of the center of mass in the X-direction is prevented. For Y-direction earthquake excitation, the result is a simple model with only two degrees of freedom: displacement in the Y-direction of the center of mass, CM, and a rotation, θ, about a vertical axis passing through the center of mass of the model. The resisting elements of the mass eccentric model used by Guimond [10], depicted in Figure 2.1, are located at a distance of $(a + e_s)$ to the left of CM (element 1) and at a distance of $(a - e_s)$ to the right of CM (element 2).

Lateral and torsional rigidities of the model are given by:

$$K_y = \sum_i k_{iy} \tag{2.2}$$

$$K_x = \sum_j k_{jx} \tag{2.3}$$

$$K_\theta = \sum_i k_{iy} x_i^2 + \sum_j k_{jx} y_j^2 + \sum_i k_{i\theta} \tag{2.4}$$

$$K_{\theta s} = K_\theta - e_s^2 K_y \tag{2.5}$$

where K_y is the total lateral stiffness of elements oriented along the Y-direction, K_x is the

total lateral stiffness of elements oriented along the X-direction, $k_{i\theta}$ is the torsional stiffness of an element about its own axis (omitted for planar members), K_θ is the torsional rigidity of the structure about the center of mass, CM, and $K_{\theta s}$ is the torsional rigidity of the structure about the center of stiffness, CS.

The center of stiffness of a structure, CS, is defined as that point along the deck where an applied static elastic load causes no rotation of the deck. The distance between CS and CM is the elastic stiffness eccentricity and is denoted by e_s. In order to evaluate the lateral-torsional dynamic response of the structure the static plastic eccentricity is required. The center of resistance, CR, of a structure is defined as that point along the deck where an applied load of sufficient magnitude causes all the resisting elements to reach their yield limit at the same instant. The distance between the center of resistance and the center of mass is called the plastic eccentricity or strength eccentricity and is denoted by e_p. Consequently, four eccentricities can be defined for the model:

$$e_s = \frac{1}{K_y}\sum_i k_{iy}x_i \tag{2.6}$$

$$e_p = \frac{1}{R_y}\sum_i R_{yi}x_i \tag{2.7}$$

$$e_s^* = \frac{e_s}{\rho} \tag{2.8}$$

$$e_p^* = \frac{e_p}{\rho} \tag{2.9}$$

where e_s^* represents the static stiffness eccentricity, normalized with respect to ρ, resulting from an uneven distribution of stiffness and mass, and e_p^* denotes the normalized static strength eccentricity resulting from unequal yield strengths of the resisting elements. R_y represents the total resistance of the structure and is given by:

$$R_y = \sum_i R_{yi} \tag{2.10}$$

where R_{yi} is the yield resistance of the individual elements. Yielding of the resisting

elements is ensured by restricting the yield capacity of the member to a fraction of its theoretical maximum elastic seismically induced force, $R_{elastic}$. For a corresponding elastic symmetric structure, the ratio chosen is governed by the code applied force reduction factor, R. Thus, R_y is described as:

$$R_y = R_{elastic}/R \tag{2.11}$$

This study uses a value of R = 4.0, which represents the maximum allowable reduction factor for structures demonstrating a high level of ductility according to the 1990 NBCC [15]. Also, the resisting elements of the structure are assumed to exhibit elastoplastic behavior. Thus, a strain hardening behavior of $k_2 = 0.00001k$ is assigned to the plastic portion of the curve for numerical stability, where k is the elastic stiffness of the resisting element.

The uncoupled lateral frequency and the uncoupled torsional frequency about the center of mass can now be defined as:

$$\omega_y = (K_y/m)^{1/2} \tag{2.12}$$

$$\omega_\theta = (K_\theta/m\rho^2)^{1/2} \tag{2.13}$$

Two other torsional frequencies which have been used in the literature are [16]:

$$\omega_{\theta s} = (K_{\theta s}/mr^2)^{1/2} \tag{2.14}$$

$$\omega_{\theta o} = (K_{\theta s}/m\rho^2)^{1/2} \tag{2.15}$$

where r is the mass radius of gyration about the center of resistance, CR, of the structure. Consequently, three uncoupled torsional to lateral frequency ratios, can be defined:

$$\Omega^2_{CM} = \omega^2_\theta/\omega^2_y \tag{2.16}$$

$$\Omega^2_{CR} = \omega^2_{\theta s}/\omega^2_y \tag{2.17}$$

$$\Omega^2_o = \omega^2_{\theta o}/\omega^2_y \,. \tag{2.18}$$

The importance of introducing Ω_o, and $\omega_{\theta o}$ is evidenced by the fact that, once set,

the value of Ω_o is constant and independent of the eccentricity of the structure, thereby simplifying the analysis of the results [16]. Moreover, the two coupled natural frequencies of the system can be found from:

$$\omega_{1,2}^2 = \left[\frac{1 + \Omega_o^2 + e_s^{*2}}{2} \pm \sqrt{\frac{(1 - \Omega_o^2 - e_s^{*2})^2 + e_s^{*2}}{4}} \right] \omega_y^2 . \qquad (2.19)$$

Considering that the maximum benefit of friction dampers is obtained for the design of multi-storey buildings of intermediate height, a period of vibration of T = 1.0 sec. is specified. In addition, since the lateral-torsional coupling in elastic structures is most critical when the torsional to lateral frequency ratio is near unity, Ω_o = 1.0 will be adopted for the models used in this study. The remaining variables are thereby adjusted to ensure the specified T and Ω_o.

2.2.1 Positioning the Resisting Elements

Determination of the physical position of the resisting elements within the plan layout of the model is carried out according to the equations set forth in Reference [4]. Considering the generalized system of Figure 2.2, the resisting elements of this mass eccentric system are located according to:

$$\frac{d}{\rho} = \frac{\sqrt{\gamma_x}\,\Omega_o}{\omega_x / \omega_y} \qquad (2.20)$$

$$\frac{a_1}{\rho} = \sqrt{(1 - \gamma_x)\,\Omega_o^2} - e_s^* \qquad (2.21)$$

$$\frac{a_2}{\rho} = \sqrt{(1 - \gamma_x)\,\Omega_o^2} + e_s^* \qquad (2.22)$$

where ω_x / ω_y is the lateral vibration frequency ratio and is equal to $(K_x / K_y)^{1/2}$, and γ_x is defined as the relative torsional stiffness of frames oriented along the X-direction to the total torsional stiffness and is given by:

$$\gamma_x = (\sum_i k_{ix} y_i^2) / K_{\theta s}. \tag{2.23}$$

This ratio can be set equal to zero if there are no resisting elements oriented in the X-direction.

Since the eccentricity in a mass eccentric structure is obtained by moving the center of mass away from the center of stiffness, the required stiffness of the resisting elements can be considered independent of their position and is calculated according to:

$$\frac{k_{1y}}{m} = \frac{k_{2y}}{m} = \frac{\omega_y^2}{2} \tag{2.24}$$

$$\frac{k_{3x}}{m} = \frac{k_{4x}}{m} = \frac{\omega_y^2}{2}\left(\frac{\omega_x}{\omega_y}\right)^2. \tag{2.25}$$

2.2.2 Strength Symmetric and Strength Eccentric Models

As mentioned earlier, this study considers two types of mass eccentric structures in the analysis: a strength symmetric model and a strength eccentric model (see Figure 2.3). The fundamental parameters for each model are determined from their stiffness and mass and are calculated according to the above equations. The difference between the models arises from a difference in the yielding characteristics of the resisting frames and is expressed by e_p.

In the case of the strength symmetric model, $e_p = 0$. This means that the resisting frames have varying strength, R_{yi}, such that the CM and CR of the system coincide, although the stiffnesses remain identical. Such a model could be representative of a structure having two different types of resisting frames (e.g. a moment resisting frame and a concrete shear wall). The wall and the frame could be built with the same stiffness characteristics, although the difference in material properties would make it difficult to have them yield at the same R_{yi}.

The strength eccentric model has $e_p \neq 0$. This means that there is no restriction as

to the strength that each element is permitted to have. However, to simplify the study, e_p is restricted to vary with e_s such that $e_p = e_s$. This means that CR and CS will coincide for each system, although their position will be different from CM. This type of model would be representative of a steel or concrete structure having two identical resisting frames.

2.3 DESCRIPTION OF THE STIFFNESS ECCENTRIC MODEL (Without Braces)

This section describes the basic stiffness eccentric model used in this study, as well as two of its variants: the strength symmetric model and the strength eccentric model. These models are considered because most multi-storey buildings, although composed of various resisting elements having differing stiffness or strength characteristics, have one major point in common: a uniform distribution of mass at each floor. The braces have been neglected for the time being, and their addition will be discussed in a separate section.

The general layout of the stiffness eccentric model is the same as that outlined for the mass eccentric model, and equations (2.1) through (2.19) apply. The difference between these two models comes from differing assumptions used as to the cause of the eccentricity. These are characterized by changes in the equations used to position the resisting frames within the plan layout of the structure. In contrast to a mass eccentric structure where the CS is fixed and the CM is shifted in order to produce the eccentricity, here, the CM is fixed and the CS is shifted to produce the desired eccentricity.

2.3.1 Positioning the Resisting Elements

In the stiffness eccentric structure of Figure 2.4, the center of mass coincides with the geometric centroid of the deck, and the resisting frames are positioned symmetrically about this point. The eccentricity results from different stiffnesses assigned to the resisting frames. Determining the actual in-plan position of the resisting elements is done according

to the equations set forth in Reference [4]. Considering the generalized system of Figure 2.4, the resisting elements of this stiffness eccentric system are located according to:

$$\frac{d}{\rho} = \frac{\sqrt{\gamma_x}\Omega_o}{\omega_x/\omega_y} \tag{2.26}$$

$$\frac{a}{\rho} = \sqrt{(1-\gamma_x)\Omega_o^2 + e_s^*} \tag{2.27}$$

$$\frac{k_{1y}}{m} = \frac{\omega_y^2}{2}\left(1 - \frac{e_s^*}{a/\rho}\right) \tag{2.28}$$

$$\frac{k_{2y}}{m} = \frac{\omega_y^2}{2}\left(1 + \frac{e_s^*}{a/\rho}\right) \tag{2.29}$$

$$\frac{k_{3x}}{m} = \frac{k_{4x}}{m} = \frac{\omega_y^2}{2}\left(\frac{\omega_x}{\omega_y}\right)^2 \tag{2.30}$$

2.3.2 Strength Symmetric and Strength Eccentric Models

As for the mass eccentric structures, two types of stiffness eccentric structures were considered: a strength symmetric model and a strength eccentric model, shown in Figure 2.5. In the case of the strength symmetric model, $e_p = 0$, and the resisting frames have identical strength, R_{yi}, thereby causing CM and CR to coincide, although the stiffnesses are permitted to vary.

The strength eccentric model has $e_p \neq 0$. This means that there is no restriction as to the strength that each element is permitted to have. However, as in the case of the mass eccentric model, e_p is restricted to vary with e_s such that $e_p = e_s$. This means that CR and CS will coincide for each system, although their position will be different from CM.

2.4 ADDING FRICTION DAMPER EQUIPPED BRACES

Braces are very much like frames in that they have specific strength and stiffness

characteristics. The difference between regular X or K bracing and friction damper equipped braces is that the yield point of conventional bracing is usually the load at which the friction dampers begin to slip. Hence, the friction-damper equipped brace does not experience conventional yielding until it has reached its maximum slip displacement. A typical friction damper is shown in Figure 2.6.

Given this similarity between braces and frames, the equations presented earlier are easily applied to the bracing. Of particular interest are the equations dealing with the strength and stiffness eccentricity, e_s and e_p. In order to keep the notations clear, new subscripts are introduced to distinguish between frame properties and brace properties. Hence, the frame properties can be rewritten as:

$$e_{sf} = \frac{1}{KF_y}\sum_i kf_{iy}x_i \tag{2.31}$$

$$e_{pf} = \frac{1}{RF_y}\sum_i RF_{yi}x_i \tag{2.32}$$

and the brace properties can be expressed as:

$$e_{sb} = \frac{1}{KB_y}\sum_i kb_{iy}x_i \tag{2.33}$$

$$e_{pb} = \frac{1}{RB_y}\sum_i RB_{yi}x_i \tag{2.34}$$

where e_{sb} represents the distance between the center of mass of the structure and the center of stiffness of the braces, and e_{pb} is the distance between the center of mass of the structure and the slip load center of the braces. The slip load center of the braces is defined as that point along the deck where the application of a force of sufficient magnitude causes all the braces to slip at the same time.

The premise behind the friction damped braces is that the compression diagonal buckles under small loads, and this causes the device to activate and keep this member taut. The resulting behavior, which has been verified by Filiatrault and Cherry, produces a rectangular hysteresis loop exhibiting virtually no degradation [17, 18]. A typical

hysteresis loop is shown in Figure 2.7 [10].

For both the braced and the unbraced frames, stiffness is defined as the force required to cause a storey drift of one unit. The frame resistance, RF_{yi}, is defined as the force needed to bring about the onset of yielding in one of the resisting members, and the brace strength, RB_{yi}, is defined as the force which causes the friction damper to activate and slip at a constant load. Having defined individual strength and stiffness for the braced and the unbraced frame (shown in Figure 2.8), two new variables can be introduced: the ratio of total brace stiffness to total frame stiffness, KB / KF, and the ratio of total brace strength to total frame strength, RB / RF.

Optimization of KB / KF and RB / RF has been carried out by other researchers and will not be reproduced here [2, 3, 10]. Each of these studies investigated the ratio of total strength or stiffness by using two dimensional analysis, and each made some simplifying assumptions to help accelerate the investigation. The main assumption made in each case was that the resisting frames, regardless of their actual plan-wise position within the structure, would be identical in stiffness and strength, and that the braces assigned to each frame would also have identical slip loads and stiffnesses. From these studies, it was concluded that the optimum response of a structure would be obtained when the RB / RF ratio was at, or near, unity and KB / KF was greater than seven. The present investigation examines the effect of changes in distribution of RB_{yi} and kb_{iy} while RB / RF and KB / KF remain constant.

2.5 COMPUTER MODELLING OF STRUCTURES CONSIDERED

Analysis of the mass eccentric and stiffness eccentric models will be done through the use of DRAIN-2D, a two dimensional dynamic analysis program [13]. The structures of Figures 2.2 and 2.4 are idealized to those shown in Figure 2.9. Figure 2.9 represents the plan view of the structures to be modelled. The rigid deck is modelled as a series of

infinitely rigid beam elements whose material properties reflect those of the rigid deck, and whose lengths are equivalent to the distance between control points. The frames and braces are modelled as simple truss elements, each having the stiffness and yielding properties of the resisting elements. In the case of the friction brace, the yield resistance specified for the truss element equals the slip load of the brace.

The use of beam elements for the deck and truss elements for the resisting members is justified by the design assumptions that have been made. It is assumed that the mass of each floor considered is concentrated at the floor level, hence it is possible to assign the total mass of a floor level to that point along the rigid beam designated as the center of mass, CM. Also, the frames are assumed to act as massless, planar springs which carry only tension or compression; hence the use of truss members which also act solely in tension or compression. It should be noted that if a brace element is assigned either a KB or RB value of zero, the frame to which the element is attached is assumed to be braceless. Control points are located at the edges of the model ($\pm$ 1.5 ρ), at the location of the resisting elements, and at the CS and CM points. Finally, positioning of the resisting elements and the structural properties governing their behavior is dictated by equations (2.1) to (2.30).

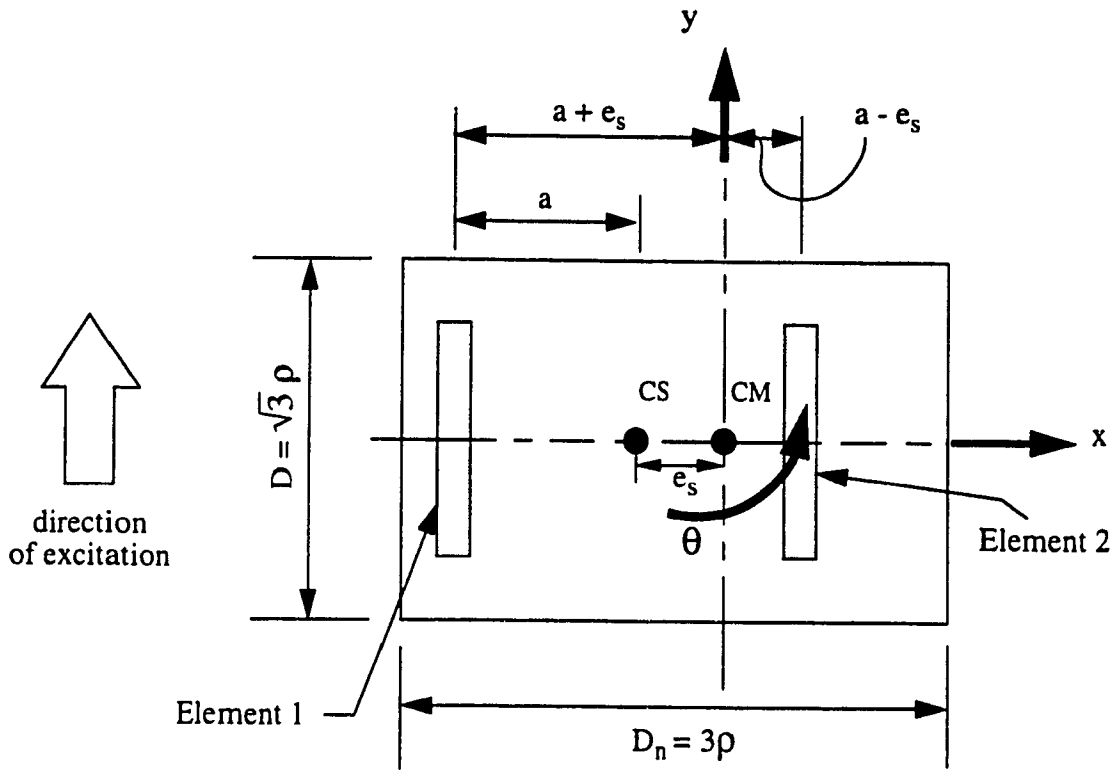

Figure 2.1. Mass eccentric model used in previous study [10].

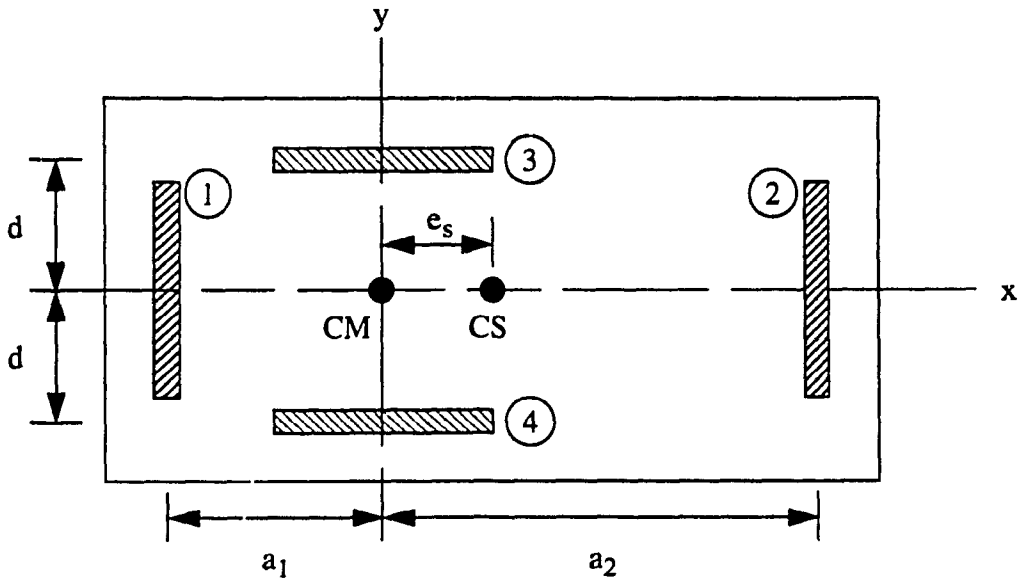

Figure 2.2. Generalized mass eccentric model.

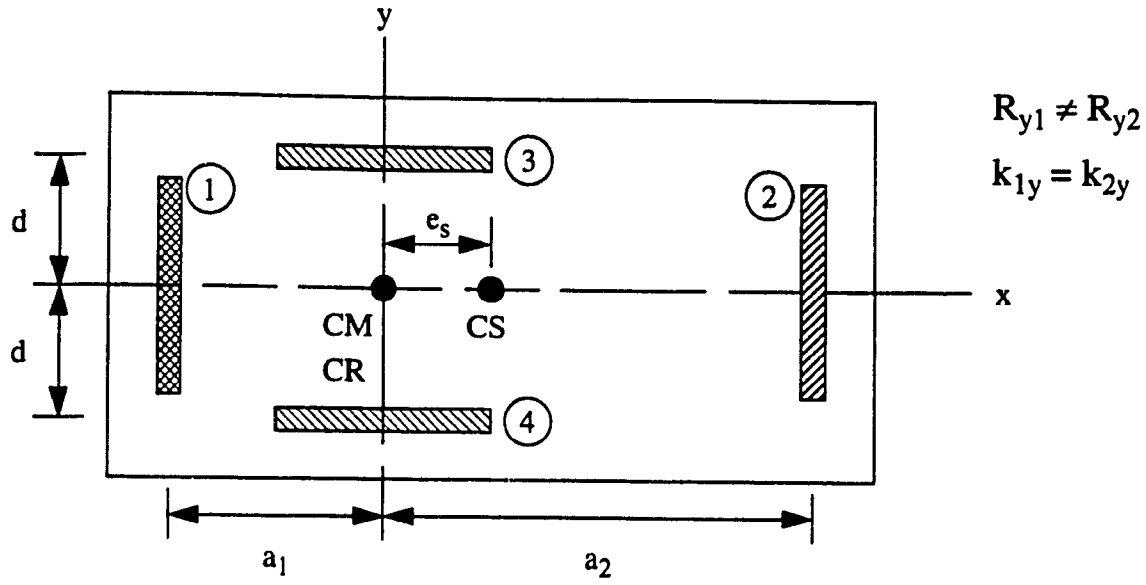

a) Strength symmetric model, $e_p = 0$.

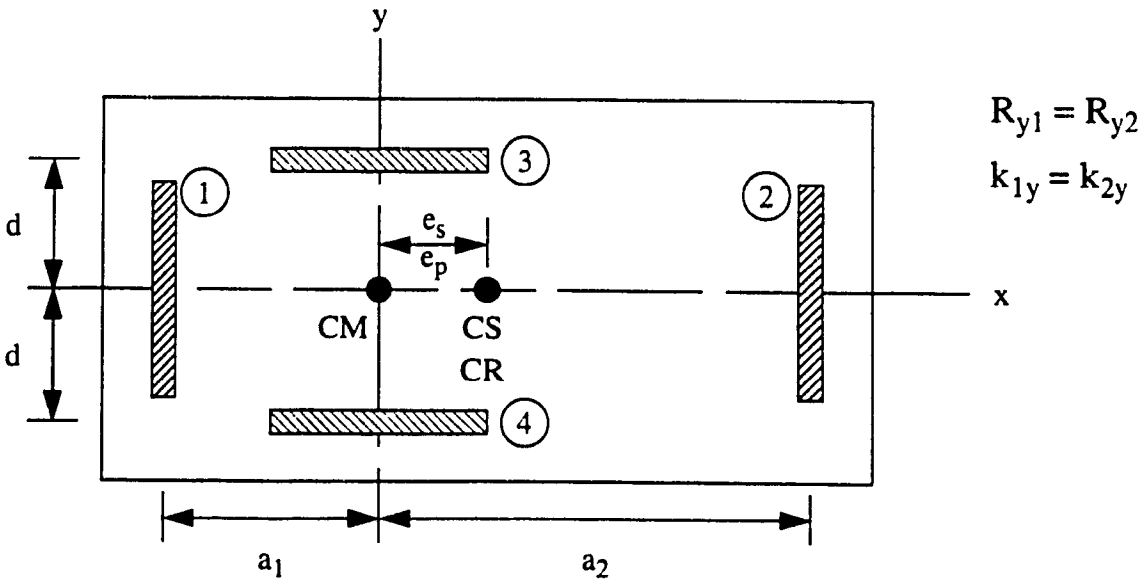

b) Strength eccentric model, $e_p = e_s$.

Figure 2.3. Strength symmetric and strength eccentric models for structures with eccentricity due to mass.

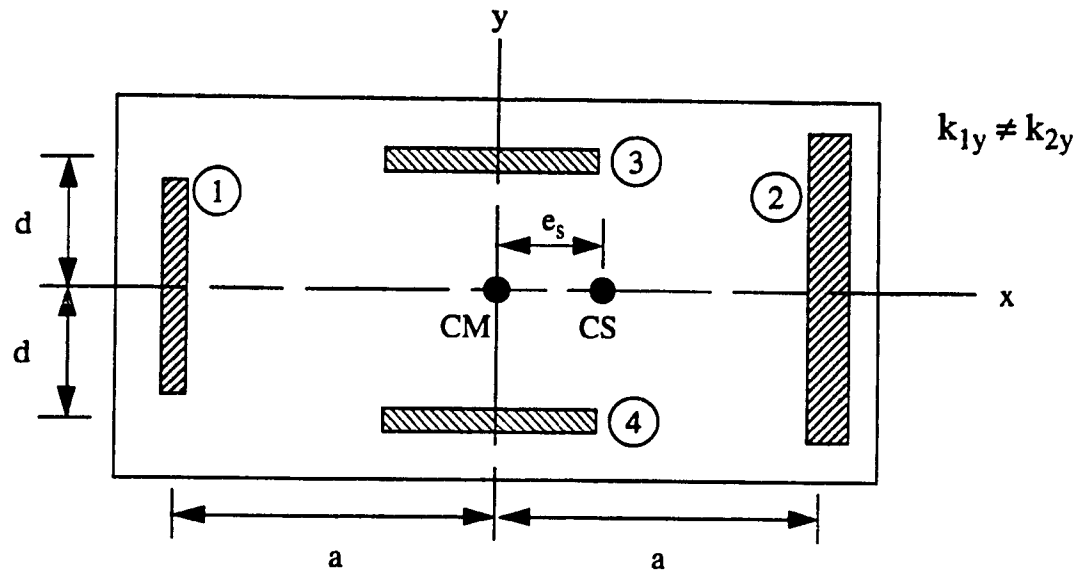

Figure 2.4. Generalized stiffness eccentric model.

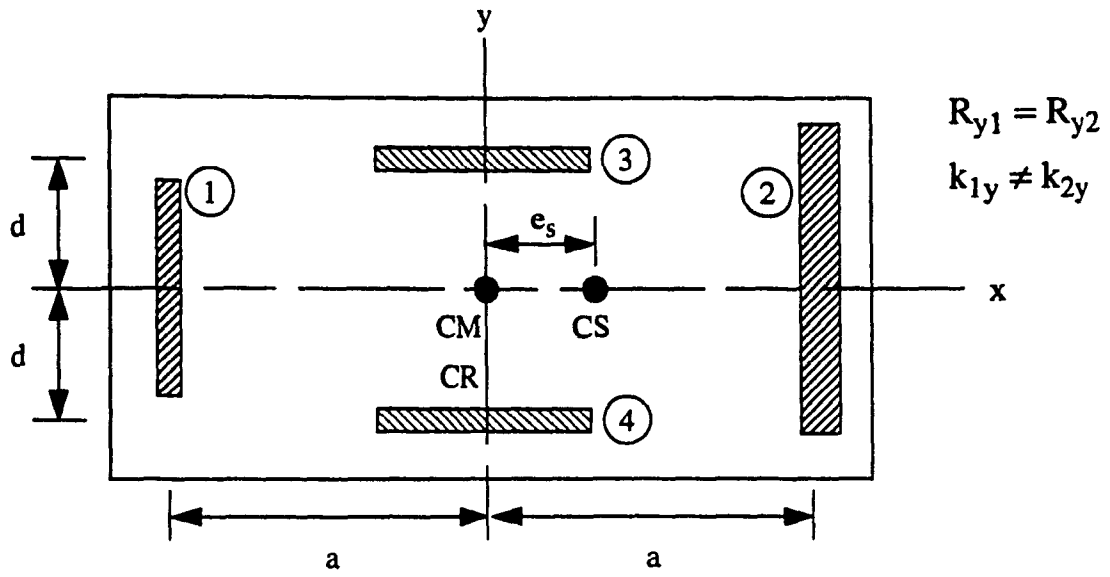

a) Strength symmetric model ($e_p = 0$).

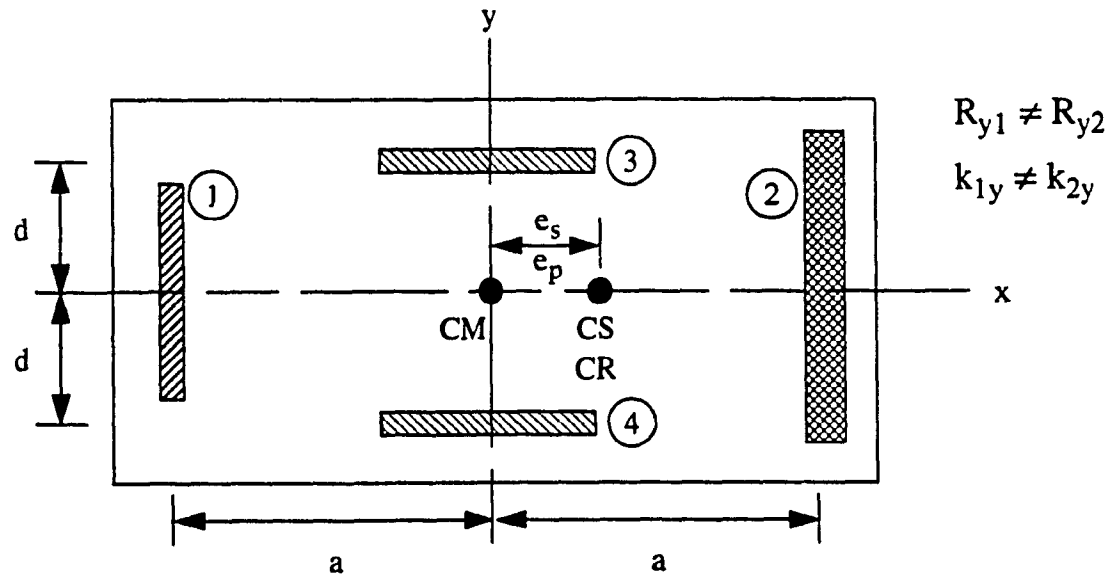

b) Strength eccentric model ($e_p = e_s$).

Figure 2.5. Strength symmetric and strength eccentric models for structures with eccentricity due to stiffness.

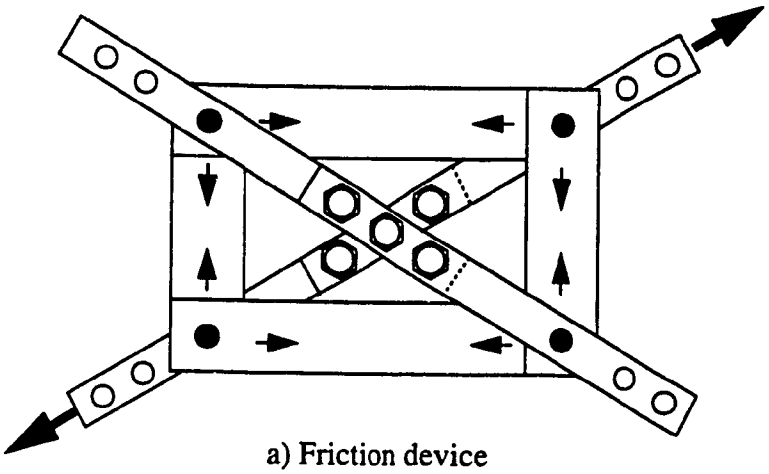

a) Friction device

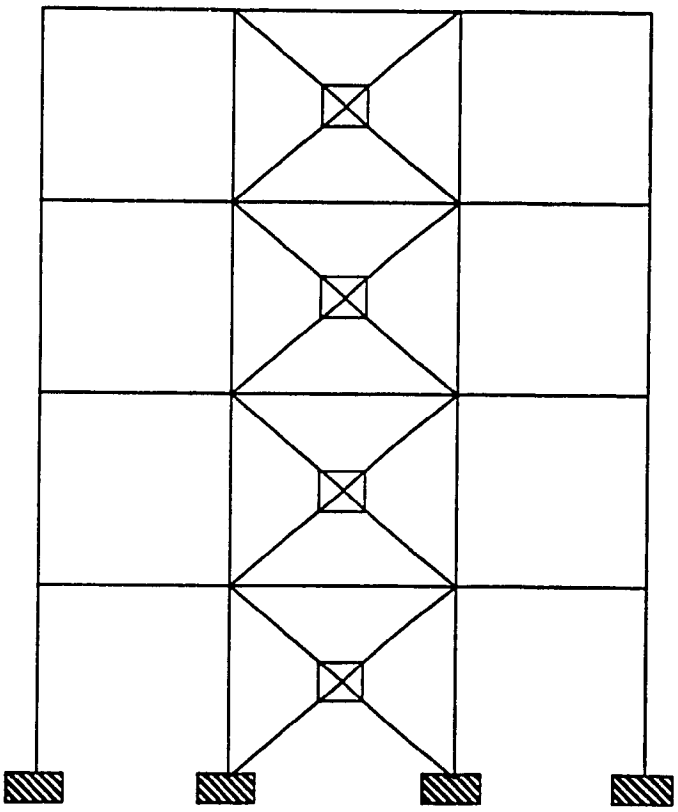

b) Typical frame with friction device

Figure 2.6. Typical friction device and placement within frame.

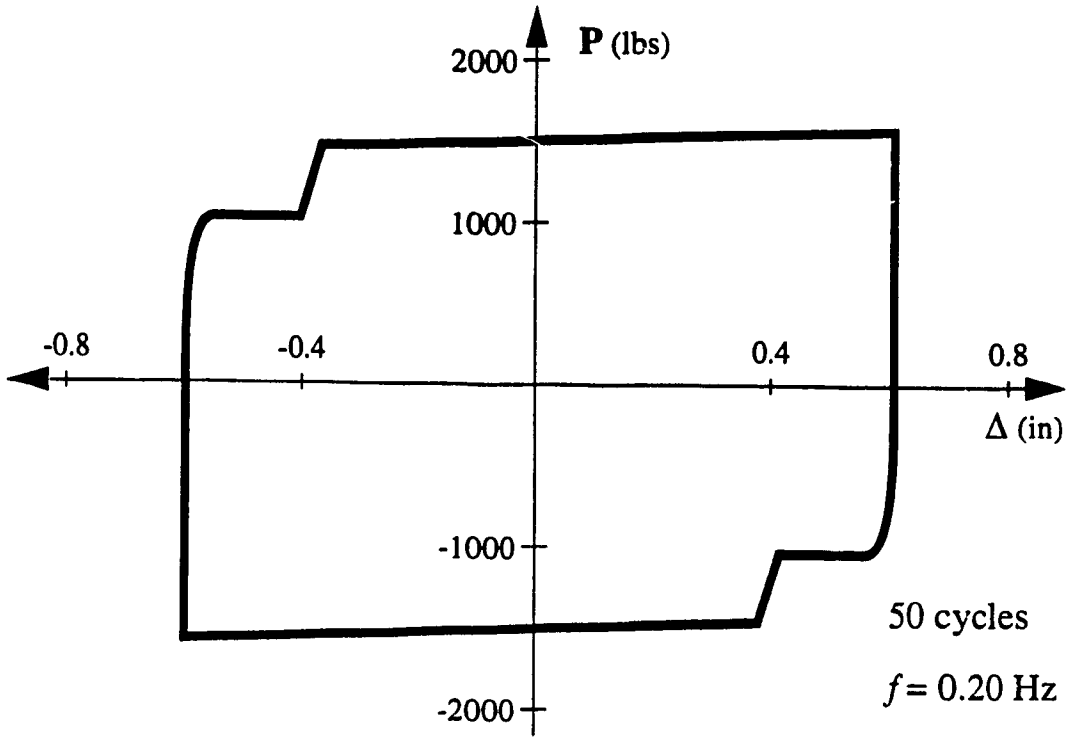

Figure 2.7. Hysteresis loop of a typical friction device [10].

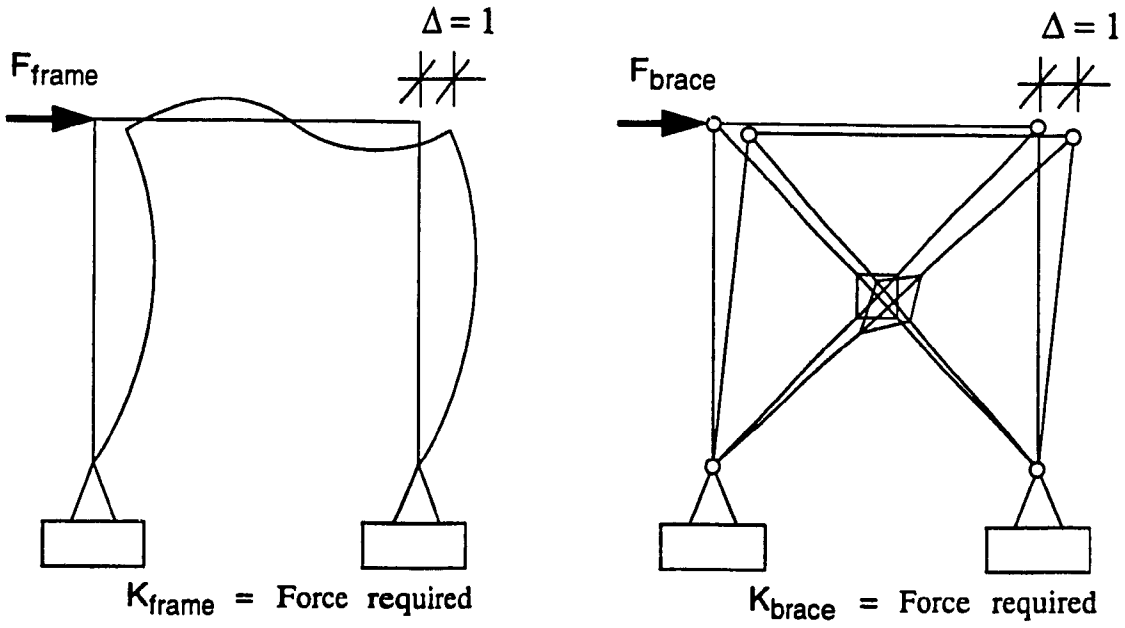

Figure 2.8. Definition of stiffness [10].

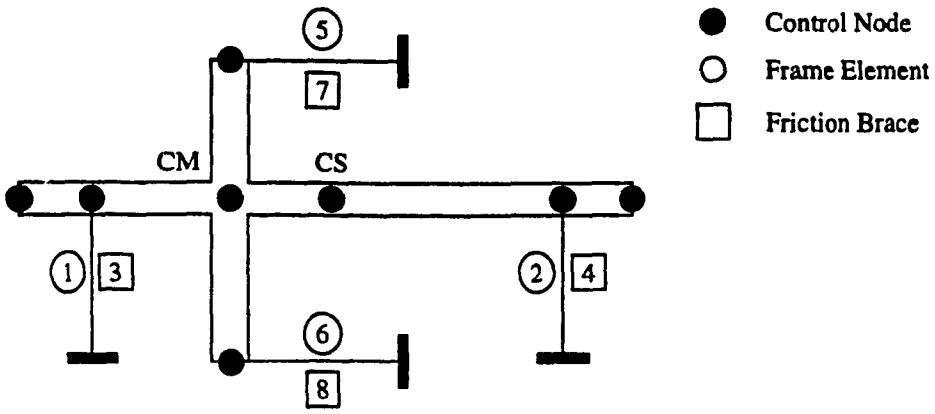

a) Idealized computer model for mass eccentric model.

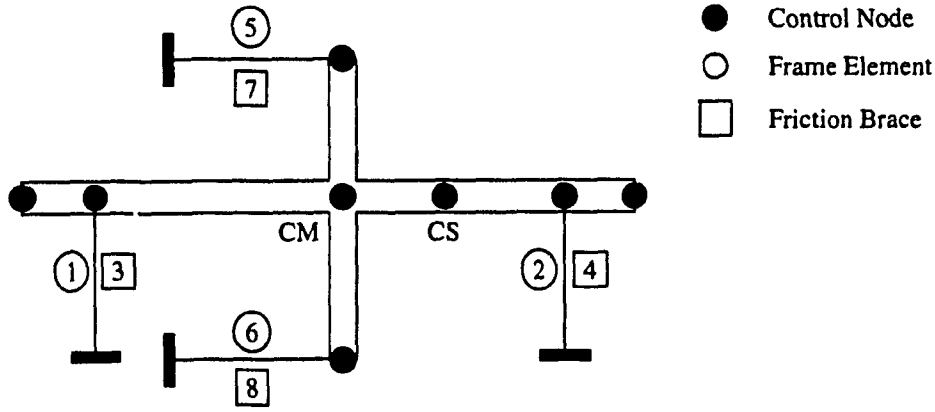

b) Idealized computer model for stiffness eccentric model.

Figure 2.9. General models idealized for computer analysis.

CHAPTER 3

ANALYSIS OF 2-D MODELS SUBJECT TO CHANGES IN SLIP LOAD AND STIFFNESS DISTRIBUTION

3.1 INTRODUCTION

The initial phases of the research programme require the determination of the optimum slip load and stiffness distribution between the friction braces. The basis for the research in these phases is the results obtained by Baktash [2]. Baktash determined that the optimum ratio of slip load to frame strength, RB / RF, was equal to unity, although her work concentrated on the effect of lateral forces on one frame of a multi-storey symmetric building. These findings were later confirmed by the research of Pekau and Guimond [3] who demonstrated that this optimum value could also be used when attempting to control the seismic response of asymmetric structures.

Because of the young nature of this field, neither of these works focused on determining how the optimum strength ratio should be distributed between the friction damped braces of the structure. The focus was on the establishment of the structural limits that were needed in order to design the friction damped braces for multi-storey and asymmetric buildings. The research herein aims to determine how the limits established by Baktash, Pekau and Guimond can best be utilized to minimize the response of the models chosen. Optimum stiffness and slip load distribution is determined by the procedure described in the following paragraphs.

3.2 PHASE I: OPTIMIZATION OF STRENGTH DISTRIBUTION

The strengths and stiffnesses of the structures of Chapter 2 were initially made to reflect those used in Reference [3]. That is, the ratio of slip load to frame strength, RB / RF

was set to unity, and the ratio of brace stiffness to frame stiffness, KB / KF, was maintained at a value greater than seven. For the stiffness eccentric structure used in this study, preliminary analysis showed that KB / KF = 10 was satisfactory.

The structural parameters allowed to vary include the normalized stiffness eccentricity $e_s^* = e_s / \rho$, the normalized strength eccentricity of the unbraced frame e_{pf}^*, and the normalized slip load eccentricity of the friction damped braces e_{pb}^*. As in Reference [3], e_s^* was allowed to vary from 0 - 1.5, thereby providing results for structures having no eccentricity to those having eccentricity equal to 50 percent of their plan dimension. The distribution of the frame strength, e_{pf}^* was also permitted to vary between 0 - 1.5, thereby giving rise to the two types of models described in Chapter 2, namely the **strength symmetric** model, where $e_{pf}^* = 0$, and the **strength eccentric** model, where $e_{pf}^* = e_s^*$. This approach, however, caused an inconsistency when preparing the data file for the case where $e_s^* = e_{pf}^* = 1.5$. The resisting frames of the stiffness eccentric structure would have to be placed beyond the established plan dimensions of the deck. This presented no problem as far as the numerical analysis was concerned since the plan dimension could simply be increased to reflect the required position of the resisting frames; however, this practice limited the comparisons between the current models used and those of Reference [3] since the plan dimensions perpendicular and parallel to the excitation would no longer be the same. Due to this, the effective range of comparison has been reduced to systems of e_s^* varying between 0 and 1.2.

The total slip load required for the braces was calculated as the sum of all the strengths of the frames in which the braces were to be placed, and this slip load was assigned to the brace located on the stiff side of the structure. The response of the model was then obtained using DRAIN-2D. For subsequent runs, the slip load of the brace on the flexible side was gradually increased while that of the stiff side was decreased so as to create the desired slip load distribution while maintaining RB / RF = 1.0 for the overall

system. This practice continued until the total slip load was concentrated on the brace located on the flexible side of the structure.

By proceeding in this fashion, six eccentricities ($e_s^* = 0, 0.3, 0.5, 0.75, 0.9, 1.2$) and four earthquakes (1940 El Centro N-S, 1952 Taft S69E, 1977 Romania N90W, and the Newmark-Blume-Kapur artificial excitation) were processed. Figure 3.1 depicts the response of the one-storey structure to variations in slip load distribution. For each stiffness eccentricity given, normalized response is plotted versus normalized slip load eccentricity. The response was normalized by taking the maximum edge response of the structure and dividing it by the corresponding maximum edge response of the unbraced symmetric structure. The significance of these results is discussed below.

3.2.1 Results of Strength Analysis

If one stops to consider how the presence of the braces affects the behavior of the frames, one realizes the following. Braces inherently add stiffness and strength to a frame. Hence, their effect is somewhat equivalent to providing frames having increased stiffness and a higher yield strength, except that the friction damper-equipped braces are not expected to fail under excessive deformations.

Consequently, one would expect that an optimum solution involving the slip load and stiffness distribution of the braces would try to reduce the strength and stiffness eccentricities present in the unbraced structure.

Alternatively, if it is indeed true that the braces behave much like the unbraced frames in which they are located, then one may draw on the research of Ayala, Garcia and Escobar [6], Tso and Ying [7], and Sadek and Tso [8] for a potential solution. These researchers were investigating the effect of strength distribution on overall displacement of structures equipped with ductile moment resisting frames as it pertains to the seismic design portion of the Mexico building code. Their investigation demonstrated that structures having strength eccentricity negative that of stiffness eccentricity generally

performed better during severe earthquakes, and recommendations for changes to the code reflected these results. Therefore, it may be possible to obtain an optimum solution by providing braces with characteristics which mimic those used in the above-mentioned research.

Each of the strength symmetric and strength eccentric models subsequently tested showed a reduction in maximum edge displacement as the center of resistance of the braces moved from the stiff side to the flexible side of the structure. Figure 3.1 shows that, in general, the minimum displacements occur when the normalized slip load eccentricity, e_{pb}*, equals -e_s*. Thus, the optimum normalized response occurs when the eccentricity in slip load distribution equals that of the elastic stiffness of the structure, but on the opposite side.

Closer analysis of these curves, however, suggests that a more practical distribution for design purposes is one in which equal slip loads are assigned to the friction braces (i.e. e_{pb}* = 0) regardless of the elastic stiffness eccentricity. This approach, although not yielding the lowest response, yields displacements that are within 15 percent of the lowest responses recorded for the range of eccentricities considered.

3.2.2 Comparison of The Two Models for Eccentricity with Respect to Strength

Comparisons between the strength symmetric and strength eccentric models show that their behaviors are virtually identical. Responses for the two models vary by approximately ten percent at large eccentricities (e_s* = 1.2) and by less than five percent for eccentricities as large as e_s* = 0.75. These results are displayed in Figure 3.2.

Increase in structure performance may be measured by comparing the optimum response obtained to the response obtained from accepted design practice. Acknowledging that the current accepted practice consists of setting the slip load of the friction damper equal to the strength of the frame in which it is located, comparison of these results, shown in Figure 3.3, shows a dramatic reduction for the strength eccentric case and only a

moderate improvement in the strength symmetric case. The difference can be explained by the use of two different 'starting points' along the curves shown in Figure 3.2. For the strength symmetric case, the response has been reduced from that at $e_{pb}^* = 0$ to that of $e_{pb}^* = -e_s^*$, which is a drop of less than 15 percent. On the other hand, the strength eccentric case sees its response decrease from that of $e_{pb}^* = e_s^*$ to that of $e_{pb}^* = -e_s^*$, a reduction of as much as 70 percent. For the 'suggested design' distribution, the reduction in response for the strength symmetric case would be zero since 'optimum' is at $e_{pb}^* = 0$, and for the strength eccentric case the reduction would be approximately 50 percent.

Where the results differ the most is in the comparison of ductility demand. Ductility demand for an element is defined as the ratio of maximum displacement to yield displacement for the element. Figures 3.4 and 3.5 show the ductility demand for the stiff side and flexible side elements for both the strength eccentric ($e_{pf} = e_s$) and strength symmetric ($e_{pf} = 0$) models. As it can be seen in the strength eccentric case, the ductility demand decreases with increase in e_s^* on the stiff side, and increases with increase in e_s^* on the flexible side. In the case of $e_{pf} = 0$, the reverse trend is true. More importantly, the ductility demand with variation of slip load distributions shows that, regardless of the model chosen, the best results are obtained when $e_{pb}^* = -e_s^*$. It can be seen that reductions in ductility demand are the greatest for the strength eccentric case, and, in general, both the $e_{pb}^* = -e_s^*$ and the $e_{pb}^* = 0$ cases perform well in maintaining the ductility demand either below that of $e_{pb} = e_s$ or below unity (when ductility demand is below unity, the element remains elastic). Similar results for the unbraced system have been obtained by Sadek and Tso [8].

3.2.3 Mass Eccentric vs. Stiffness Eccentric Structures

Based on conflicting conclusions between researchers using mass eccentric models and those using stiffness eccentric models, Goel and Chopra [4] undertook an extensive research programme to help clarify the results through a detailed understanding of the

similarities and differences of mass eccentric and stiffness eccentric structures. They revealed the importance of selecting the appropriate numerical model when analyzing the inelastic response of torsionally coupled buildings. The study also revealed that the main cause of eccentricity in multi-storey structures was an uneven distribution of plan-wise strength and stiffness. Based on these observations, primary consideration of the stiffness eccentric models in the current research is made.

Although this choice was made for the sake of modelling real structures, some comparisons between the mass eccentric and stiffness eccentric models are still warranted if the optimization process is to be considered as generally applicable. Obviously, if results obtained regarding improved response and performance are shown to be independent of the model utilized, more credibility and validity may be attributed to the conclusions drawn.

Recognizing that there are some fundamental behavioral differences between the models as outlined by Goel and Chopra [4], the intent is not to show that both models will provide identical responses and ductility demands, but rather, to show that the improvement obtained once the optimization is complete should be similar. However, in the course of preparing the data, two limitations for comparison were discovered. First, the mass eccentric model has a restricted range of slip load eccentricities compared to the stiffness eccentric model. Second, a stiffness eccentric model could not be created for the case of $e_s^* = 1.5$ without modifying the dimensions of the rigid deck. Having already addressed the latter limitation in a previous section, some attention is now devoted to clarifying the limitation of restricted range.

Consider the mass eccentric structure shown in Figure 3.6 and let RB_{yj} represent the slip load of the j^{th} friction damper-equipped brace oriented in the Y-direction and located at a distance x_j from CM, and let $RB_y = \sum RB_{yj}$ represent the total slip load required for the system in the Y-direction. Consequently, the slip load eccentricity of the system is located at a distance

$$e_{pb} = \frac{1}{RB_y}\Sigma(RB_{yj} \cdot x_j) \tag{3.1}$$

from the center of mass, CM, along the X-direction. For the mass eccentric structure of Reference [3], $RB_{y1} = RB_{y2}$ and e_{pb} becomes

$$e_{pb} = 0.5\,(x_2 - x_1)\,. \tag{3.2}$$

Substituting $x_1 = a\text{-}e_s$ and $x_2 = a+e_s$ into the above equation gives

$$e_{pb} = 0.5\,(a + e_s - a + e_s) \tag{3.3}$$

which reduces to $e_{pb} = e_s$. If RB_{y1} and RB_{y2} are allowed to vary so that an optimum distribution may be obtained, then $RB_{y2} = RB_y - RB_{y1}$ and

$$e_{pb} = \frac{1}{RB_y}\,(RB_y x_2 - RB_{y1} x_2 - RB_{y1} x_1)\,. \tag{3.4}$$

Rearranging this equation gives

$$e_{pb} = x_2 - \frac{RB_{y1}}{RB_y}\,(x_2 + x_1)\,. \tag{3.5}$$

Consequently, substituting for x_1 and x_2 gives

$$e_{pb} = a + e_s - \frac{RB_{y1}}{RB_y}\,(a + e_s + a - e_s) = a + e_s - \frac{2aRB_{y1}}{RB_y}\,. \tag{3.6}$$

If $e_{pb} = -e_s$ (optimum determined earlier) then the above equation becomes

$$-e_s = a + e_s - \frac{2aRB_{y1}}{RB_y}\,, \tag{3.7}$$

or,

$$\frac{e_s}{a} = \frac{RB_{y1}}{RB_y} - 0.5\,. \tag{3.8}$$

Remembering that $a = \rho$ in Reference [3], this equation becomes

$$e_s^* = \frac{RB_{y1}}{RB_y} - 0.5. \tag{3.9}$$

Since $0 \leq RB_{y1} / RB_y \leq 1$, then from equation (3.9) $-0.5 \leq e_s^* \leq 0.5$. This means that $e_{pb} = -e_s$ is only defined for those systems whose normalized eccentricity, e_s^*, lies between 0.5 and -0.5. Changing the value of e_{pb} changes the limits of e_s^* for which e_{pb} is defined, thereby limiting the effective use of the mass eccentric model for determining the optimized slip load distribution.

The normalized maximum edge displacements versus slip load eccentricity for the two systems are shown in Figure 3.7. Figures 3.7 (a), (b), and (c) display the results for e_s^* in which the two systems have values defined within the range of $-e_s^* < e_{pb}^* < e_s^*$. Figure 3.7 (d), (e), and (f) compares the results of the remaining eccentricities, and shows that for the mass eccentric model, e_{pb}^* is not defined for values as low as $-e_s^*$. A summary of the response plotted against e_s^* is given in Figure 3.8 for $e_{pb}^* = e_s^*$ and for $e_{pb}^* = -e_s^*$.

When comparing plots of the ductility demand versus eccentricity for the mass eccentric model (Figure 3.9) to similar plots for the stiffness eccentric model (Figure 3.4), the observation is that the optimization process utilized has the same effect on each model. Although the individual ductility demands are different, the *change* in ductility demand from one slip load eccentricity to another is independent of the model chosen. Hence, the conclusions that may be drawn based on the data obtained should be generally applicable.

3.2.4 Concluding Remarks Regarding Strength Distribution

The analysis of the possible variations in strength distribution between friction damped braces has revealed the following:

- Minimum response may be obtained when the slip load of the braces has been distributed in such a fashion as to mirror the stiffness eccentricity of the structure, i.e. $e_{pb}^* = -e_s^*$.

- Practically speaking, good response may be obtained when the slip load of the braces has been distributed so that the slip load eccentricity equals zero, i.e. $e_{pb}^* = 0$.
- Two models designated as **strength eccentric** and **strength symmetric** were created to reflect the most common types of structures in existence. Although both models give the same responses, improvements over the 'current practice' are moderately model dependent in that they give differing results when comparing ductility demands.
- Modification of the slip load distribution in brace design is best suited to strength eccentric structures since performance increases can reach 70 percent in this case, compared to 15 percent in the case of strength symmetric structures.
- At optimum distribution, the ductility demand is relatively stable and near unity for both the flexible and stiff side elements. In some cases the ductility demand is below unity which signifies that the elements remain elastic.
- The models have shown some limitations in that they cannot be compared to those of Pekau and Guimond [3] for the case of $e_s^* = 1.5$ since this eccentricity would place the resisting frames beyond the edges of the rigid deck of the model. On the other hand, the current models allow for a wider range of strength eccentricities than the models of Pekau and Guimond [3].

All results have been compiled for an ensemble of four earthquakes: 1940 El Centro N-S, 1952 Taft S69E, 1977 Romania N90W, and the artificially generated Newmark-Blume-Kapur accelerogram.

3.3 PHASE II: OPTIMIZATION OF STIFFNESS DISTRIBUTION

The second phase of the research programme focuses on the determination of a suitable stiffness distribution between the friction braces. The basis for this phase is the results obtained by the research of Pekau and Guimond [3] who recommended that for asymmetric structures the KB / KF ratio be maintained at a level higher than seven. The

KB / KF ratio in Phase I was distributed according to the current accepted design practice, whereby a stiffness ratio of KB / KF = 10 meant that the stiffness of each brace was equal to ten times that of the frame in which it was located. No particular attention was given to the distribution of the stiffness of the braces other than noting that for the practice used, the braced system had the same combined stiffness eccentricity as the unbraced system.

The same methodology employed in Phase I to determine the slip load distribution is again used to determine a suitable stiffness distribution. In this case, however, the slip loads of the braces are preset to the optimum values determined at the end of Phase I. Two trials were performed for each of the strength eccentric and strength symmetric models. For the first trial, the slip loads were set such that $e_{pb}^* = 0$, and in the second trial the slip loads were set according to $e_{pb}^* = -e_s^*$. The responses obtained in each case were almost identical.

As for the total slip load, the total required stiffness was determined as the sum of all the stiffnesses of the frames in which the braces would be inserted, multiplied by the KB / KF ratio of ten. This total stiffness was then applied to the brace on the stiff side and a response was obtained. While maintaining the total stiffness constant the concentration of brace stiffness was incrementally shifted from the stiff side to the flexible side of the structure. The procedure ended when the total stiffness was concentrated on the flexible side of the structure. Maximum displacements were then normalized by the response of the unbraced symmetric case and the results plotted.

3.3.1 Discussion of Results

With regard to notation, e_s^* refers to the normalized stiffness eccentricity of the *combined* system under consideration (i.e. braces *and* frames). Consequently, when the stiffness distribution of the braces is modified, the elastic stiffness of the structure is also modified. If the stiffness ratio is very small, KB / KF $\ll$1, the effect of the brace stiffness distribution on the eccentricity of the combined system is almost negligible. Given that

KB / KF = 10 is rather large, it is expected that the elastic stiffness eccentricity, e_s*, will be dominated by the distribution of brace stiffness and highly sensitive to its modification. In Figures 3.10 to 3.13, clarity requires that the 'ic stiffness, e_s*, be broken down to e_{sb}*, the elastic stiffness eccentricity of the friction damped braces, normalized with respect to the mass radius of gyration, and e_{sf}*, the normalized eccentricity of the unbraced structure. In Phase I of the research, e_{sf}* was equal to e_s* since the stiffness of each brace was simply ten times that of the frame in which it was located, and e_s* was unaffected by the presence of the braces.

The data shown in Figure 3.10 depicts the typical effect of varying the distribution of stiffness between the resisting braces for each of the stiffness eccentricities, e_{sf}*, considered. Although Figure 3.10 shows these effects for the strength eccentric case ($e_{pf} = e_{sf}$), plots of the strength symmetric case ($e_{pf} = 0$) are almost identical and, therefore, not shown. In each of these plots, the normalized response for the ensemble of four earthquakes is plotted against the stiffness eccentricity of the friction damped braces, e_{sb}*.

Except for those points where the stiffness is concentrated solely on the stiff side or solely on the flexible side of the structure, each graph shows a relatively uniform response. As in Phase I, two reasonable brace stiffness distributions exist. In this case, however, there is less difference between the optimum distribution and the practical distribution than that observed for the slip load analysis. Here, the optimum response is obtained at e_{sb}* = -e_{sf}*/2, while the practical response is obtained at e_{sb}* = 0. The difference between the results at these two points is less than five percent for the range of e_{sf}* considered.

These plots also reveal that the response tends to be near minimum whenever the brace eccentricity is on the flexible side of the structure (e_{sb}* < 0). Neglecting the endpoints of the plotted curves, variations of response for negative values of e_{sb}* are below ten percent, while those of positive e_{sb}* values (i.e. eccentricity tending towards the stiff side) vary by as much as 50 percent. For most eccentricities, the optimum response is

approximately 25 percent that of the unbraced symmetric structure. In the case of $e_{sf}^* = 1.2$ the optimum is approximately 35 percent that of the unbraced symmetric response.

3.3.2 Notes and Caution Regarding Distribution of Brace Stiffness

For simplicity, the above analysis was performed using the 'suggested design' slip load distribution of Phase I (i.e. $e_{pb}^* = 0$). Some doubts existed, however, as to whether or not these results would be improved if the analysis had been performed for $e_{pb}^* = -e_{sf}^*$. Rather than going through the entire procedure above for $e_{pb}^* = -e_{sf}^*$, an additional computer run was made for $e_{pb}^* = -e_{sf}^*$ with $e_{sb}^* = 0$. The results, not shown, indicated that there is no benefit in favouring $e_{pb}^* = -e_{sf}^*$ over $e_{pb}^* = 0$ in the design of the braces for the KB / KF ratio chosen. In both cases, the maximum normalized response was reduced to 25 percent that of the unbraced symmetric structure.

This indicates that differences in results after the system has been optimized with respect to slip load distribution (curves $e_{pb} = 0$ and $e_{pb} = -e_s$) are eliminated once the system is further optimized with respect to stiffness distribution between braces. This tendency, however, may stem more from the magnitude of KB / KF than from the distribution of KB / KF.

The effect of placing braces of equal stiffness in both frames is best described by the results of Figure 3.11. In Figure 3.11(a), the response is plotted versus e_{sf}^* to show the effect on the initial system, while Figure 3.11(b), with response plotted against e_s^*, demonstrates the overall effect of introducing highly stiff, highly symmetric elements to an initially eccentric structure. As it can be seen, the elastic stiffness eccentricity of the combined system is reduced to a range that lies below $e_s^* = 0.2$. That is, the braces are so stiff in comparison to the frames they are inserted into, that they simply dominate the structural response. Consequently, highly eccentric structures have their combined eccentricities reduced almost to zero. Thus, it is not unreasonable to expect that for lower values of KB / KF, the response will be closer to that expressed by the slip load

redistribution alone (i.e. curves for $e_{pb}^* = 0$ or $e_{pb}^* = -e_{sf}^*$ in Figure 3.11). Also, given that the normalized displacements for $e_{pb} = 0$, $e_{sb} = 0$ in Figure 3.11 are almost identical to those of $e_{pb} = -e_{sf}$, $e_{sb} = -e_{sf}$, one may conclude that the distribution of KB / KF is not as critical in the design of the friction damped braces as the magnitude of KB / KF or the distribution of RB / RF.

3.3.3 Effect of Stiffness Distribution on Ductility Demand

As in the case of slip load distribution, plots were also made to determine the effect of the brace stiffness distribution on the ductility demands of the resisting elements. The curves showing these effects have been added to Figures 3.4 and 3.5 and are displayed as Figures 3.12 and 3.13.

Each successive stage of research has produced lower ductility demands in the resisting elements and this continued progression is shown in these curves. At the end of Phase I, two slip load distributions had been retained, namely, $e_{pb} = -e_s$ and $e_{pb} = 0$. As it can be seen, the case with $e_{pb} = 0$, $e_{sb} = 0$ stabilizes the ductility demand at values near those of the braced symmetric structure.

As previously mentioned, optimization of the strength symmetric model yielded virtually identical responses to those of the strength eccentric model. Although the ductility demands are not identical, the effects of the KB / KF distribution are. That is, for $e_{pb} = 0$, $e_{sb} = 0$, the ductility demand is similar to that of the braced symmetric ($e_{sf} = 0$) structure. These trends may be observed in Figure 3.13.

3.3.4 Concluding Remarks Regarding Optimum Stiffness Distribution

The analysis of the possible variations in stiffness distribution between friction damped braces has revealed the following:

- Minimum response may be obtained when the stiffness of the braces has been

distributed such that $e_{sb}^* = -e_{sf}^*/2$.

- Practically speaking, excellent response may be obtained when the stiffness of the braces has been distributed such that $e_{sb}^* = 0$.
- Given the influence of the large KB / KF ratio used on e_s^*, it is probable that for lower values of KB / KF, the effect of stiffness redistribution between the braces will be attenuated.
- Given that displacements for $e_{pb} = 0$, $e_{sb} = 0$ are similar to those of $e_{pb} = -e_{sf}$, $e_{sb} = e_{sf}$, one need not consider the KB / KF distribution if the slip load distribution has already been adjusted.
- The two models designated as **strength eccentric** and **strength symmetric** give the same responses, and model dependency is almost nonexistent when comparing ductility demands.

All results have been compiled for an ensemble of four earthquakes: 1940 El Centro N-S, 1952 Taft S69E, 1977 Romania N90W, and the artificially generated Newmark Blume Kapur accelerogram.

At the end of these two phases of research, it may be possible to conclude that, although the best distribution of slip load and stiffness has $e_{pb} = -e_{sf}$ and $e_{sb} = -e_{sf}/2$, the best practical distribution of slip load and stiffness is one in which the center of resistance and center of stiffness for the braces remain coincident with the center of mass of the unbraced structure (i.e. $e_{pb} = 0$ and $e_{sb} = 0$).

3.4 PHASE III: ENERGY CURVES

The research carried out thus far has helped establish distributions of slip load and brace stiffness so as to minimize edge displacement response and ductility demand for the structures studied. This phase of research proposes to determine the benefit, if any, of the new distribution schemes on the way energy is dissipated by the structures. Of particular

interest is the fraction of seismic energy imparted to a structure that will be dissipated by the friction braces of the structure.

There has been some discussion between researchers as to which method must be employed when calculating the energy imparted to a structure by seismic excitations. Protagonists in this debate fall into two categories: those who favour the 'absolute' energy method and those who prefer the 'relative' energy concept [19]. The SDOF system of Figure 3.14 is useful in explaining the fundamental difference between these two methods. Using the SDOF system of Figure 3.14(a), the equation of motion with regard to **absolute** energy may be written as:

$$m\ddot{v}_t + c\dot{v} + f_s = 0 \tag{3.10}$$

where m = mass of system, c = coefficient of viscous damping, f_s = restoring force, $v_t = v + v_g$ (total displacement of mass), v = relative displacement of mass to ground and v_g = ground displacement due to seismic excitation [19]. Equation (3.10) may be rearranged by letting $\ddot{v}_t = \ddot{v} + \ddot{v}_g$ thereby obtaining the equation of motion with regard to **relative** energy as:

$$m\ddot{v} + c\dot{v} + f_s = -m\ddot{v}_g \ . \tag{3.11}$$

For convenience, the system of Figure 3.14(a), which includes ground displacements in addition to relative mass to ground displacements, may be replaced by the equivalent fixed-base system of Figure 3.14(b) in which the relative mass displacement is employed and the effect of the ground displacement is considered by adding a forcing function equal to $-m\ddot{v}_g$. Analysis of the system of Figure 3.14(b) thus employs the 'relative' energy concept. This latter approach was the one adopted herein.

Thus, in terms of relative energy, integration of equation (3.11) with respect to v gives

$$\int m\ddot{v}dv + \int c\dot{v}dv + \int f_s dv = -\int m\ddot{v}_g dv \ . \tag{3.12}$$

The first term on the left-hand-side of this equation represents the relative kinetic energy of the system; the second term is the damping energy of the system; and the third term represents the energy absorbed by the system in the form of irrecoverable hysteretic energy and recoverable elastic strain energy. The right-hand-side term is then defined as the input energy of the system. Generalizing, equation (3.12) may be written as:

$$E_i = E_k + E_\xi + E_a \tag{3.13}$$

where [19],

$$\begin{aligned} E_i &= -\int m\ddot{v}_g dv \\ E_k &= \int m\ddot{v} dv = \frac{m(\dot{v})^2}{2} \\ E_\xi &= \int c\dot{v} dv \\ E_a &= \int f_s dv \end{aligned} \tag{3.14}$$

Extending this concept to the two DOF system utilized (Figure 3.15) requires the addition of an equation to account for the rotation of the system. The equation of motion in this case can be described by:

$$\begin{bmatrix} m & 0 \\ 0 & m\rho^2 \end{bmatrix} \begin{Bmatrix} \ddot{v}_y \\ \ddot{v}_\theta \end{Bmatrix} + [C] \begin{Bmatrix} \dot{v}_y \\ \dot{v}_\theta \end{Bmatrix} + \{F\} = -\begin{Bmatrix} m\ddot{v}_y \\ 0 \end{Bmatrix}. \tag{3.15}$$

When integrated with respect to v, the first term leads to the kinetic energy of the system; the second term yields the damping energy of the system; and the third term gives rise to the stored elastic and irrecoverable plastic energy. The resisting force vector, {F}, in incremental form, may be written as [20]:

$$\{\Delta F\} = \begin{bmatrix} \Sigma K_i & \Sigma K_i x_i \\ \Sigma K_i x_i & \Sigma K_i x_i^2 \end{bmatrix} \begin{Bmatrix} \Delta v_y \\ \Delta v_\theta \end{Bmatrix} \tag{3.16}$$

where K_i is the stiffness of frame i located at a distance x_i from the center of mass, CM.

The effect of the friction damped braces is included in the formulation of the energy equation presented above. Therefore, in order to compare the energy dissipated by the friction braces to that imparted to the structure, it becomes necessary to extract the energy absorbed by the braces from the left hand side of equation (3.15). In general, the energy dissipated by a friction device is expressed as the product of the slip load of the device and the total slip travel incurred by the device. If, however, the slip load is set too high, the device will not slip and no friction energy will be dissipated. Set too low, the device will slip, but the energy dissipated will be almost negligible [18]. When multiple devices are used, such as in the models chosen, the total energy dissipated by friction may be expressed as the product of the slip load and the total slip travel of *all* the friction devices in the building. Expressed in symbolic form this means that the total friction energy dissipated by the braces is

$$E_{(brace)} = \Sigma RB_{yi} \times |\Delta_{(slip)\,i}| \tag{3.17}$$

where RB_{yi} represents the slip load of brace i, and $|\Delta_{(slip)i}|$ is the cumulative (absolute) slip travel.

3.4.1 Regarding the Computation of the Energy Equation

The simplicity of the equations presented above belies the effort involved when solving for the various components. The most important aspect to consider is the time step that needs to be chosen so that the various integrations and summations can be considered accurate. This required a two-step approach. First, a reasonable time step had to be

selected so that results could be obtained from DRAIN-2D. Using the results obtained from DRAIN-2D, a separate program was run to calculate the different components of equation (3.15). The time step was then reduced and new results were obtained. When the difference between successive attempts was negligible, the process was ended and the time step was established. The time step thus chosen was $\Delta t = 0.005$ seconds.

3.4.2 Discussion of Results

Simply presenting energy curves for the stiffness eccentric and stiffness symmetric models at various eccentricities and for different earthquake records would be useless if the results obtained could not be generalized in some fashion. Universal applicability of any conclusions drawn forces the choice of an appropriate normalization scheme. In keeping with the spirit of the research conducted in Reference [3], the energy curves obtained for the various eccentricities are normalized either according to the energy imparted to the braced symmetric model, or with respect to the energy dissipated by the braces of the symmetric structure. Thus, the energy curves presented hereafter depict the effect that increasing eccentricity has on the energy imparted to the structure, as well as the dissipative ability of braces with slip load according to the current design ($e_{pb} = e_s$), the suggested design ($e_{pb} = 0$), and the optimum slip load eccentricity ($e_{pb} = -e_s$).

Figure 3.16 shows the averaged, normalized, energy curves for each of the eccentricities considered for the strength eccentric structure ($e_{pf} = e_s$). These curves were plotted with respect to the duration of the ground motion and can be grouped into two sets. Curves between 1.0 and 1.6 represent the energy input to the structure, while those located between 0.5 and 0.6 represent the energy dissipated by the friction damped braces. At every eccentricity, the energy absorbed by the braces approaches the approximate value of sixty percent of the total energy input into the structure, thereby indicating that the braces are dissipating most of the energy that would otherwise be dissipated by the resisting frames as nonrecoverable hysteretic energy.

Some researchers, however, have noted that the amount of energy imparted to a structure is essentially governed by the ground motion chosen as well as the natural period of the structure and is, thereby, independent of eccentricity, strength, or stiffness distribution [21]. This idea is somewhat reflected by Figure 3.16, although the difference between the input energies for the range of eccentricities considered might be explained by considering the effect of the Romania earthquake on the results obtained. Note that in Figures 3.16 to 3.26 normalization of the curves for times less than two seconds becomes quasi-impossible because most of the original curves, depicted by Figure 3.17, have energy input very near zero in this range, thereby causing division by zero errors when normalization is attempted. Also, small numerical differences when calculating the low amounts of accumulated energy in the early portions of the curves may explain the uncharacteristic peaks obtained.

Figure 3.18 provides a comparison of energy curves before and after slip load optimization for the ensemble of earthquake records considered. As it can be seen, optimization of the brace equipped structure with respect to slip load distribution reduces the energy input to the structure by approximately 15 percent as e_{pb} moves from $e_{pb} = e_s$ to $e_{pb} = -e_s$. For $e_{pb} = 0$, the energy dissipated by the braces is expected to be twice that of $e_{pb} = e_s$ at large eccentricities ($e_s^* = 0.9$ and 1.2), and approximately equal to that of $e_{pb} = e_s$ for small and medium eccentricities ($e_s^* = 0 - 0.75$). In contrast, $e_{pb} = -e_s$ shows the same energy dissipation as $e_{pb} = e_s$ at large eccentricities, and approximately half that of $e_{pb} = e_s$ at small and medium eccentricities. Results obtained for the strength symmetric model were virtually identical to those of Figure 3.18 and, therefore, not shown.

A possible explanation for this contradiction in results may be gleaned by examining Figures 3.3 and 3.4 in conjunction with Figure 3.19 and recalling that energy dissipation is a function of slip load and displacement. Figure 3.3 showed that the maximum displacements for $e_{pb} = 0$ were half those of $e_{pb} = e_s$, and that those of $e_{pb} = -e_s$ were one fourth of those of $e_{pb} = e_s$. Similarly, Figure 3.4 showed that the ductility

demands for $e_{pb} = 0$ were half of those at $e_{pb} = e_s$, and that $e_{pb} = -e_s$ caused the peak ductility demand of the structure to drop to 25 percent that of $e_{pb} = e_s$.

Consequently, it would be expected that the energy curves follow the trends set forth by Figures 3.3 and 3.4, until consideration is given to the physical behavior of the structure as e_{pb} is moved from e_s to $-e_s$. For $e_{pb} = e_s$, the brace on the flexible side is subjected to large displacements while having a low slip load, while that of the stiff side is subjected to small displacements and a larger slip load. This combination results in high ductility demands (compared to $e_{pb} = 0$ and $e_{pb} = -e_s$), and low energy dissipation. Consequently, the braces help the behavior of the structure, but they are not being used as effectively as they could be. Reducing the slip load eccentricity to $e_{pb} = 0$ means increasing the slip load of the flexible side brace and reducing that of the stiff side brace. Coupling this load with the displacements obtained results in a more effective brace arrangement which lowers ductility demand, and the combination of a larger flexible side slip load and medium size displacements results in a higher energy dissipation. For $e_{pb} = -e_s$, another increase in the slip load on the flexible side is required along with a reduction in the slip load of the stiff side. This results in a brace arrangement which reduces the ductility demands and displacements to half of those obtained for $e_{pb} = 0$. However, because the displacements have decreased by a significant amount compared to the increase in flexible side slip load, the resulting energy dissipated by the braces is relatively low compared to the other slip load distributions. Hence, the results of Figure 3.19, which at first seem contradictory, are in fact a reflection of the physical behavior of the structure.

Figure 3.20 shows the difference between the energy imparted to the structure and the energy dissipated by the braces. As it can be seen, the smallest difference occurs for $e_{pb} = 0$, thereby indicating that this slip load distribution is the most effective at dissipating the input energy. This figure also implies that $e_{pb} = e_s$ and $e_{pb} = -e_s$ are equally effective configurations since each is expected to dissipate approximately the same fraction of input energy.

Figure 3.21 shows the energy dissipated by the braces of the strength symmetric model (e_{pf} = 0) according to the current design (e_{pb} = 0) and optimum slip load eccentricity (e_{pb} = -e_s). Comparing this figure to that of Figure 3.19 demonstrates that the energy dissipated by braces having a large KB / KF ratio is minimally affected by a modification of the strength eccentricity of the frames.

3.4.3 The Effect of the Romania Earthquake

Reference has been made to the effect of the Romania excitation on the results obtained. Comparisons between the Romania earthquake and the other excitations used in this study (Figure 3.22) illustrate the degree of difference which exists between the energy content of the Romania earthquake and the other excitations. In contrast to the other excitations which are characterized by a series of random peaks of short duration, the Romania earthquake (Figure 3.22(b)) is characterized by an almost sinusoidal arrangement of high amplitude, long duration pulses.

Given that the energy content is essentially represented by the area under the pulses or peaks of an excitation, it is evident that the Romania excitation has a very high energy content when compared to the rest of the ensemble. Hence, some of the results obtained in the analysis are skewed to the high side when all the earthquakes of the ensemble are considered. In fact, for the other earthquakes considered, as the eccentricity increased, both the energy input to the structure and the energy dissipated by the braces decreased. In contrast, for the Romania excitation, as the eccentricity increased, so did the energy input to the structure and the energy dissipated by the braces. Typically, the increase was such that at e_s^* = 1.2, the energy (input or dissipated) was three times that at e_s^* = 0. If the results of the Romania excitation are omitted from the averaging process and the results replotted, it becomes clear that the structure behaves as explained in Reference [22]. Figure 3.23 illustrates this by presenting the normalized energy curves for the strength symmetric model without the Romania excitation.

Figure 3.24 depicts the results for the strength eccentric model considering and neglecting the Romania excitation. The author believes that the curves of Figure 3.24(a), which neglect the Romania earthquake, are more representative of the effect that optimization has on the ability of the structure to dissipate large amounts of energy through the friction damped braces. This plotted data reveals that for $e_s^* < 0.75$, all e_{pb} distributions will dissipate similar amounts of energy. For $e_s^* > 0.75$, $e_{pb} = 0$ should dissipate twice the energy of $e_{pb} = e_s$, while $e_{pb} = -e_s$ is expected to dissipate 50 percent more energy than $e_{pb} = e_s$, in contrast to the 10 percent reduction shown in Figure 3.24(b). Where previously the results showed a continuous increase in energy input with increase in e_s^*, the new results show a stabilization of energy input at 0.8 - 1.2 times that of $e_s^* = 0$.

Figure 3.25, which omits the input energy and normalizes the results with respect to the energy dissipated by the braces of $e_s^* = 0$, clearly demonstrates that the $e_{pb} = 0$ configuration expects to dissipate twice the energy of $e_{pb} = \pm e_s$. In addition, Figure 3.25(a), which neglects the Romania excitation, shows that for any e_s^*, the braces will dissipate less energy than those of $e_s^* = 0$.

Figure 3.26 shows the energy dissipated by the braces of the strength symmetric model ($e_{pf} = 0$) including and neglecting the Romania excitation. As expected, omitting this earthquake produces curves that are similar to those of Figure 3.25.

3.4.4 Concluding Remarks Regarding Energy Curves

Analysis of the results relating energy imparted to the structure and energy dissipated by the FDBF has revealed the following information:

- For the strength eccentric model, the optimum scheme has $e_{pb} = 0$ and causes the braces to dissipate twice the energy of $e_{pb} = e_s$ for $e_s^* > 0.75$, and up to 60 percent of the energy imparted to the structure.
- For $e_s^* < 0.75$, $e_{pb} = \pm e_s$ and $e_{pb} = 0$ dissipate approximately the same amount of energy.

- As far as energy dissipation is concerned, the braces of the strength symmetric structure behave exactly as those of the strength eccentric structure.
- Analysis of Figures 3.3 and 3.4 in conjunction with Figure 3.19 suggests that the earlier scheme of Reference [3] adopted for the distribution of slip load was inefficient in dissipating the energy imparted to the structure because it forced the frames to dissipate too much energy, as indicated by the high ductility demand of the frames and the low level of energy dissipation by the braces.
- Including the high energy Romania excitation in the averaging process significantly affects the results obtained for both the strength symmetric and strength eccentric models. Omission of this excitation provides what is believed to be a more accurate rendering of the structural behavior.

This phase of the research has demonstrated that with a distribution of slip load according to the methods outlined earlier, it can be expected that the structure, regardless of its eccentricity, will be subject to the same levels of energy input as the braced symmetric structure. The amount of energy dissipated by the reconfigured braces is not necessarily greater than in the corresponding symmetric structure, but reduced displacement response is nonetheless achieved.

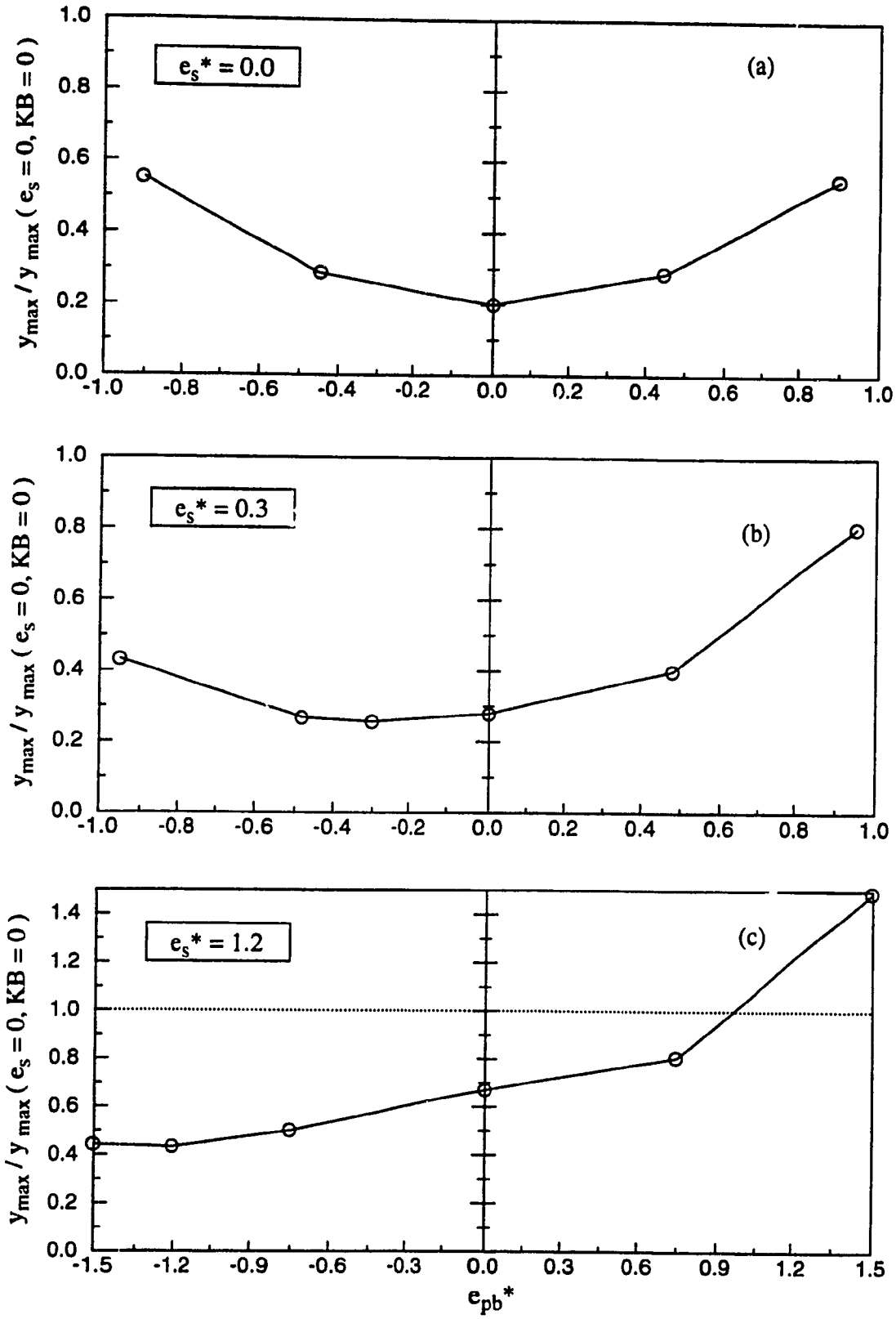

Figure 3.1. Typical response of stiffness eccentric structure with variation in slip load eccentricity e_{pb}^* of the braces.

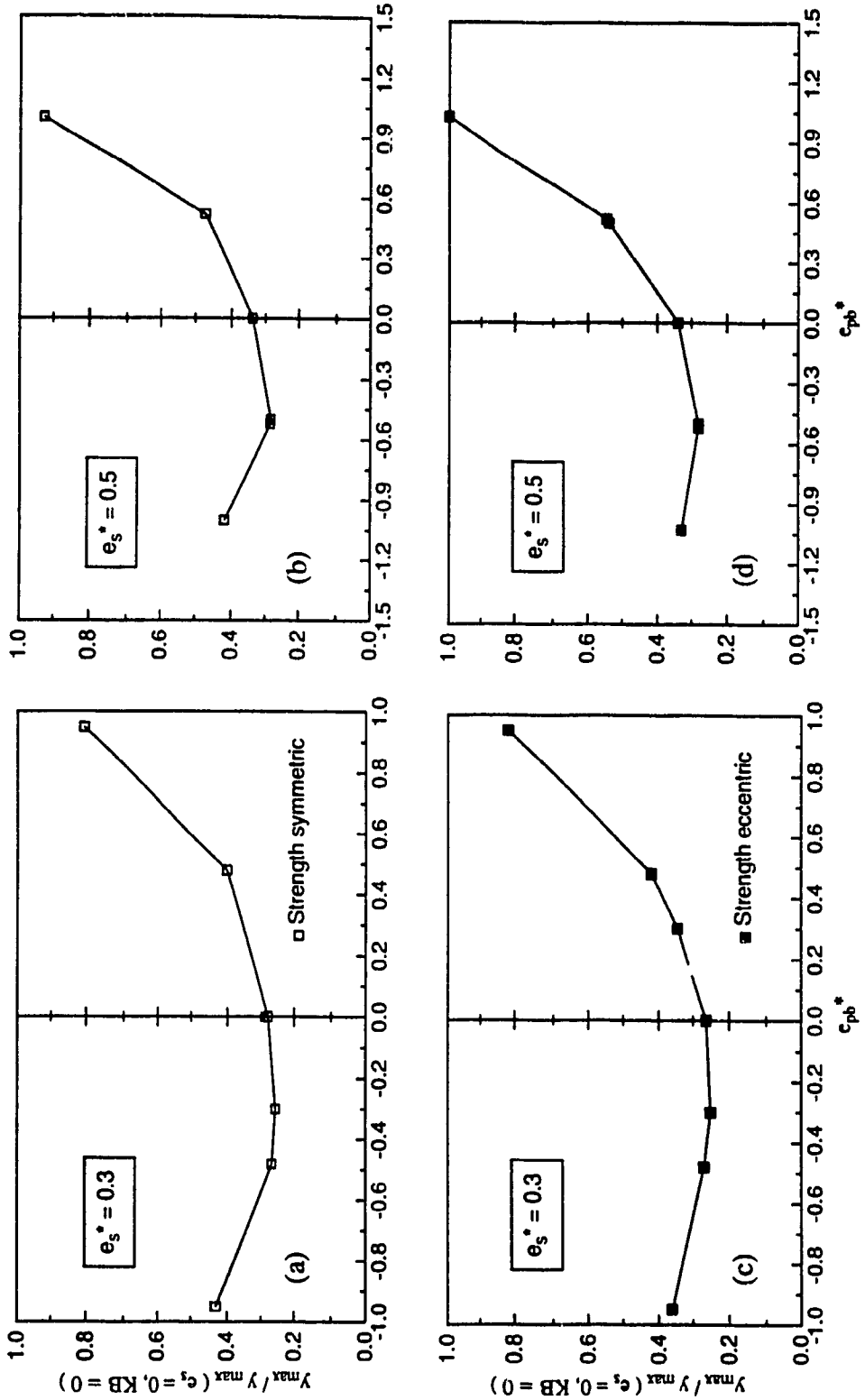

Figure 3.2. Comparison of stiffness eccentric models for $e_s^* = 0.3$ and 0.5.
(a, b) Strength symmetric ($e_{pf} = 0$). (c, d) Strength eccentric ($e_{pf} = e_s$).

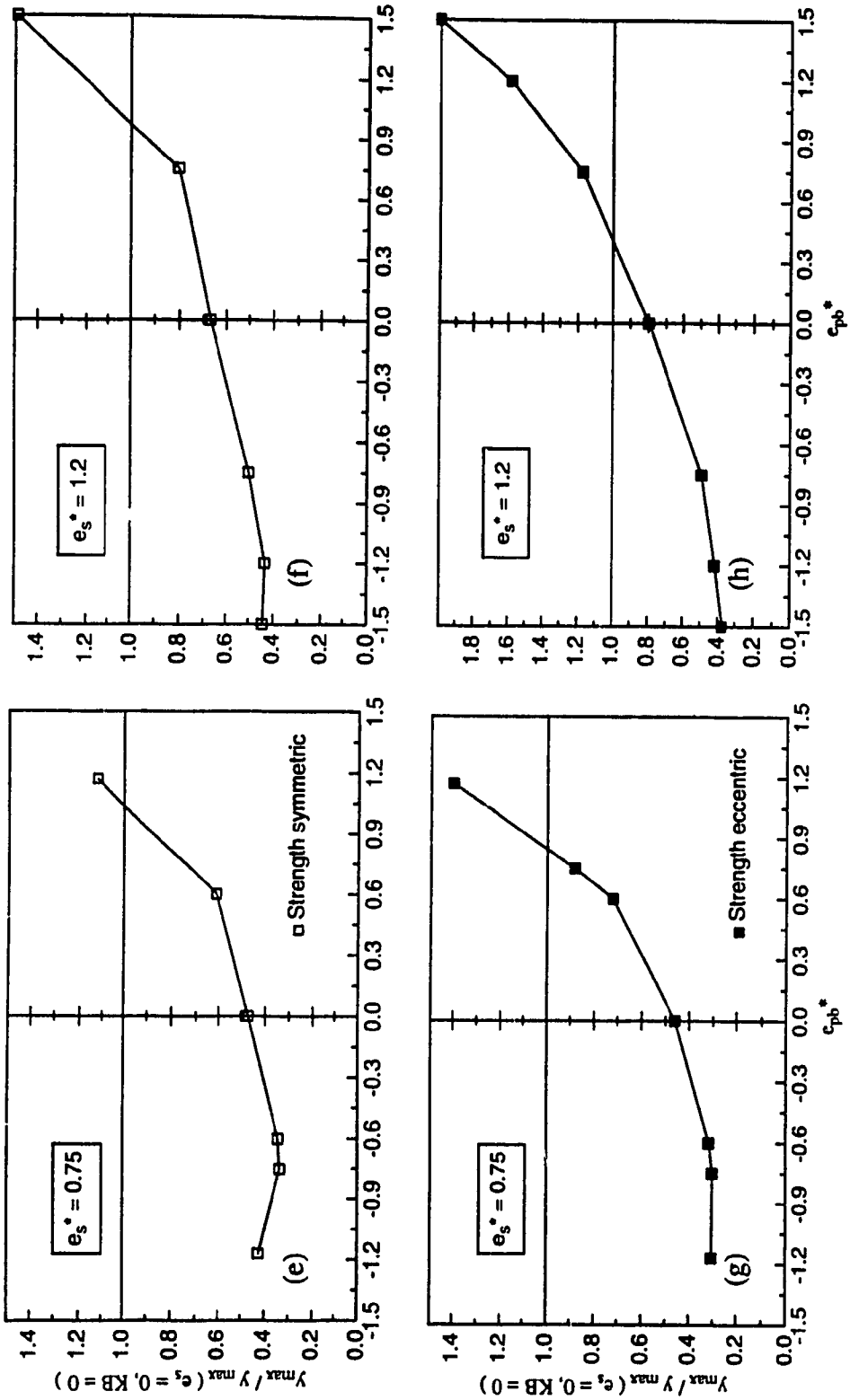

Figure 3.2 (Cont'd). Comparison of stiffness eccentric models for $e_s^* = 0.75$ and 1.2.
(e, f) Strength symmetric ($e_{pf} = 0$). (g, h) Strength eccentric ($e_{pf} = e_s$).

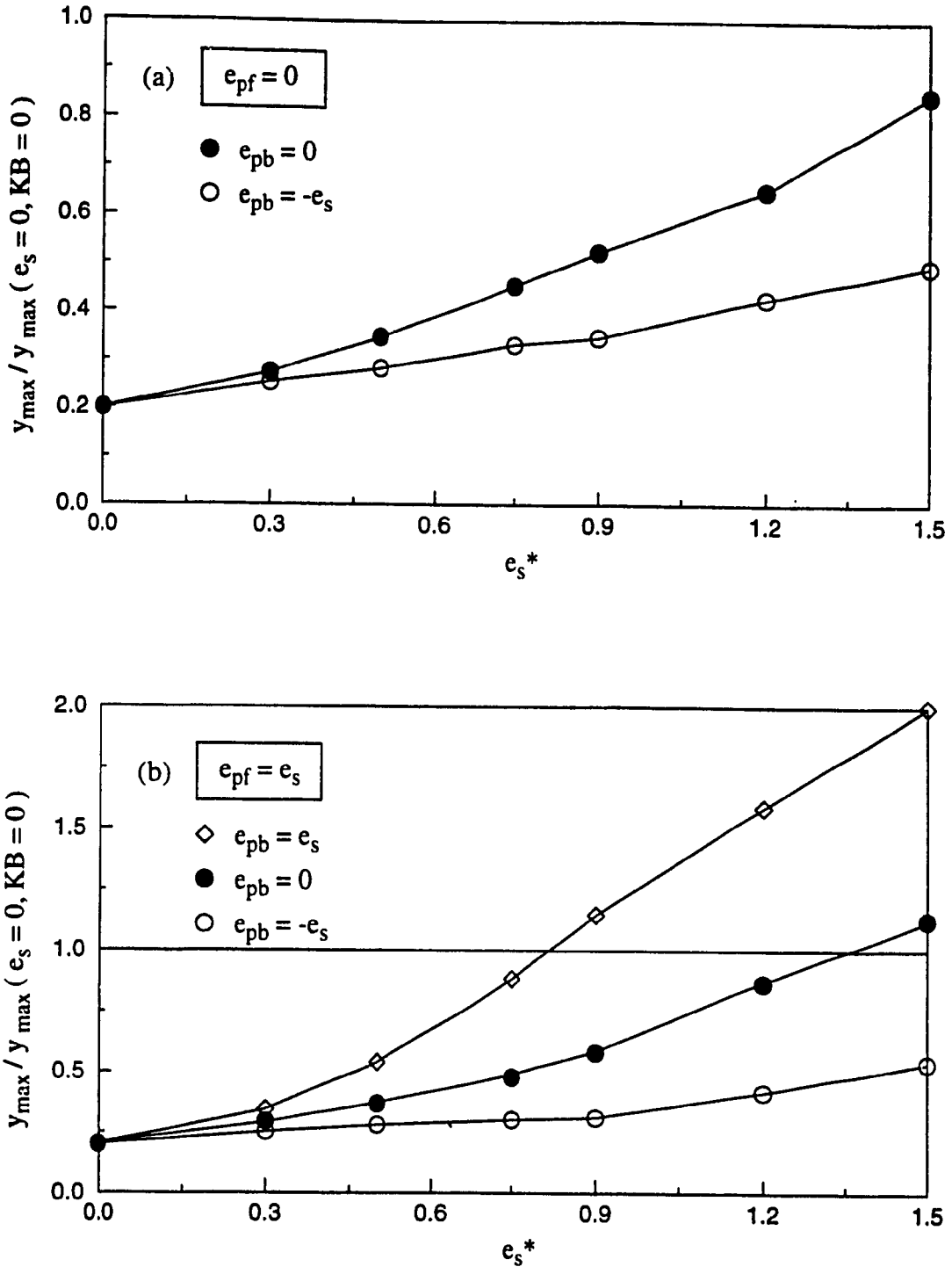

Figure 3.3. Comparison of response over stiffness eccentricity e_s^* for current design ($e_{pb} = e_{pf}$) and optimum ($e_{pb} = -e_s$) slip load eccentricity. (a) Strength symmetric ($e_{pf} = 0$). (b) Strength eccentric ($e_{pf} = e_s$).

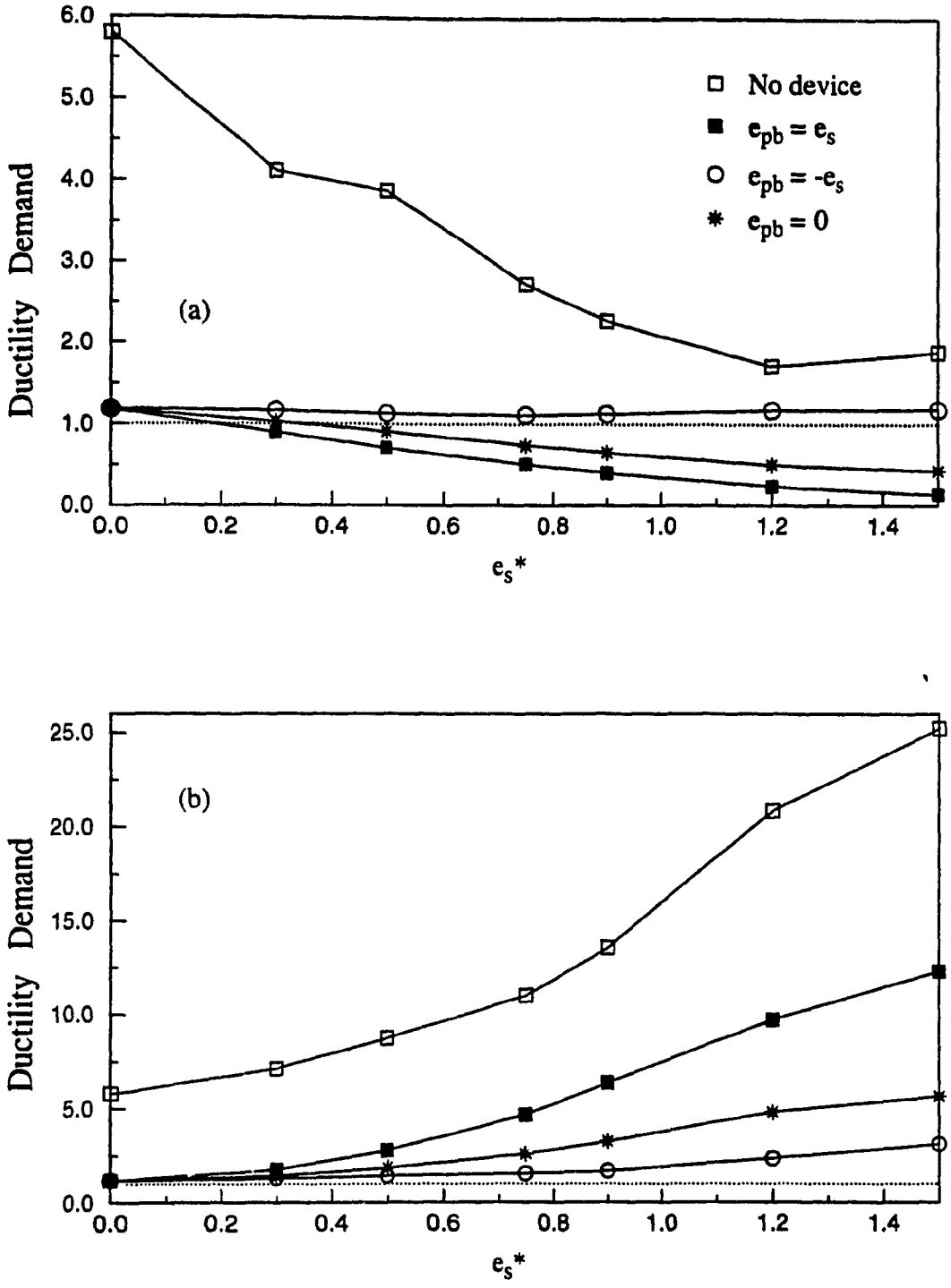

Figure 3.4. Effect of slip load eccentricity of bracing on ductility demand for strength eccentric model ($e_{pf} = e_s$). (a) Stiff side. (b) Flexible side.

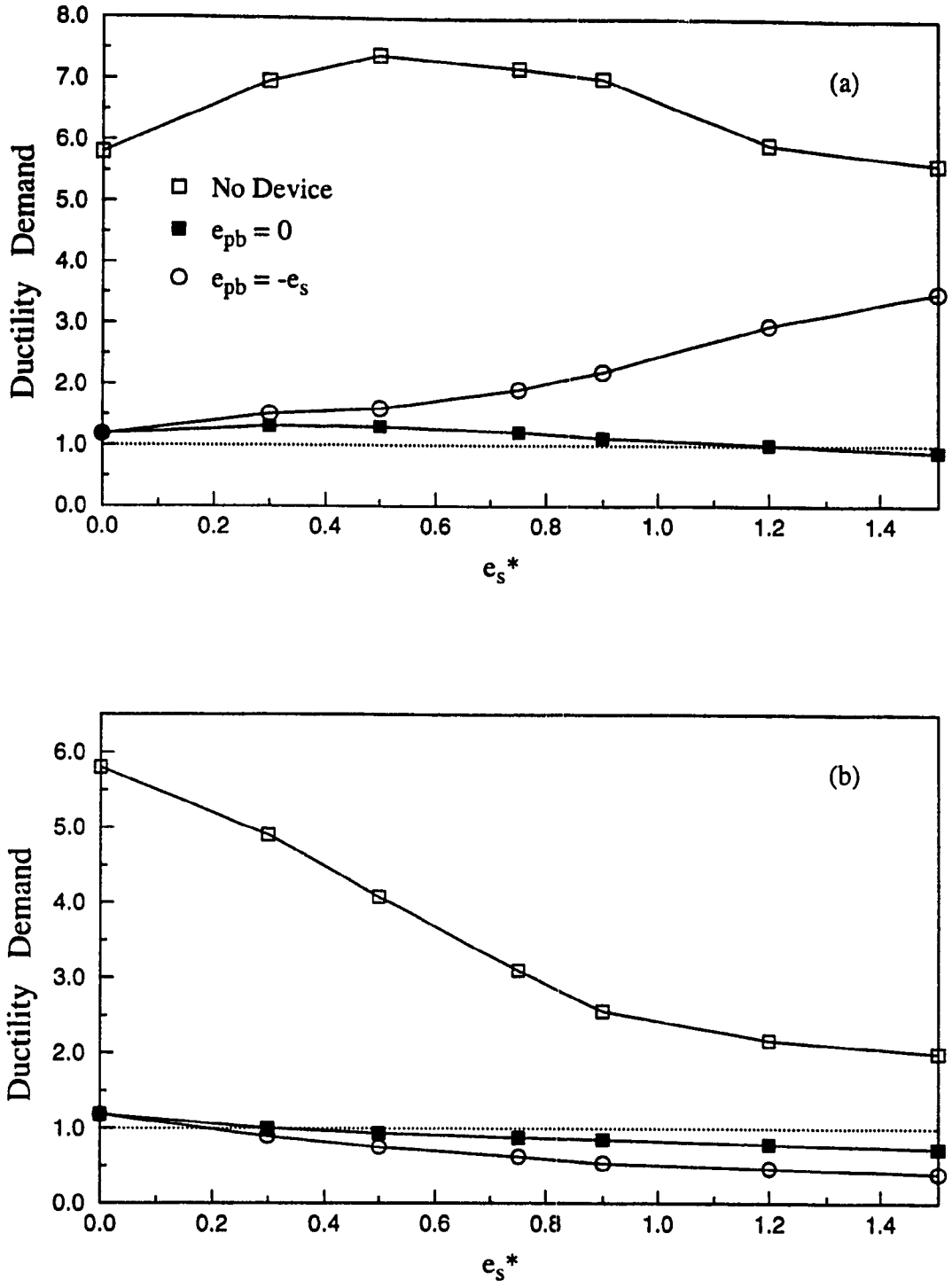

Figure 3.5. Effect of slip load eccentricity of bracing on ductility demand for strength symmetric model ($e_{pf} = 0$). (a) Stiff side. (b) Flexible side.

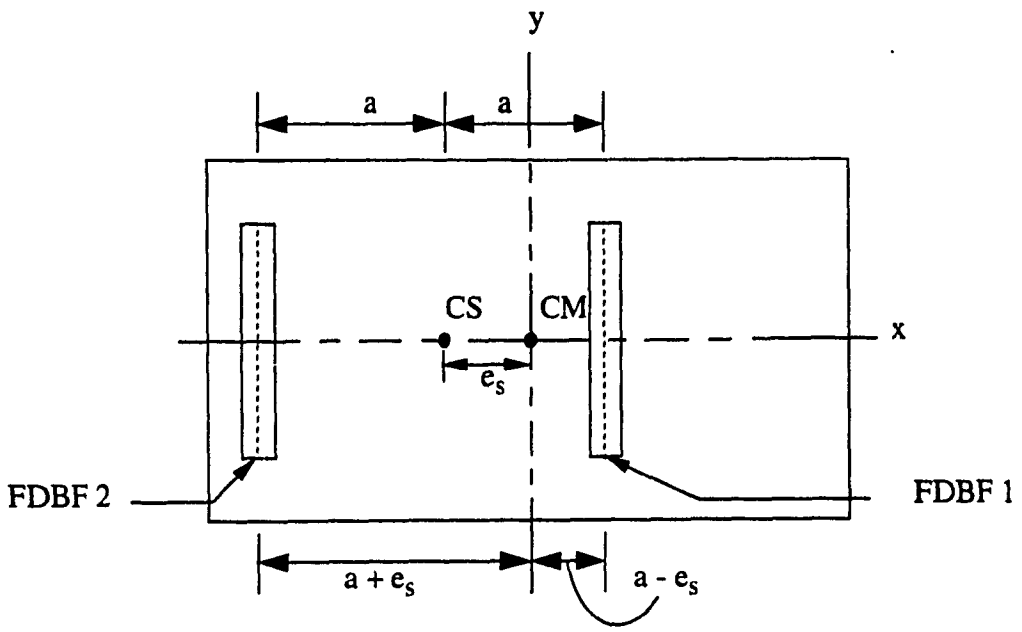

Figure 3.6. Model used in previous study [10].

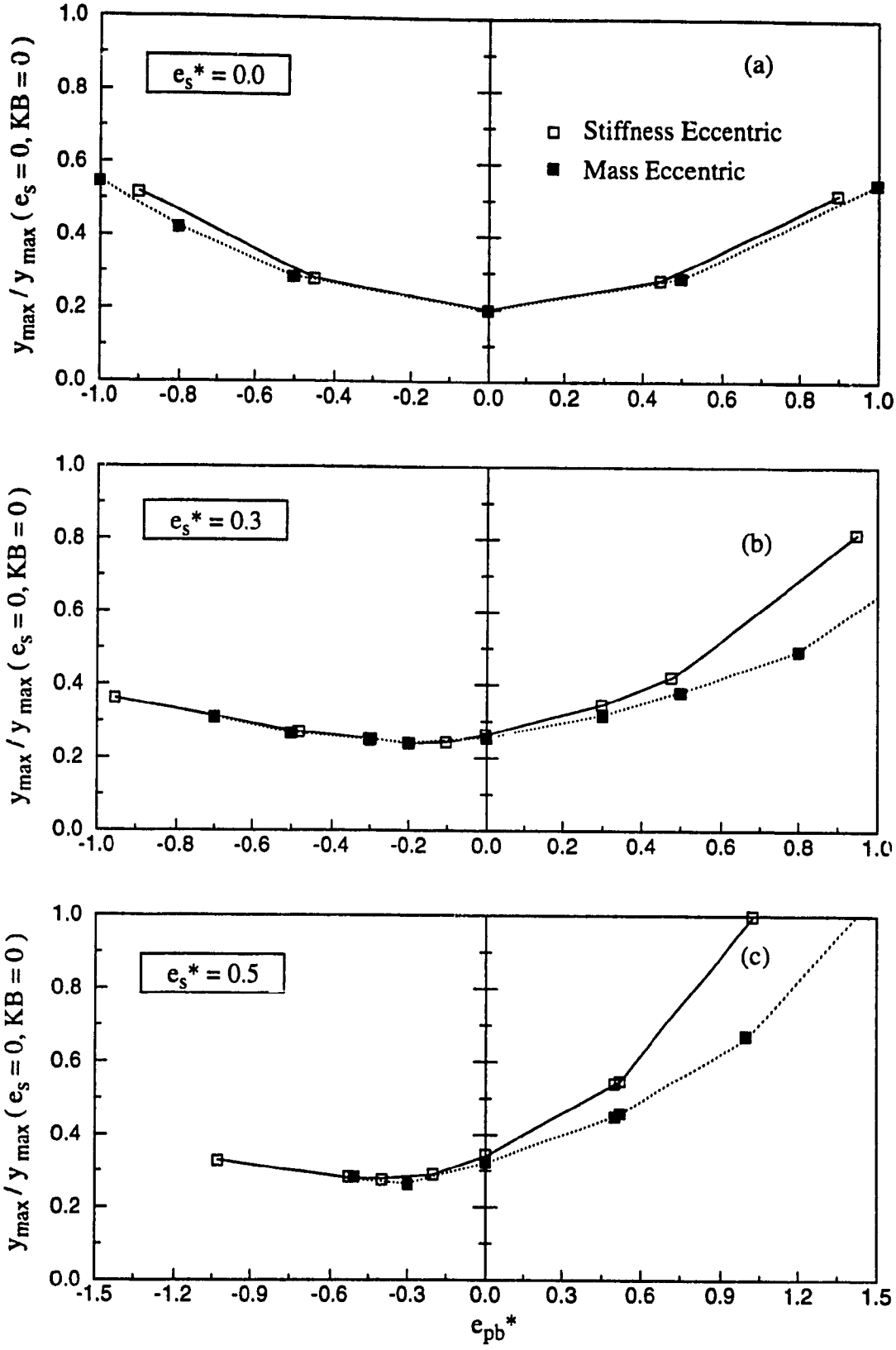

Figure 3.7. Comparison of response of structures studied to variation in strength eccentricity e_{pb} of the braces.

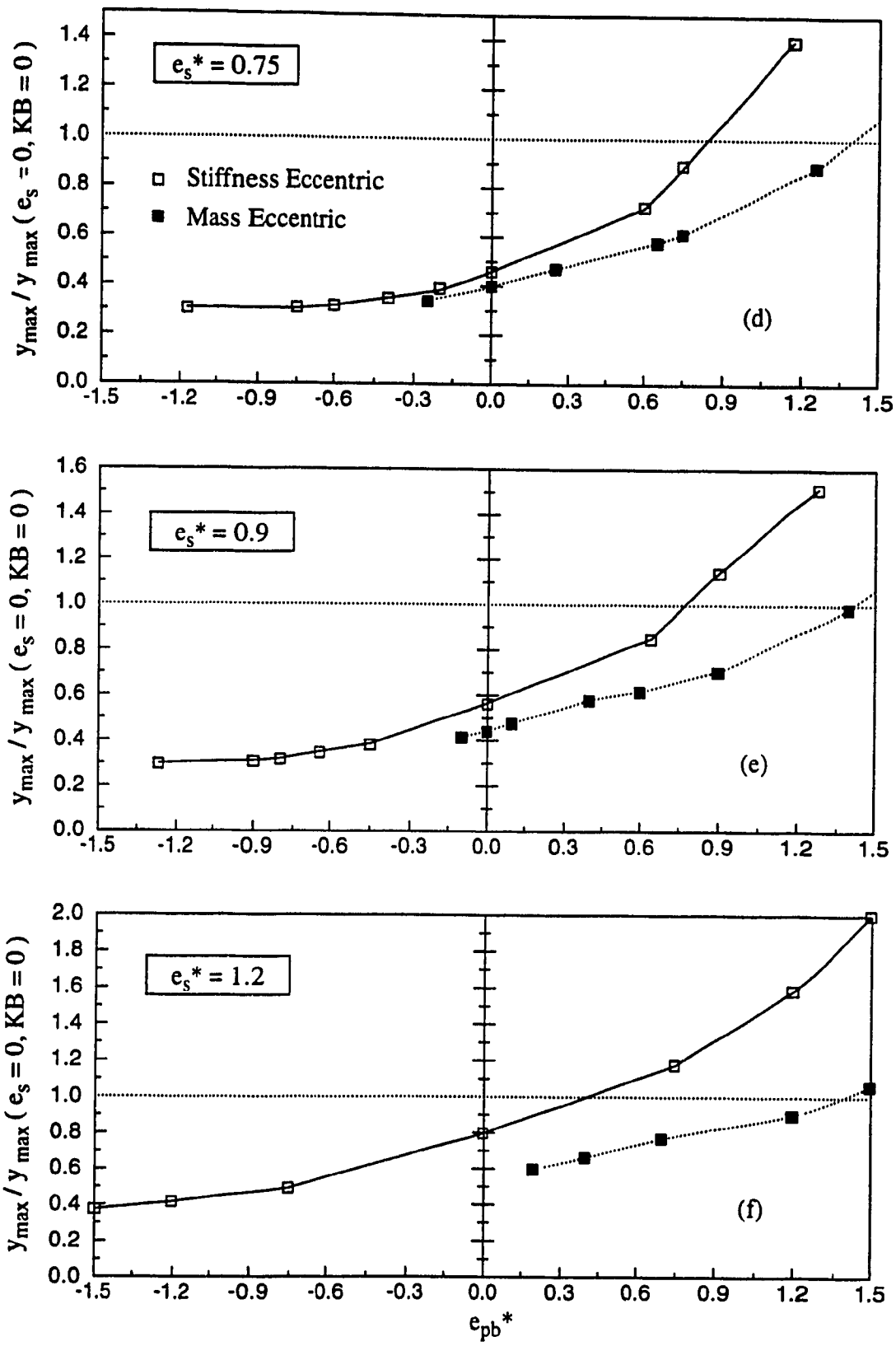

Figure 3.7 (Cont'd). Comparison of response of structures studied to variation in strength eccentricity e_{pb} of the braces.

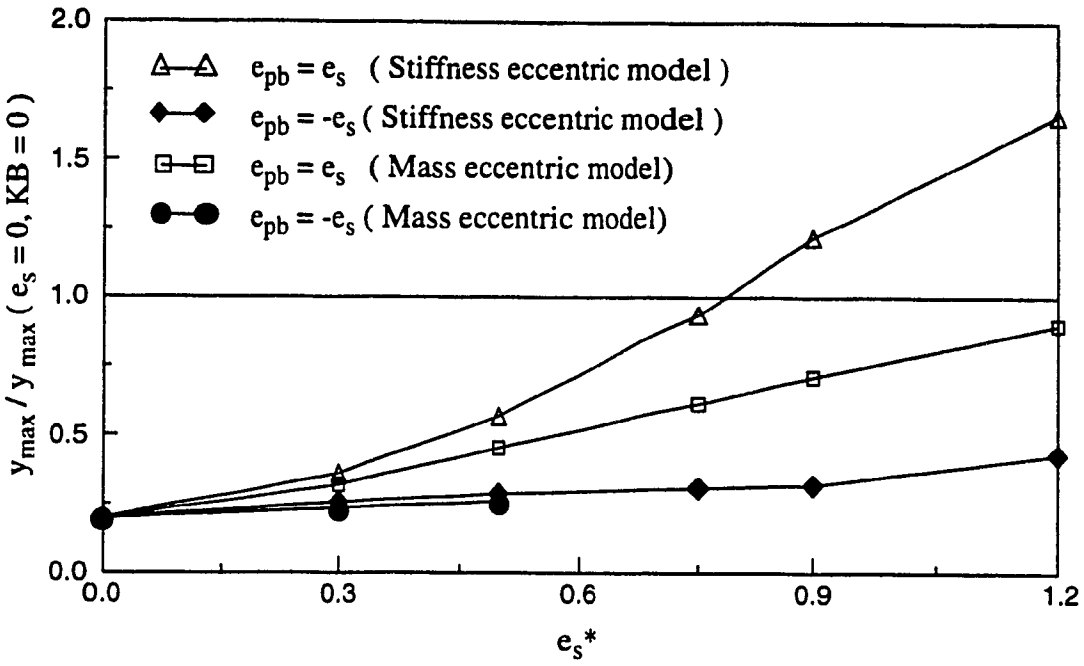

Figure 3.8. Comparison of response between stiffness eccentric and mass eccentric structures over eccentricity e_s* for current design ($e_{pb} = e_s$) and optimum ($e_{pb} = -e_s$) slip load eccentricity.

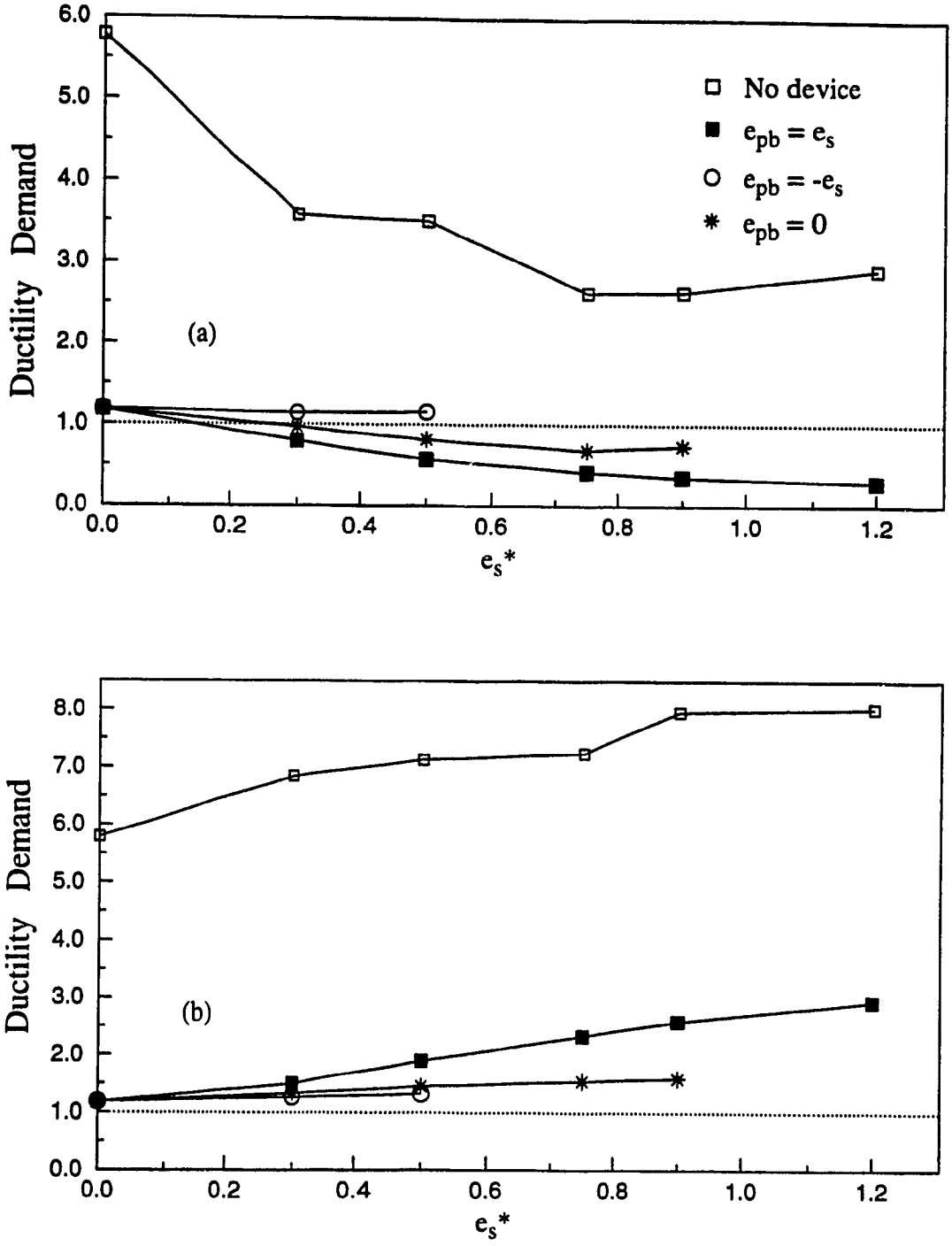

Figure 3.9. Effect of slip load eccentricity of bracing on ductility demand of mass eccentric structure with $e_{pf} = e_s$. (a) Stiff Side. (b) Flexible side.

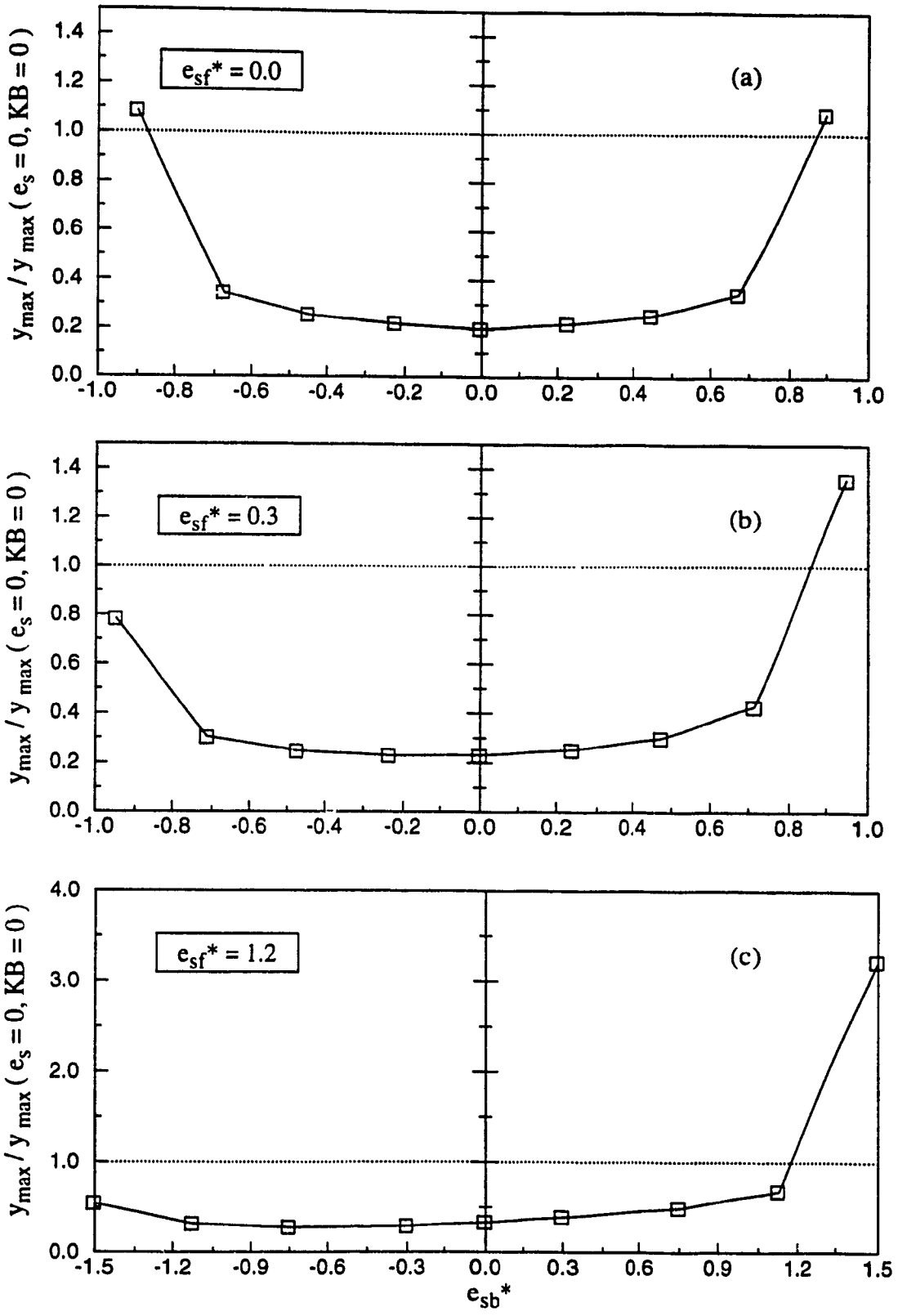

Figure 3.10. Typical response of stiffness eccentric structure ($e_{pf} = e_{sf}$) with variation in stiffness distribution e_{sb}^* of the braces.

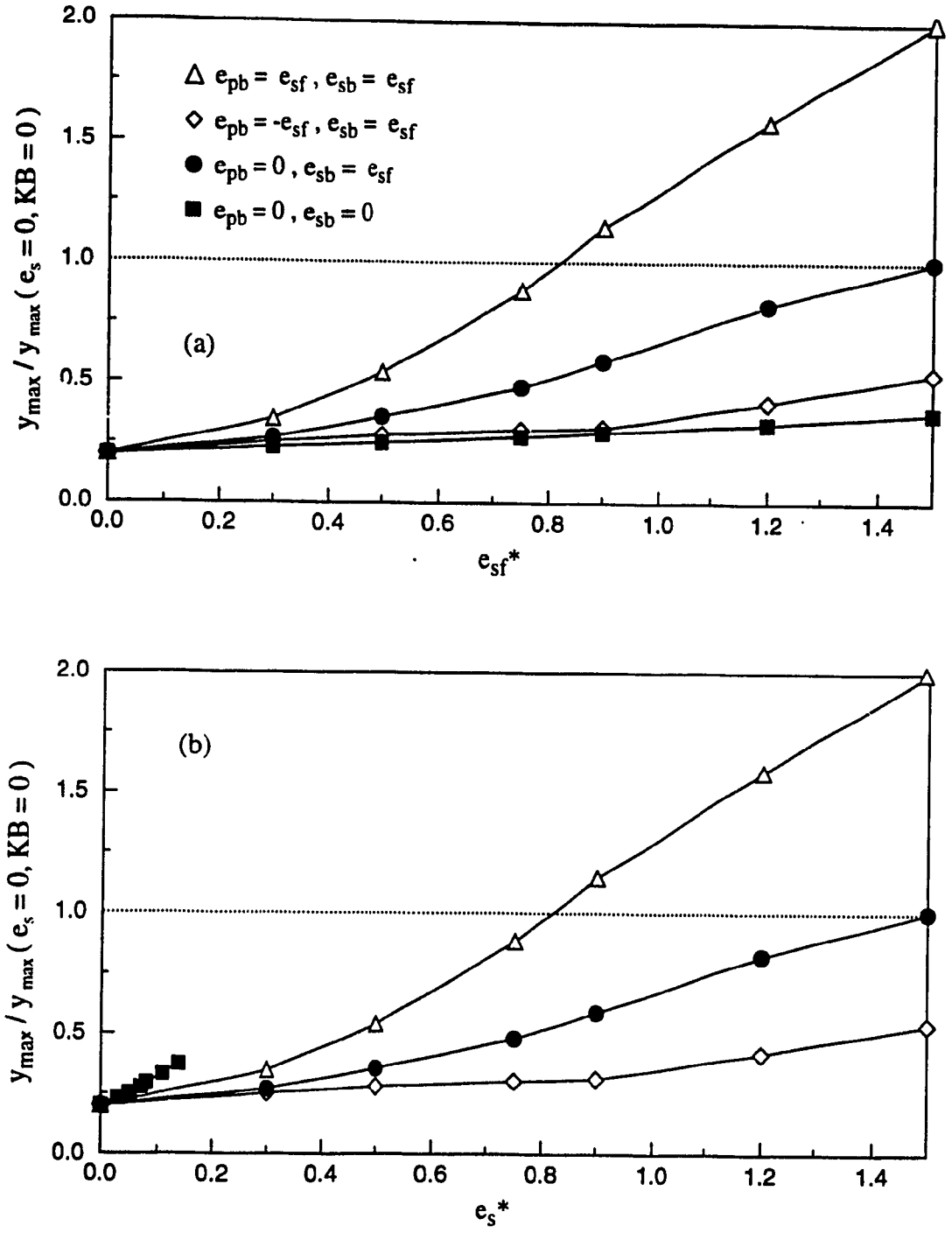

Figure 3.11. Comparison of response over stiffness eccentricity for current design ($e_{pb} = e_{sf}$, $e_{sb} = e_{sf}$) and other slip load and brace stiffness eccentricities. (a) Neglecting effect of e_{sb} on e_s*. (b) Including effect of e_{sb} on e_s*.

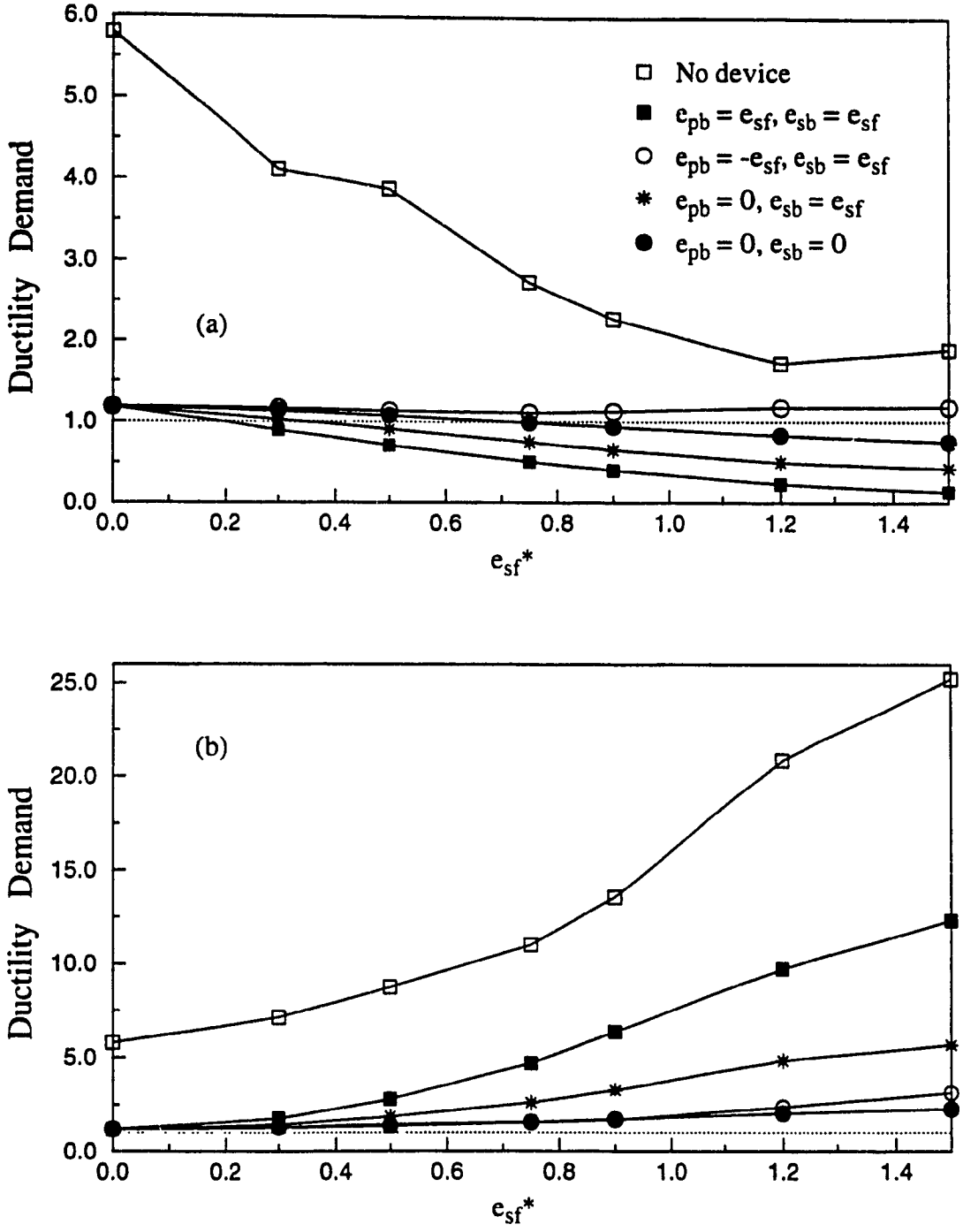

Figure 3.12. Summary of effects of slip load and stiffness eccentricity of bracing on ductility demand for strength eccentric model ($e_{pf} = e_{sf}$). (a) Stiff side. (b) Flexible side.

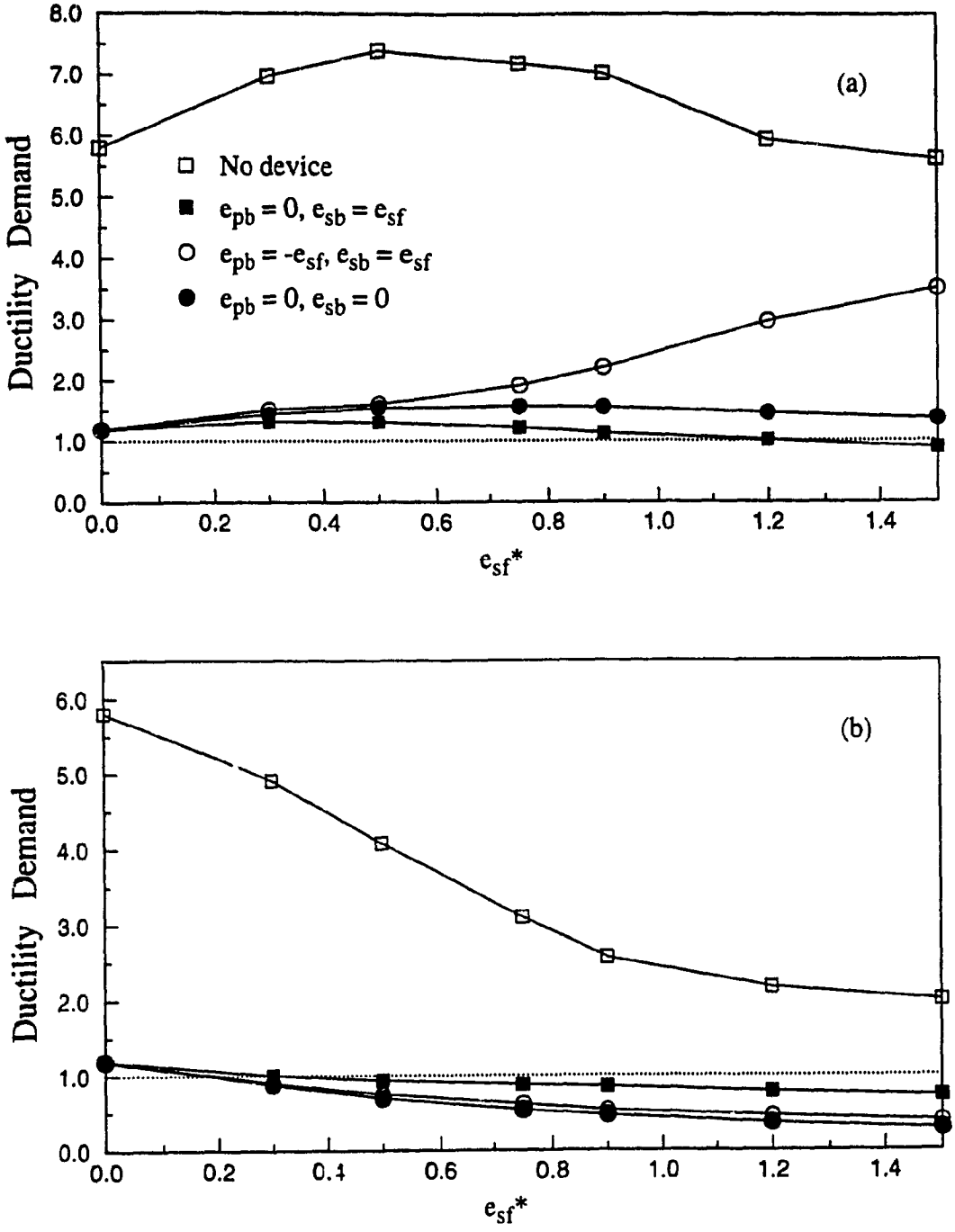

Figure 3.13. Summary of effects of slip load and stiffness eccentricity of bracing on ductility demand for strength symmetric model ($e_{pf} = 0$). (a) Stiff side. (b) Flexible side.

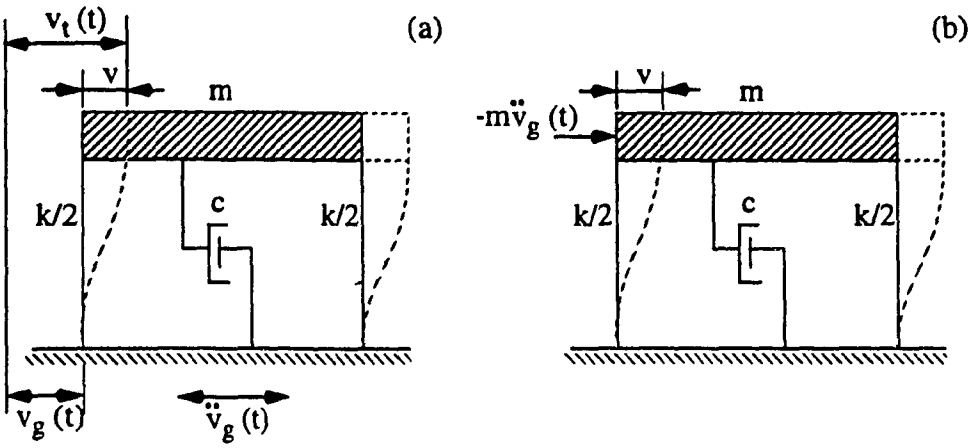

Figure 3.14. Idealized SDOF systems subjected to earthquake ground motion.
(a) 'absolute' motion. (b) Equivalent 'relative' displacement.

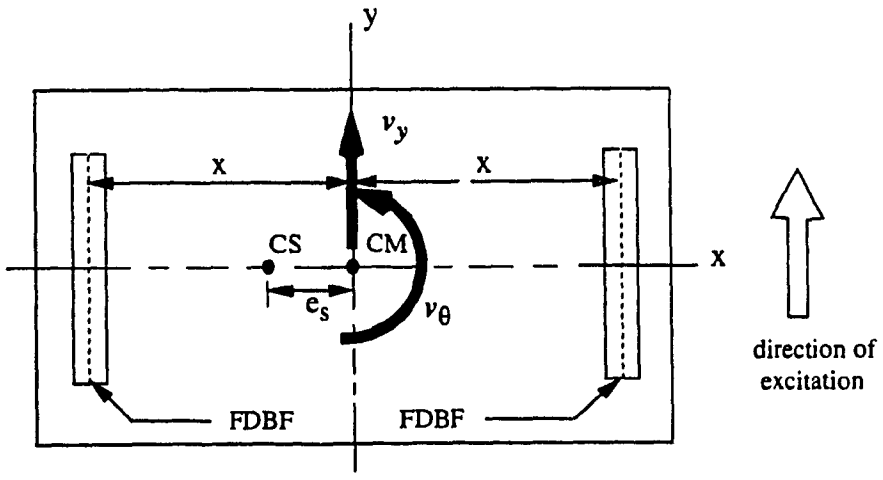

Figure 3.15. Idealized 2-DOF model of eccentric structure used in current study.

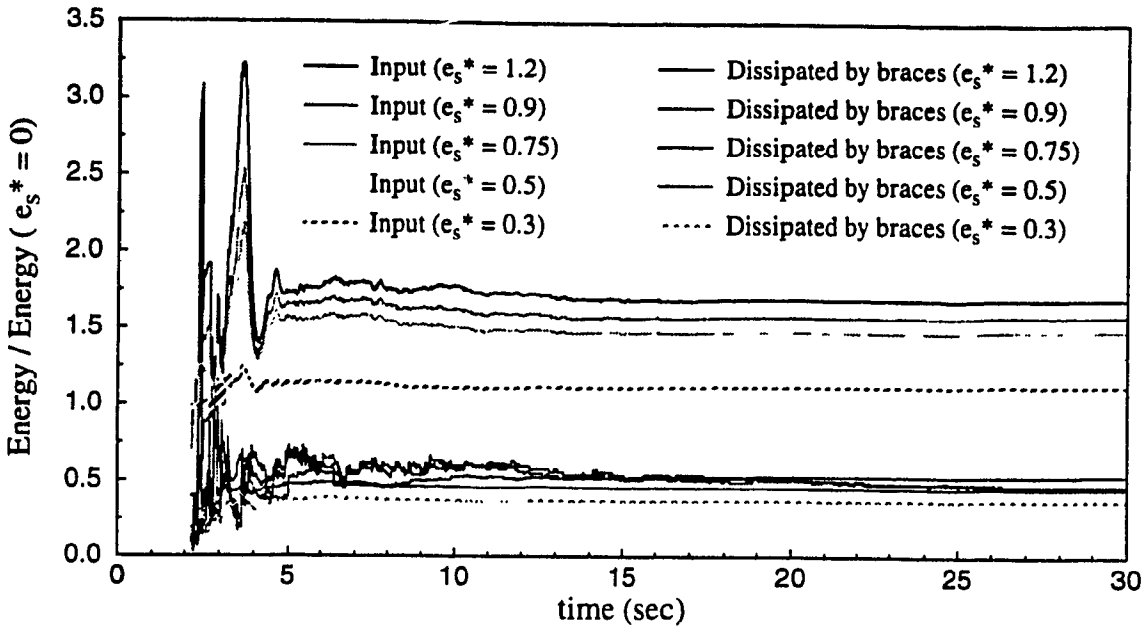

Figure 3.16. Energy curves for strength eccentric model ($e_{pf} = e_s$) with current design braces ($e_{pb} = e_s$).

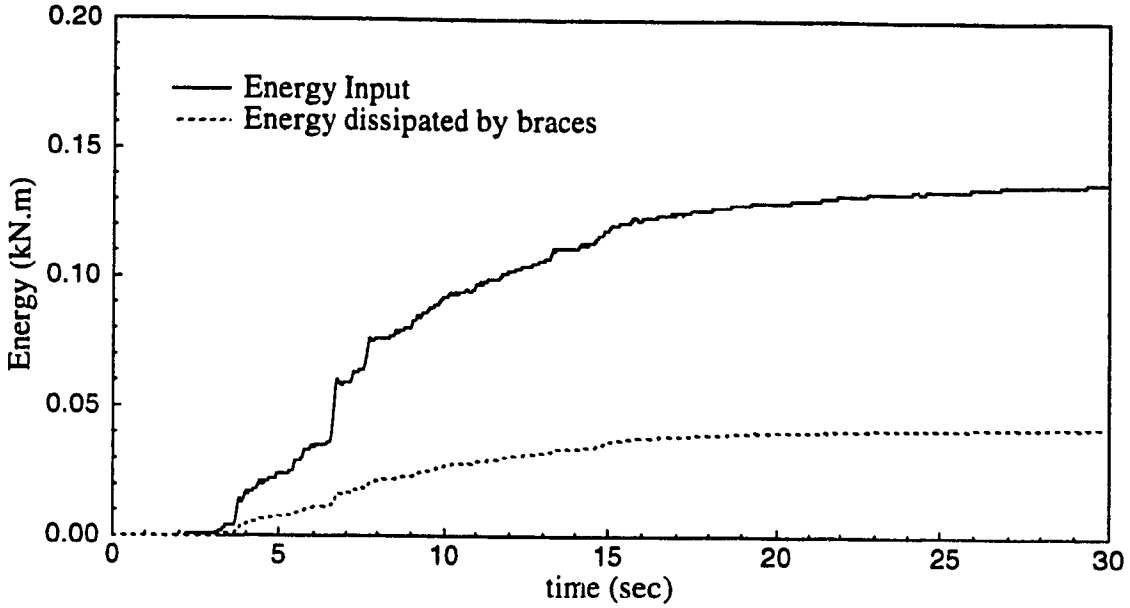

Figure 3.17. Typical energy relations for strength eccentric model ($e_{pf} = e_s$) subjected to Taft excitation with $e_{pb} = 0$ and $e_s^* = 0.3$.

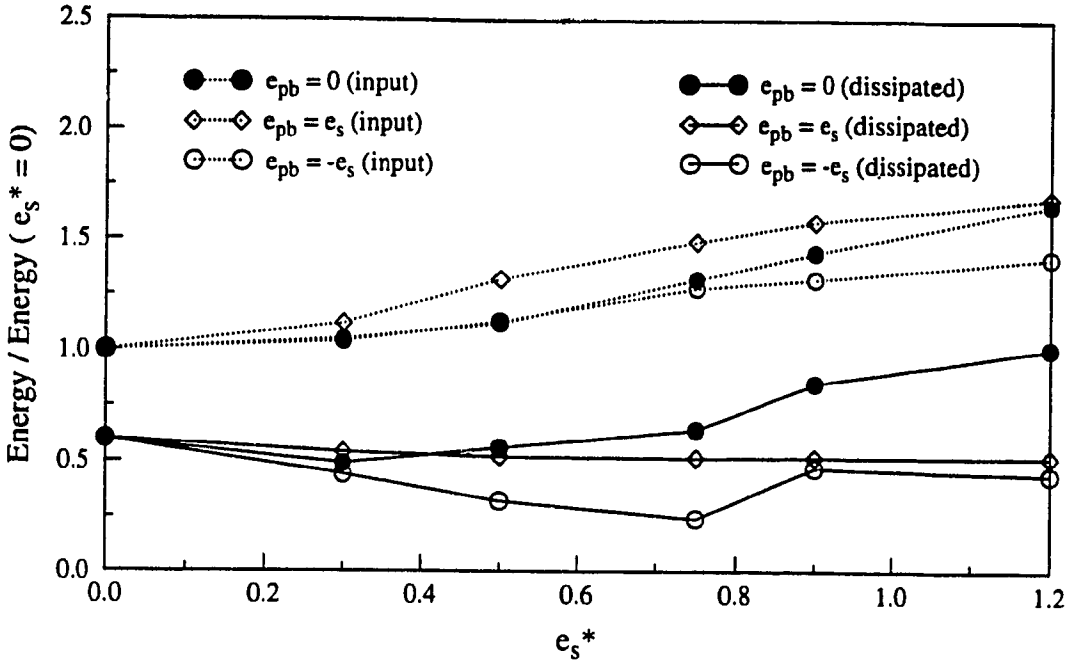

Figure 3.18. Comparison of energy input to structure and dissipated by braces over stiffness eccentricity e_s^* for current design ($e_{pb} = e_s$), suggested design ($e_{pb} = 0$) and optimum slip load eccentricity ($e_{pb} = -e_s$).

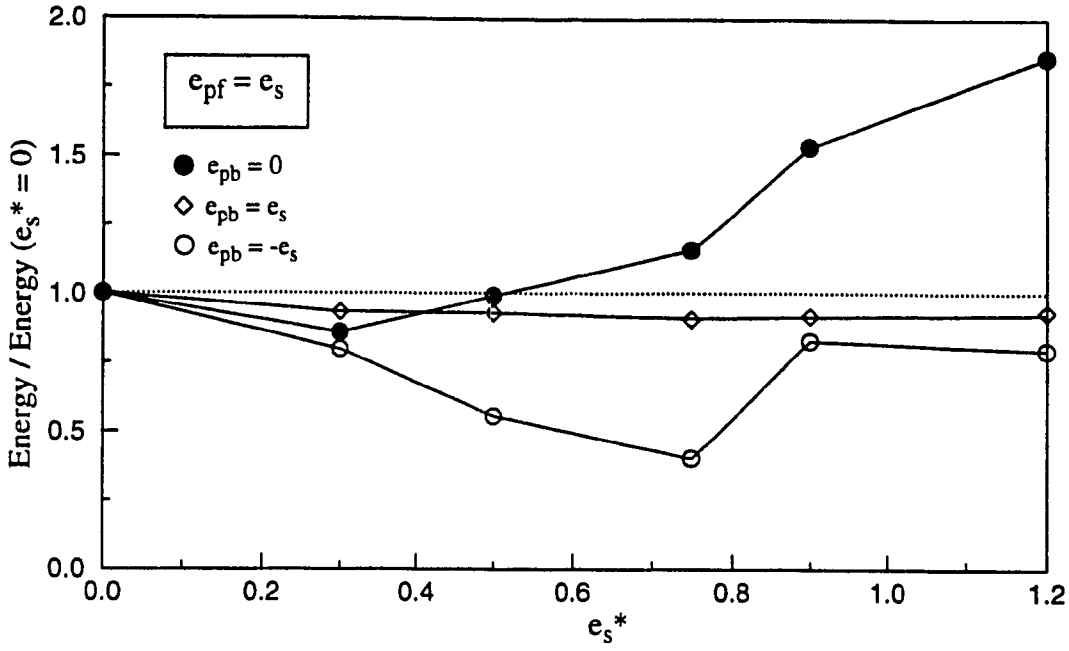

Figure 3.19. Energy dissipated by braces of strength eccentric model ($e_{pf} = e_s$) according to current design ($e_{pb} = e_s$), suggested design ($e_{pb} = 0$), and optimum slip load eccentricity ($e_{pb} = -e_s$).

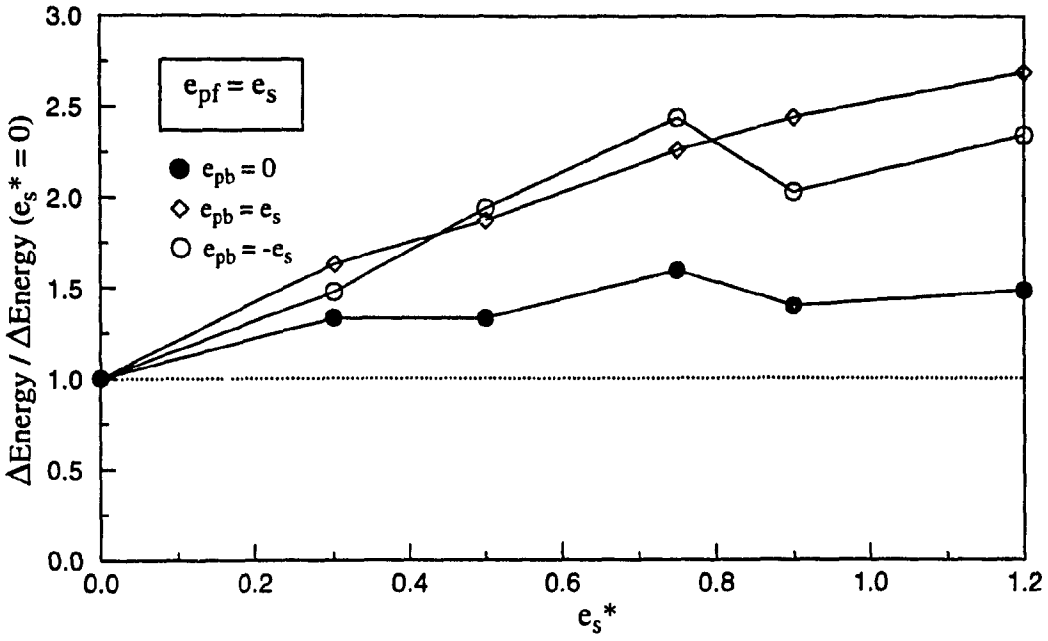

Figure 3.20. Difference between energy input to structure and energy dissipated by braces of strength eccentric model according to current design ($e_{pb} = e_s$) suggested design ($e_{pb} = 0$) and optimum slip load eccentricity ($e_{pb} = -e_s$).

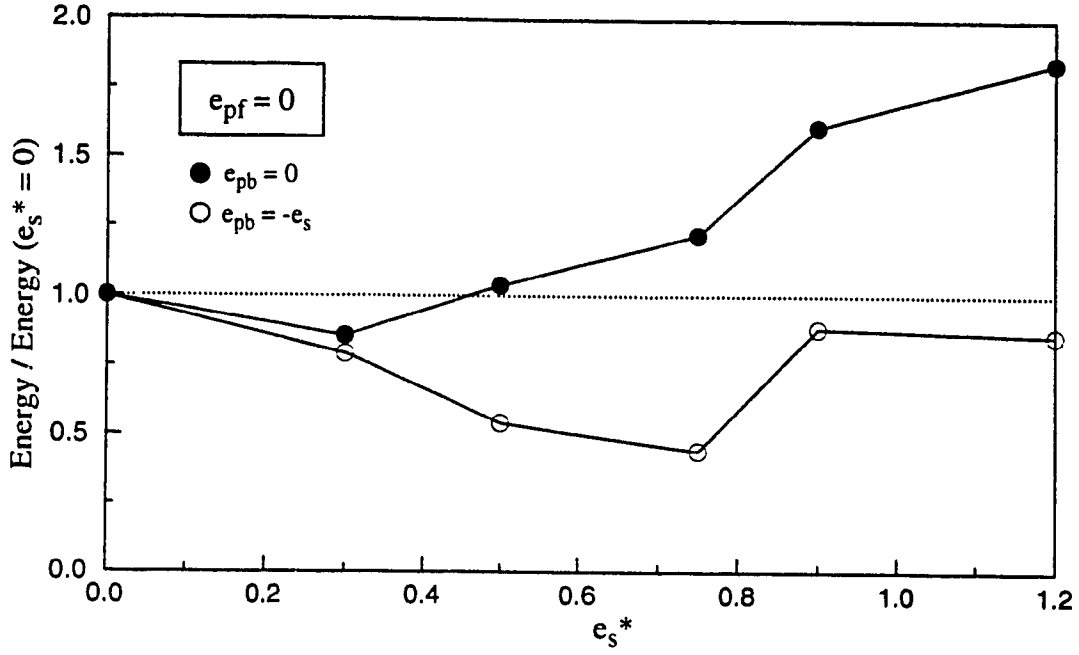

Figure 3.21. Energy dissipated by braces of strength symmetric model ($e_{pf} = 0$) according to current design ($e_{pb} = 0$) and optimum slip load eccentricity ($e_{pb} = -e_s$).

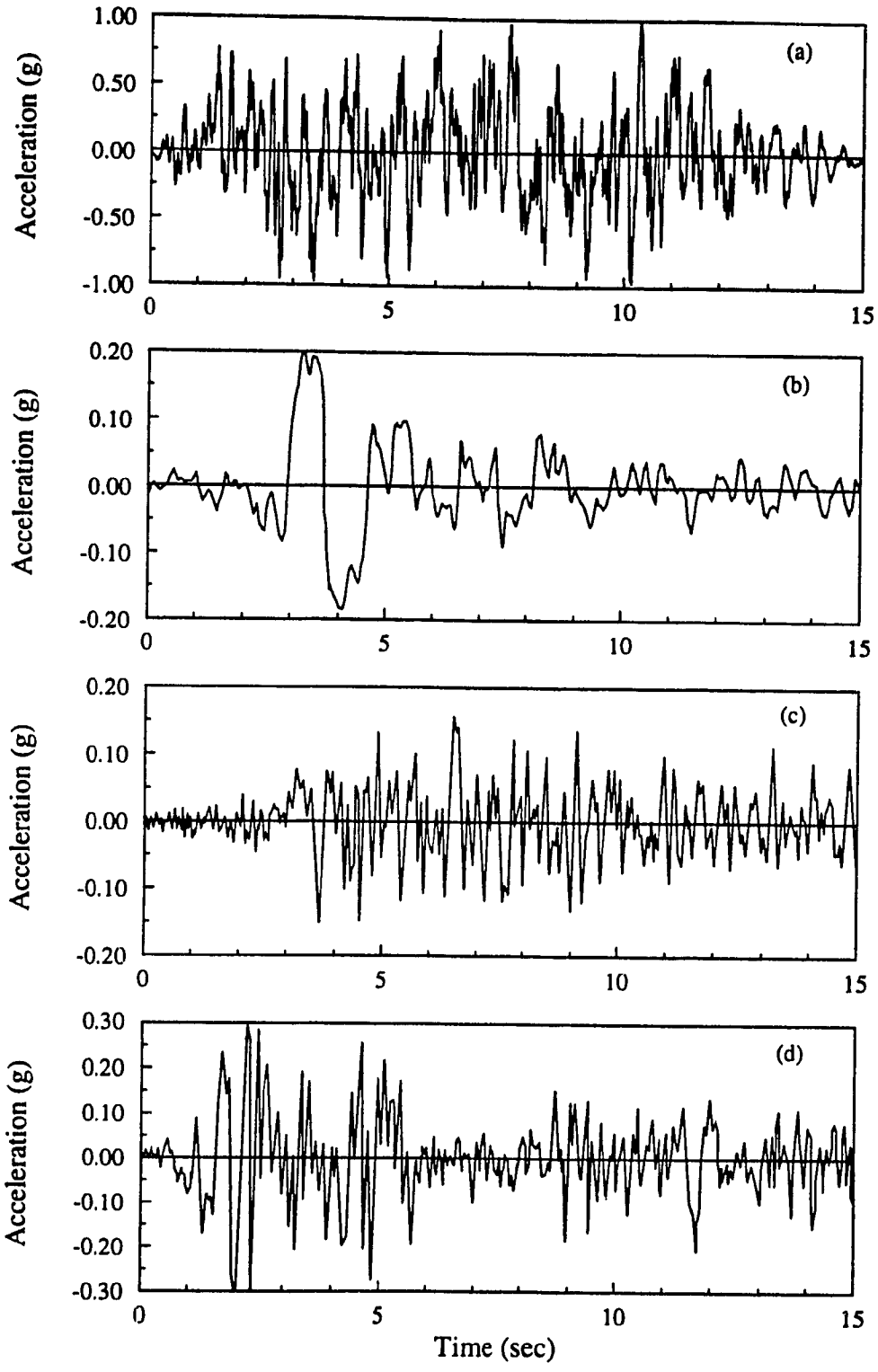

Figure 3.22. Acceleration time history for earthquake ensemble: (a) Newmark-Blume-Kapur artificial excitation; (b) 1977 Bucharest N-S; (c) 1952 Taft S69E; (d) 1940 El Centro N-S.

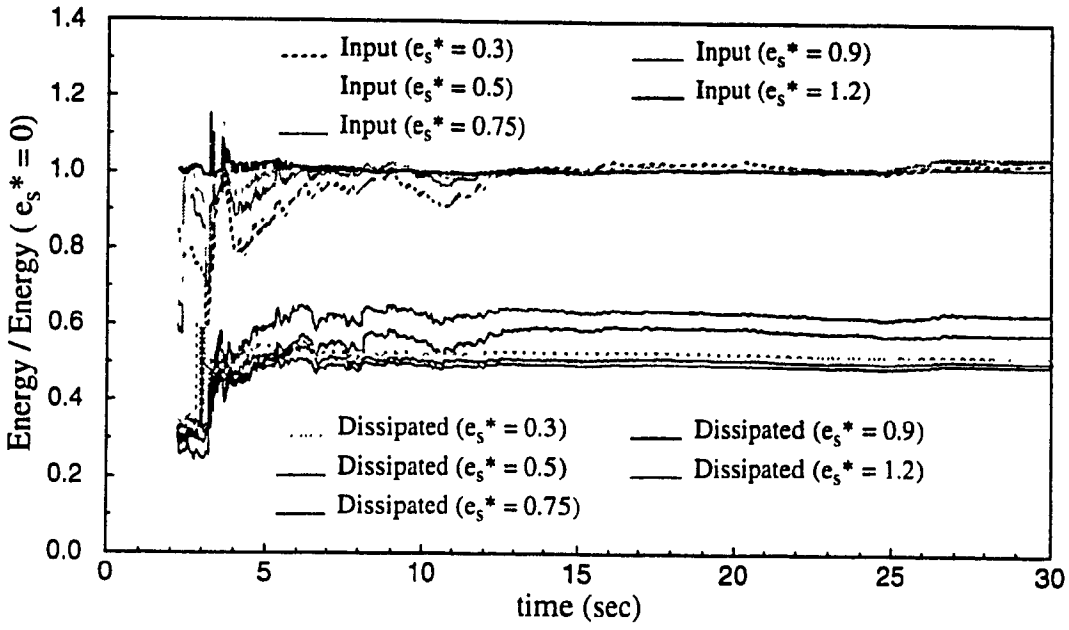

Figure 3.23. Energy curves for strength symmetric model (e_{pf} = 0) normalized with respect to energy input at e_s* =0 for e_{pb} = 0 (No Romania).

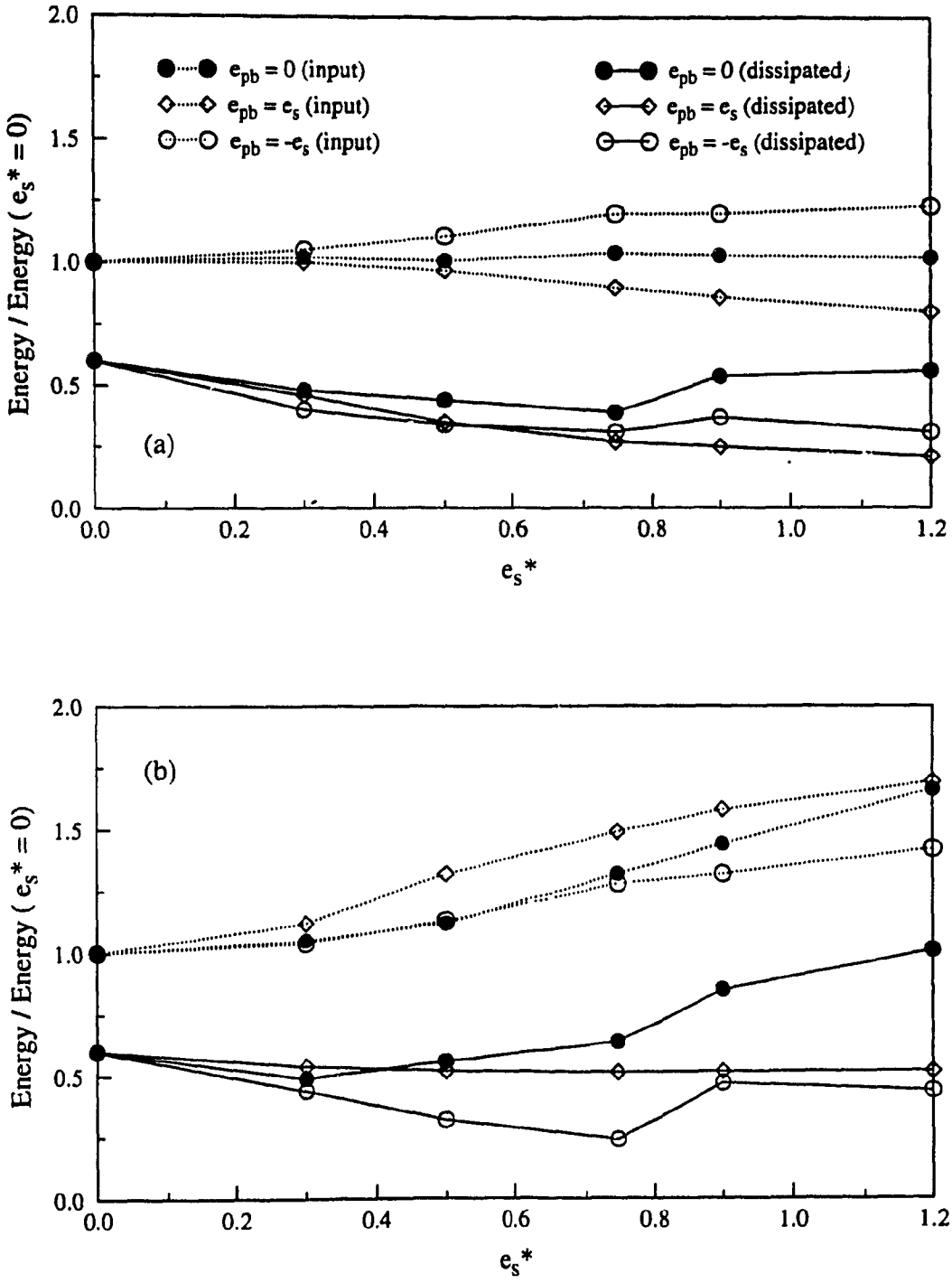

Figure 3.24. Comparison of energy input to structure and dissipated by braces over stiffness eccentricity e_s^* for current design ($e_{pb} = e_s$), suggested design ($e_{pb} = 0$) and optimum slip load eccentricity ($e_{pb} = -e_s$). (a) Romania excitation excluded. (b) Romania excitation included.

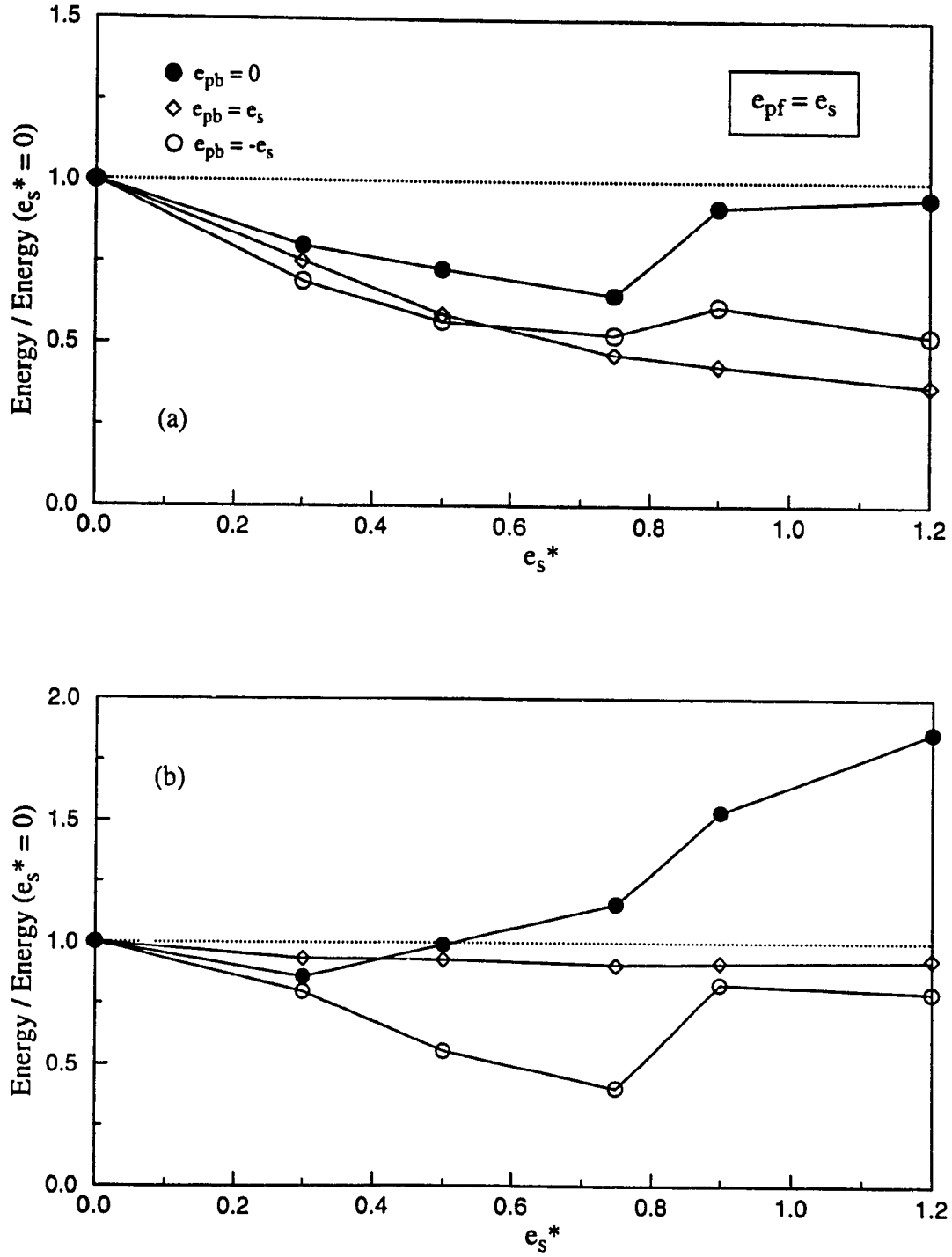

Figure 3.25. Energy dissipated by braces of strength eccentric model ($e_{pf} = e_s$) according to current design ($e_{pb} = e_s$), suggested design ($e_{pb} = 0$), and optimum slip load eccentricity ($e_{pb} = -e_s$). (a) Romania excitation excluded. (b) Romania excitation included.

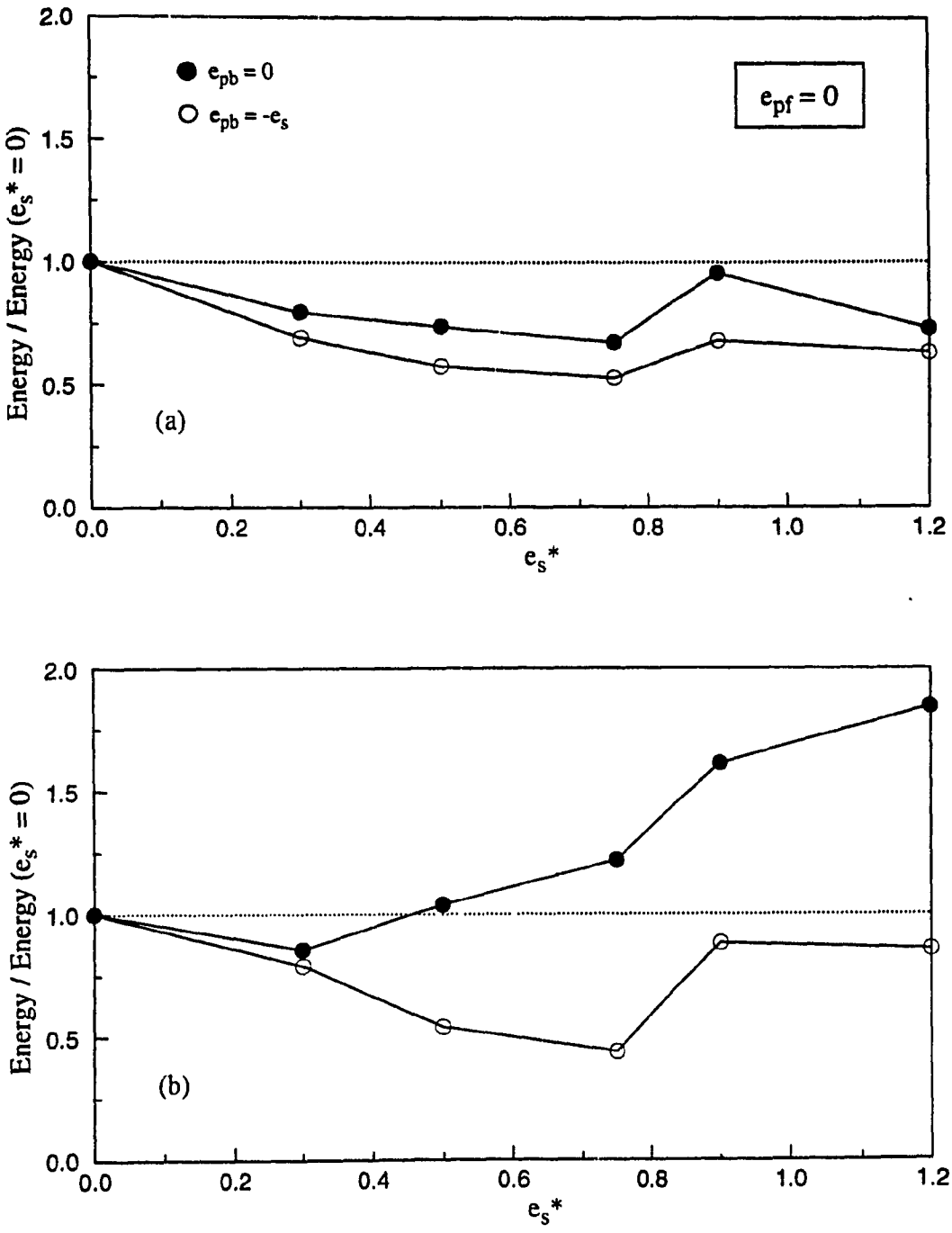

Figure 3.26. Energy dissipated by braces of strength symmetric model (e_{pf} = 0) according to current design (e_{pb} = 0) and optimum slip load eccentricity (e_{pb} = $-e_s$). (a) Romania excitation excluded. (b) Romania excitation included.

CHAPTER 4

RESPONSE OF A THREE DIMENSIONAL STRUCTURE EQUIPPED WITH FRICTION BRACES

4.1 INTRODUCTION

This chapter attempts to evaluate the performance of friction damper equipped braces installed in a prototype structure and tuned in accordance with the results obtained for the one storey, two dimensional models. The prototype structure is the same as that used by Guimond [10] and has been analyzed with the three dimensional dynamic inelastic analysis package DRAIN-Tabs [9]. The earlier study by Guimond focused on the introduction of the friction damped braces into a five storey prototype structure of the Concordia University Library Complex. Since the time of that study, however, the design of the library has undergone several changes and the prototype version is no longer a reflection of the actual library complex. Nevertheless, this prototype structure has been retained for the purpose of comparison.

Guimond introduced tension-compression braces to a reinforced concrete, moment resisting frame structure and undertook the task of tuning them for overall stiffness and slip load according to results of preliminary analyses on single storey models. The process utilized for determining the appropriate slip loads was one of trial and error which ended when a height-wise distribution was found such that each device would slip and participate in the energy dissipation under a given load. In this case, the seismic load used was the first six seconds of the Newmark-Blume-Kapur artificial earthquake scaled to a peak ground acceleration of 0.18g, which is commensurate with a 10 percent in 50 years probability of a severe earthquake in the Montreal area, in accordance with NBCC 1990 (Table J2) [15].

With the optimum slip load determined, the investigation proceeded to determine

the effect that varying the KB / KF ratio would have on maximum edge displacements as well as on ductility ratios and rotations. Reference [10] demonstrated the benefits of KB / KF ratios as low as 0.5 and that ratios of KB / KF = 1.5 could help prevent hinge formation in members even though the structure was subjected to an earthquake of 0.315g. The latter study, however, assumed that all the friction damped braces having the same orientation would have identical structural properties. Also, it neglected the effect that the incorporation of the braces would have on the overall eccentricity of the structure.

The current study adopts the same structural building parameters and height-wise slip load distribution as in the Guimond study and attempts to demonstrate the benefits of redistributing (on a per floor basis) the previously obtained optimum slip loads and stiffnesses of the friction damped braces. It is assumed that modifying the individual brace parameters while maintaining a constant slip load ratio (RB / RF) and stiffness ratio (KB / KF) should help reduce initial eccentricity while improving the overall performance of the tuned structure. For the purpose of comparison, KB / KF ratios of 1.5 and 3.0 have been utilized. Also, in order to investigate the effect of different earthquakes on the findings, four earthquake records have been used and their results averaged. The earthquakes used are the artificial Newmark-Blume-Kapur earthquake, 1940 El Centro N-S, 1952 Taft S69E, and 1977 Bucharest N-S.

4.2 DESCRIPTION OF BUILDING

A plan view of the prototype five storey building is shown in Figure 4.1, which consists of one storey of 5.3 m in height and the remaining four floors at 4.2 m. The building has a length of 36.9 m along the Y-axis and 27.6 m long along the X-axis with columns spaced, approximately, on a 9 m grid. The entire resisting structure is designed as a flat slab, reinforced concrete structure with drop panels. As it can be seen in Figure 4.1, lateral loads acting on the unbraced structure are resisted by 6 frames oriented in the X-

direction (numbered 1 to 6) and 5 frames oriented in the Y-direction (labelled A to E). The design of the building has small eccentricity about the X-axis, and a somewhat larger eccentricity exists for Y-direction excitation due to the presence of Frame B. The choice of bracing Frames 2, 6, and E has small effects on eccentricity for X-direction excitation and a potentially large eccentricity for Y-direction excitation, the latter depending on the magnitude of KB / KF for Frame E.

4.3 STRUCTURAL PROPERTIES OF PROTOTYPE

Elevations of typical frames are shown in Figures 4.2 and 4.3. Each frame is modelled by three types of elements. Truss elements used to represent the friction damped braces are designated as B#. Beam elements used to represent the flat slab are designated as S#. Finally, beam-column elements used to model the column behavior are designated as C#.The total mass of the structure assumed for the analysis was 984 000 kg for each of the floors 1 to 4 and 719 000 kg for the roof. A specific gravity of concrete of 2400 kg/m^3 was used for the calculations [10].

The moment capacity of the beam elements used to model the flat slab is approximately equal to the tributary width of the slab multiplied by 144 kN·m/m. For ease of calculation, the 330 mm thick slab was assumed to have elasto-plastic characteristics. The effective moment of inertia after cracking was assumed to be half that of the gross moment of inertia and is equal to 15.5 x 10^{-4} m^4 per metre of tributary width. Both circular and rectangular columns were used in the prototype. The structural properties of these columns are listed in Table 1. The effective moment of inertia of the columns was assumed to be 75 percent of the gross moment of inertia. Furthermore, a bilinear load-moment interaction diagram for the columns was assumed such that the change in slope occurred at $M_{max} = 1.2M_o$ and $P = 0.6P_o$, where P_o is the crushing load of the column under pure axial load, and M_o is the maximum moment under pure bending. The structural

material properties of the building are as follows: for concrete, $f'c = 40$ MPa, $E_c = 31\ 600$ MPa, and $\nu_c = 0.15$; for steel, $f_y = 300$ MPa, $E_s = 200\ 000$ MPa, and $\nu_s = 0.3$. ν_c and ν_s, respectively, denote the Poisson's ratio for concrete and steel [10].

Table 1: Structural properties of columns in prototype building.

Column Type and Orientation	Storey	Effective Inertia (m^4)	Moment Capacity (kN·m)	Axial Capacity (kN)
Rectangular				
	3 - 4 - 5	14.3×10^{-4}	295	6800
weak direction	2	14.3×10^{-4}	395	7500
	1	14.3×10^{-4}	505	7650
	5	115×10^{-4}	665	7050
strong direction	3 - 4	115×10^{-4}	905	8450
	2	115×10^{-4}	1115	8750
	1	115×10^{-4}	1500	9300
Circular				
	5	47.7×10^{-4}	525	6800
	2 - 3 - 4	47.7×10^{-4}	655	7500
	1	47.7×10^{-4}	725	7650

The steel areas for the braces oriented in the Y-direction have been set to 550, 1100, 1650, 2750, and 4125 mm^2 for storeys 5 to 1 respectively. For braces oriented along the X-direction, the areas used are dependent on the KB / KF ratio chosen and are proportioned according to Table 2:

Table 2: Area distribution for braces.

Storey	Area Used for Braces (mm^2)
5	**A**
4	**2 A**
3	**4 A**
2	**6.667 A**
1	**9.333 A**

where **A** = brace area required for a given KB / KF ratio as determined in Reference [10].

A simplified structural period in the direction of excitation according to NBCC 1990 is given as $T = 0.09\ h_n/\sqrt{D_s}$ for a braced structure, where h_n is the height of the building in metres and D_s is the length of the lateral supporting elements in metres. For a moment resisting frame the period is given as $T = 0.1N$, where N is the number of storeys. Therefore, for a 9 m braced bay, $T_{FDBF} = 0.663$ sec. and for a 5 storey moment resisting frame, $T_{MRF} = 0.5$ sec. [15].

Preference, however, is given to the more refined analysis of NBCC 1985 which uses pseudo-static displacements and the Rayleigh approximation [11]

$$T = 2\pi \left\{ \left(\sum_{i=1}^{n} W_i (\Delta_i)^2 \right) \Big/ \left(g \left[\left(\sum_{i=1}^{n-1} F_i \Delta_i \right) + (F_t + F_n)\, \Delta_n \right] \right) \right\}^{0.5} \qquad (4.1)$$

to determine the structural period. In the above equation, F_i is the force applied at floor i, and Δ_i is the corresponding displacement. W_i is the weight of floor i, and F_t is the portion of the minimum lateral seismic force that is applied at the top of the structure. Using this method, the structural period for Y-direction excitation is calculated as: $T_{FDBF} = 1.115$ sec. and $T_{MRF} = 1.261$ sec. Periods corresponding to X-direction excitations of the braced structure depend on the KB / KF ratio and will be dealt with in a later section. For the

moment resisting frame, T_{MRF} = 1.227 sec.

As mentioned previously, the optimum slip load was determined by a trial and error procedure with load increments of 50 kN. It was also observed that the higher storeys required a slip load reduction. Thus, the total slip load required for the braces used in this study is found in Table 3. Note that this table presents *total* slip loads at each floor for braces oriented along the X-direction and Y-direction instead of the slip loads for the *individual* braces. This is due to the fact that the slip load redistribution will cause changes in the value of the slip load of the individual braces for the direction having multiple plan-wise braces.

Table 3: Optimum slip loads

Storey	in X-direction (kN)	in Y-direction (kN)
5	75	100
4	150	200
3	300	300
2	500	500
1	700	750

4.4 KB / KF RATIO OF THE PROTOTYPE STRUCTURE

Defining the stiffness of a multiple storey structure is a relatively complicated process because of the dependency of the structure on such items as inter-storey shears, edge deflections, center of mass displacements, and center of resistance displacements. The stiffness of the current structure is determined by using the same procedure as that employed in Reference [10]. Pseudo-static forces distributed according to NBCC 1990 act through the center of resistance of each floor, and the stiffness of the structure is subsequently defined as the ratio of the base shear to the displacement of the center of

resistance at the top of the structure [15]. Consequently, the stiffness ratio KB / KF may be calculated according to:

$$KB/KF = \frac{\Delta_{MRF} - \Delta_{FDBF}}{\Delta_{FDBF}} \tag{4.2}$$

For the prototype structure, displacements at the top due to Y-direction pseudo-static forces were found to be 20.4 mm for the MRF structure and 16.5 mm for the FDBF structure, thereby giving KB / KF = 0.25 for the slip loads of Table 3 [10].

Alternatively, if the structural periods for the MRF and FDBF structures are readily available, the KB / KF ratio may be calculated as:

$$KB/KF = (T_{MRF}/T_{FDBF})^2 - 1.0 \tag{4.3}$$

Thus, for T_{MRF} = 1.261 sec. and T_{FDBF} = 1.115 sec., KB / KF = 0.28.

4.5 CENTER OF RESISTANCE

Defining the center of resistance of a multi-storey building is not an easy task. For the one storey structures previously studied, the center of resistance was simply calculated as that unique point along the deck through which a force could be applied which would cause all resisting frames oriented in the direction of the force to move simultaneously, without causing rotation to the deck. Wall-frame interaction, as well as brace-frame interaction, in multi-storey buildings has somewhat complicated this definition of center of resistance. Humar defined the center of rigidity of a floor as that point through which the resultant lateral force acting at that level causes no rotation of the floor, although other floors may rotate [12]. Cheung and Tso defined the center of rigidity of a multi-storey structure as the locus of points from each floor such that a given distribution of forces passing through them causes no rotation of the structure about a vertical axis [23]. Although there is no clear consensus on the matter, researchers have recognized that

buildings with identical floor plans will have differing centers of resistance depending on the floor level being considered, as well as the point of application of the lateral loads.

This study utilizes a simplified procedure which combines the above definitions of center of resistance [10]. An elastic, three-dimensional computer analysis is used whereby a horizontal torque couple is applied at a floor level in order to determine the point through which rotation occurs for that level. This process is repeated for each of the five floors of the prototype and for each of the two cases considered (MRF and FDBF). The center of rigidity of the entire building is then defined as the locus of these points.

4.6 DISCUSSION OF RESULTS

The analysis consisted of subjecting the prototype structure to the first 6 seconds of an ensemble of earthquakes consisting of the Newmark-Blume-Kapur artificial excitation, 1940 El Centro N-S excitation, 1952 Taft S69E, and 1977 Bucharest N-S earthquakes. The analysis was performed using the computer program DRAIN-Tabs, running on a 4/670 Sun Microsystems computer. The 6 seconds time limit was imposed primarily to reduce computer costs since each run of the ensemble of excitations required 3600 sec of CPU time. Figure 4.4 shows the earthquake time histories for each of the excitations considered. Since many large magnitude accelerations occur within the first six seconds, the assumption is made that the results obtained will still be valid. Also, to ease energy calculations, no structural damping is specified. The time step used for the analyses is 0.01 seconds. In order to obtain an average result for the ensemble of earthquakes, a normalization procedure was employed whereby each earthquake in the ensemble was scaled so as to produce identical base shears in the direction of the excitation. For the purpose of verifying the procedure used, the Newmark-Blume-Kapur excitation of Reference [10], scaled to 0.36g, was used, with the other excitations scaled so as to produce the same base shear for each slip load and stiffness distribution.

The building was analyzed for X-direction excitation and assuming a shift in the center of mass from the geometric centroid of $-0.35D_n$ along the Y-axis, thereby creating a large eccentricity for X-direction excitations. Results obtained allow for a comparison of the structural behavior for three slip load and stiffness distributions. Setting the cross-sectional areas of the braces oriented along the X-axis equal to those oriented along the Y-axis leads to an initial KB / KF ratio of approximately 0.5 for X-direction excitations. Any modification of KB / KF from this initial setting requires only a proportional modification of the cross-sectional area of the friction damped braces.

4.7 KB / KF USED IN STUDY

The next logical step in the design process requires the determination of a reasonable value of KB / KF that may be applied to the prototype structure. The results of References [3] and [10] suggest that KB / KF > 7 is necessary to maintain the response below that of the unbraced symmetric structure for structures having large eccentricities ($e_s^* > 0.75$). Expanding on the results obtained in Chapter 3, it would be ideal if KB / KF = 10 could be provided. Using the pseudo-static force distribution method described earlier to determine the stiffness of the braced structure subjected to X-direction loading, curves relating the brace area required and the associated displacement to the KB / KF ratio may be created. Figures 4.5 and 4.6 show that there exists a logarithmic relation between brace area and KB / KF and displacement and KB / KF.

Two important conclusions are obtained from these graphs. First, Figure 4.5 stops at 40 times the brace area required for KB / KF = 0.5, with a resulting KB / KF ratio of only 3.6. This, combined with the exponential growth of the curve indicates that the stiffness ratio cannot realistically be set to 10, and that a revised (lower) ratio will be necessary for the structure. An analysis was done with braces having 10,000 times the area required for KB / KF = 0.5 and the resulting stiffness ratio was only 4.5. Second, Figure

4.6 shows that for KB / KF > 3.0 there is relatively no improvement in the response of the structure with increase in brace area. Consequently, the largest realistic stiffness ratio that may be attained for this structure is assumed to be KB / KF = 3.0. This may be achieved with a twenty-fold increase of the brace areas provided for KB / KF = 0.5.

4.7.1 Results of 1-Storey Model for KB / KF = 3.0

Since KB / KF = 10 cannot be achieved, part of the analysis conducted in Chapter 3 is repeated to verify that $e_{pb} = -e_s$ and $e_{pb} = 0$ still provide the best responses for the single storey structure having $e_{pf} = e_s$ and KB / KF = 3.0 (i.e. the single storey representation of the prototype structure).

Using the same procedure as that employed in Phase I of Chapter 3 to determine the response of the model with varying slip load distribution, graphs similar to those of Figure 3.2 for $e_{pf} = e_s$ were generated for the range of eccentricities considered (Figures 4.7 (a) to (f)). As expected, the lower value of KB / KF = 3.0 gives normalized displacements that are higher than those obtained for KB / KF = 10, but the general behavior of the model is still the same as that predicted by Figure 3.2. Figure 4.7 shows that the optimum response still occurs at $e_{pb} = -e_s$. Figure 4.8 compares the normalized response of the three possible design cases considered. Figure 4.8(a) compares the current design approach ($e_{pb} = e_s$) to the optimum observed response ($e_{pb} = -e_s$) for the range of eccentricities investigated. It is seen that redistributing the slip load according to $e_{pb} = -e_s$ reduces the expected response to a level below that of the unbraced symmetric structure, just as in Figure 3.3 for KB / KF = 10. Using the simplified design of $e_{sb} = 0$, Figure 4.8(b) shows that the response can still be maintained below that of the unbraced symmetric structure for eccentricities as large as $e_s^* = 0.9$. At large eccentricities, $e_{pb} = 0$ reduces the response by 42 percent that of $e_{pb} = e_s$ (compared to 55 percent for $e_{pb} = -e_s$), thereby implying that the suggested design approach ($e_{pb} = 0$) of Chapter 3 is still valid in significantly reducing the expected structural response, even though KB / KF has been

considerably reduced.

Figure 4.9 shows the ductility requirements for the two resisting frames of the model and for the three design options investigated. Again, comparison of the results for KB / KF = 3.0 to those of KB / KF = 10 show a close correlation in the behaviors. Although the ductility demands are expectably higher for KB / KF = 3.0, the reductions obtained from $e_{pb} = 0$ and $e_{pb} = -e_s$ over $e_{pb} = e_s$ are comparable to those observed in Figure 3.4. What is encouraging is that even for eccentricities as large as $e_s^* = 1.0$, the suggested design distribution ($e_{pb} = 0$) is still able to maintain the ductility demand of the flexible side (Figure 4.9(b)) below that of the unbraced symmetric structure.

Finally, Figure 4.10 presents a comparison of the energy dissipated by the braces for the current design approach ($e_{pb} = e_s$) and the suggested design ($e_{pb} = 0$). These values have been normalized by the energy dissipated by the braces of the symmetric structure. The most important observation to be noted is that the $e_{pb} = 0$ design approach not only reduces the expected displacements and ductilities below that of $e_{pb} = e_s$, but it also significantly increases the participation of the braces in dissipating energy. The modified slip load distribution is expected to cause the braces to dissipate twice the energy that the current design approach permits, just as it did for KB / KF = 10 (compare Figure 4.10(a) to Figure 3.25(a)). Also of note, the presence of the Romania excitation affects the results to a lesser degree than it did for KB / KF = 10.

The analytical procedure of Chapter 3 has been used on a single storey model having the same stiffness ratio as that which will be applied to the prototype structure. It has been demonstrated that the behavior of the structure with KB / KF = 3.0 reflects that of KB / KF = 10 and that for a prototype structure having $e = -0.35D_n$ ($e_s^* = 1.0$), further reductions in the neighborhood of 30 percent over those of $e_{pb} = e_s$ can be expected for both displacements and maximum ductility demand by simply changing the slip load distribution to $e_{pb} = 0$. The above shortened analysis thereby generalizes the results obtained in Chapter 3 and also serves as a reference for the expected improvements of the

prototype structure having KB / KF = 3.0.

For sake of comparison, two stiffness ratios are employed, namely, KB / KF = 1.5 and KB / KF = 3.0. This is done to illustrate the difference between the structure studied in Reference [10] and the same structure with the stiffness ratio increased to its maximum realistic value.

4.8 X-DIRECTION EXCITATION

4.8.1 Periods Corresponding to Change in KB / KF

As noted previously, the structural period and KB / KF ratio are interdependent in accordance with equation (4.2). Since the focus of this study is on the behavior of the prototype structure when subjected to X-direction excitations, the period of the structure in this direction will vary according to the predetermined KB / KF ratio. As noted earlier, braces oriented in the Y-direction have been preset to those slip loads deemed optimum by the study of Reference [10]. Hence, the period and KB / KF ratio is fixed for this direction. There is no intention to modify the braces oriented along the Y-direction since these are concentrated in a single frame and offer no possibility of redistributing the slip load or stiffness as do the braces oriented along the X-direction.

As initially designed, the X-direction braces had minimum possible areas, with the value of A, to be used in accordance with Table 2, equal to 412.5 mm^2. Correspondingly, braces oriented along the X-axis have areas equal to 3850, 2750, 1650, 825, and 412.5 mm^2 for storeys 1 - 5, respectively [10]. Given these areas, application of equation (4.1) gives periods for the X-direction of: T_{FDBF} = 0.998 sec. and T_{MRF} = 1.227 sec. Employing equation (4.3) yields KB / KF $\approx$ 0.5. Applying a fourfold increase in the areas of the braces augments this ratio to KB / KF $\approx$ 1.5 and causes the period of the braced structure to become T_{FDBF} = 0.774 seconds, while a twenty-fold increase in the areas gives KB / KF = 3.0 and T_{FDBF} = 0.614 seconds. T_{MRF} remains unchanged.

4.8.2 Structures Considered

Three prototype variants were subjected to X-direction excitations: the 'current design' prototype used in the Guimond study; a 'suggested design' prototype in which the slip load distribution between the braces is altered according to $e_{pb} = 0$, but the stiffness distribution between the braces remains unchanged; and an 'alternative design' in which both the slip load and the stiffness distribution is changed according to $e_{pb} = 0$ and $e_{sb} = 0$.

4.8.3 Distribution of Slip Loads Among Resisting Braces

Many variations in slip load distributions were considered in the study of the simple one storey models. At the conclusion of that study, two particular distributions were retained: one in which the center of strength of the braces coincided with the center of mass of the structure ($e_{pb} = 0$); and the other in which the center of strength of the braces was located on the opposite side of the center of stiffness of the unbraced structure ($e_{pb} = -e_{sf}$). The first ($e_{pb} = 0$) merited consideration because of its ease of application in the design office since it only requires the determination of the center of mass in order to distribute the slip loads. The second ($e_{pb} = -e_{sf}$) merited consideration because it provided the lowest observed displacements for the single storey model. The problem with this distribution, however, is that it requires the knowledge of the location of the center of resistance of each floor in order to distribute the slip loads correctly. Given that the procedure necessary to determine this location is already a disputed topic [12, 23], the employment of a slip load distribution based on the center of resistance is not practical. Hence, structures designated as 'suggested design' ($e_{pb} = 0$) and 'alternative design' ($e_{pb} = 0$, $e_{sb} = 0$) have slip load distributions such that the center of strength of the braces for each floor coincides with the location of the center of mass of the floor slab being supported.

4.8.4 Distribution of KB / KF Among Resisting Braces

Some variations of the stiffness distribution between fiction damped braces were also considered in Chapter 3 once an optimum slip load distribution had been determined. It was evident that the most effective scheme for installing the braces involved the minimization of their effect on the initial stiffness eccentricity of the structure. To this end, two possible distributions were retained: the center of stiffness of the friction damped braces should either coincide with the center of mass of the unbraced structure ($e_{sb} = 0$), or, the center of stiffness of the friction damped braces should be located at $e_{sb} = -e_{sf} / 2$. For $e_{sb} = 0$, ease of implementation is a practical design asset. For $e_{sb} = -e_{sf} / 2$, the responses obtained were the lowest. In contrast to the slip load where the choice of distribution hinged on the ability to locate the center of resistance, for stiffness, the choice is much clearer. For the 'alternative design', distributing the stiffness of the friction damped braces according to $e_{sb} = 0$ was noted to lead to a difference in response between $e_{sb} = 0$ and $e_{sb} = -e_{sf} / 2$ which is less than five percent. Bearing in mind that modification of the stiffness distribution between braces alters the overall behavior of the structure in the elastic region, the results include the 'alternative design' only as a comparative alternative, not as a realistic design option.

4.8.5 Edge Displacements

The uncertainty of the direction of an earthquake excitation forces the designer to assume that it will be directed along the worst possible orientation of the building considered. This, in practice, means that the building needs to be analyzed in the two orthogonal directions which match its principal axes. This study, however, only investigates the effects of earthquake excitations oriented along the structure's X-axis. As mentioned previously, excitations along the Y-direction have been neglected because the purpose of this investigation is to study the effects of changing the distribution of slip load

and stiffness between the FDBF. The presence of a single brace oriented along the Y-direction prohibits any such investigation.

4.8.5.1 Structures with CM @ -0.35 D_n

Since the main function of the prototype structure was to house the new Concordia University Library, consideration was given to the effect that the shelved books may have on the eccentricity of the structure. Given that books are usually stacked in one area with study spaces located in another, this imposes a non-uniform distribution of mass on the structure, thereby creating an eccentricity between the center of mass and center of resistance of each floor. Assuming that the live load (7.2 kN/m^2) is placed on the lower half of the floor plan, this creates an eccentricity along the Y-axis of approximately -0.08D_n. In addition, if there are variations in strength of the members due to construction which causes an additional eccentricity of -0.10D_n, it becomes possible to encounter an accidental eccentricity along the Y-axis of -0.18D_n. This corresponds to a structure having a medium eccentricity of e* = 0.5. Reference [10] considered the effects of eccentricity e* = 0.75 for Y-direction excitations with favorable results, and an X-direction case with e = -0.35D_n was reported in reference [3]. Although the design of Figure 4.1 leads to the small eccentricities shown in Figure 4.11, the current study considers only e = -0.35D_n in the Y-direction. This corresponds to $e_{sf}^* \approx 1.0$ for the MRF, which represents an extreme eccentricity for the one storey model.

Figures 4.12(a) and 4.12(b) depict the response for KB / KF = 1.5. Installation of braces having equal properties in Frames 2 and 6, as per the 'current design' procedure, results in a decrease of stiff side displacements of up to 45 percent over those of the MRF structure (Figure 4.12(a)). Top displacement on the flexible side is reduced by 17 percent (Figure 4.12(b)). The rotations of the 'current design' distribution are also substantially lower than those of the MRF structure, as indicated by Figure 4.13. The reduction in this case is approximately 20 percent (from 0.0058 rad. to 0.0047 rad.).

Modifying the slip load distribution so that the center of strength of the braces is also located at $-0.35D_n$ ($e_{pb} = 0$ in Figures 4.12 and 4.13) increases the stiff side displacements over those of the current design by 36 percent. On the other hand, flexible side displacements show a 15 percent reduction in top storey displacement as compared to the 'current design' response. This represents a 30 percent improvement over the original response of the MRF structure (Figure 4.12(b)). This reduction of flexible side displacements is also reflected in the rotational response of the $e_{pb} = 0$ configuration. Rotations are reduced by 16 percent (from 0.0047 to 0.0040) when compared to the 'current design' values obtained (Figure 4.13).

Completing the tuning process by distributing the stiffness of the FDBF symmetrically about the center of mass of the structure ($e_{pb} = 0$, $e_{sb} = 0$) produces little improvement over the results obtained with the 'suggested design' configuration ($e_{pb} = 0$). For this case, the responses of Frame 1 and Frame 6 are virtually identical to those obtained with the $e_{pb} = 0$ distribution where only slip load was considered. Also, given that the displacements are not much different from those of $e_{pb} = 0$, it follows that the observed rotations obtained with the alternative design ($e_{pb} = 0$, $e_{sb} = 0$) are also similar to those of the suggested design ($e_{pb} = 0$).

Increasing KB / KF to 3.0 has the expected improvement in behavior. First, there is a model-wide reduction in response compared to KB / KF = 1.5. Figures 4.14 and 4.15 show the results obtained for the 'current design', 'suggested design', and 'alternative design' compared to those of MRF. Incorporating the braces according to 'current design' philosophy shows a reduction of top storey displacements of 52 percent and 20 percent for Frames 1 and 6, respectively (Figures 4.14(a) and 4.14(b)), over those obtained for the MRF structure. This is only a 3 to 7 percent improvement over the same responses obtained for KB / KF = 1.5. Changing the slip load distribution of the braces according to $e_{pb} = 0$ causes the structure to behave in a similar manner as for KB / KF = 1.5. Here, stiff side displacements increase by 48 percent when compared to the 'current design' response

(up from 36 percent for KB / KF = 1.5), and flexible side displacements are reduced by 23 percent (compared to 15 percent for KB / KF = 1.5). Further distribution of the stiffness (e_{pb} = 0, e_{sb} =0) causes no significant change in the response of Frames 1 and 6 when compared to the 'current design' (same behavior as for KB / KF = 1.5).

Figure 4.15 shows that the increase of KB / KF to 3.0 for the 'current design' prototype reduces the expected rotations of the structure by 25 percent from 0.0058 rad. to 0.0043 rad. Redistribution of properties according to the 'suggested design' (e_{pb} = 0) and the 'alternative design' (e_{pb} = 0, e_{sb} = 0) give identical results with additional reductions over those of the 'current design' by approximately 13 percent. Overall, the e_{pb} = 0 distribution causes a reduction in rotation of 35 percent for KB / KF = 3.0 (compared to 31 percent for KB / KF = 1.5) when compared to the unbraced MRF structure.

In contrast to the analysis of the one storey structure of Chapter 3 and the three dimensional analysis for KB / KF = 1.5 where redistribution of the slip load and stiffness was reflected by a progressive improvement of the structural response and rotation between the 'suggested design' and 'alternative design' prototypes, such a trend has not manifested itself for KB / KF = 3.0. Here, the 'alternative design' (e_{pb} = 0, e_{sb} = 0) has not been effective in further reducing the response (displacements and rotations) obtained from the simple slip load adjustment of e_{pb} = 0. What this analysis has also revealed is the closeness of the results obtained between KB / KF = 1.5 and KB / KF = 3.0. Although doubled in magnitude, the important increase in stiffness ratio was not reflected by an equally important reduction in response. The responses obtained for KB / KF = 3.0 were only 10 percent lower than those obtained for KB / KF = 1.5. This may suggest a more intimate relationship between KB / KF and the response of the structure than that depicted in Figure 4.6. Comparison of the improvement of the maximum edge displacements of the prototype structure to those of the single storey model (Figures 4.14(b) and 4.8(b)) shows that a good correlation exists. For e_s^* = 1.0 and e_{pb} = 0, Figure 4.8(b) shows a 35 percent reduction in maximum edge response over those of $e_{pb} = e_s$. Meanwhile, Figure 4.14(b)

shows an improvement of 23 percent for the same case.

4.8.6 Ductility Demands

The ductility demand of a structure is a measure of that structure's ability to deform inelastically without collapsing. For simple structures it is measured as a ratio of the total lateral displacement to the yield displacement of the structure. The ductility demand for a beam element, μ, is defined as the ratio of the end moment, M, to the plastic moment capacity, M_p, of that member [18]. If the member is stressed into the plastic region, then the ductility demand is defined as one plus the ratio of maximum plastic hinge rotation, $|\theta|_{max}$, to the yield rotation for a beam with equal end rotations and no transverse displacements. This can be expressed as [18]:

$$\mu = \left|\frac{M}{M_p}\right| \qquad \text{if } |M| < M_p, \tag{4.4}$$

or,

$$\mu = 1.0 + \frac{6|\theta|_{max} EI}{LM_p} \qquad \text{if } |M| = M_p, \tag{4.5}$$

where E = Young's modulus, I = moment of inertia of the beam, and L = length of the beam. The ductility demand for the column elements is defined in the same manner as that of the beams except that a modified plastic moment, M_{mp}, is considered instead of M_p to account for the strain introduced by the axial load. M_{mp} is defined as

$$M_{mp} = M_p \qquad \text{if } |P| < 0.15\, P_y, \tag{4.6}$$

and,

$$M_{mp} = 1.18\,(1 - |P|/P_y)\, M_p \quad \text{if } |P| \geq 0.15\, P_y, \tag{4.7}$$

where P = column axial load and P_y = member axial yield load [18]. Since there are

numerous resisting elements within the structure, each with a specific ductility limit, it becomes important to determine the maximum, or peak, ductility demand for a given excitation.

Figure 4.16(a) shows the ductility demand for the 'current design', 'suggested design', 'alternative design', and MRF structures when subjected to the ensemble of excitations for KB / KF = 1.5 and an eccentricity of $e = -0.35D_n$. Figure 4.16(b) omits the curve for MRF. Both these figures show that modifying the distribution of slip load and stiffness among the FDBF has a comparable effect on the ductility demand of the structure as it did on the displacements of the structure. Regardless of the distribution utilized, improvements of 30 to 45 percent over the MRF structure can be expected. Adjusting the slip load distribution according to $e_{pb} = 0$ has the effect of reducing the flexible side ductility demand (Frame 6) to 3.1, a reduction of 15 percent that expected from the 'current design' distribution of the braces. Making the center of stiffness of the braces coincident with the center of mass of the structure ($e_{pb} = 0$, $e_{sb} = 0$) further reduces the ductility demand of Frame 6 to 2.7, which represents a 24 percent decrease in demand when compared to the 'current design'. A consequence of the tuning process, however, is that the ductility demand of the stiff side (Frame 1) shows an increase to 1.25 (up from 0.75 for the 'current design' distribution).

Increasing KB / KF to 3.0 in Figure 4.17 further reduces the ductility demand of the 'current design' distribution by 10 percent (from 3.5 to 3.1). What is significant, however, is that increasing KB / KF to 3.0 causes the slip load changes to be more important than for a stiffness ratio of 1.5. In this case, the $e_{pb} = 0$ distribution reduces the ductility demand of the flexible side by 22 percent that of the 'current design' (compared to 15 percent for KB / KF = 1.5). Further adjustment of the braces according to $e_{pb} = 0$, $e_{sb} = 0$ has no effect on the braces, thereby confirming that for real structures having a reasonable KB / KF ratio, modification of the slip load distribution is sufficient to promote better response, and stiffness redistribution becomes unnecessary. This is in partial

contrast to the results obtained for the single storey structure which predicted that $e_{pb} = 0$ would reduce the displacements and ductility by approximately 35 percent (Figure 4.9 for $e_s^* = 1.0$) that of $e_{pb} = e_s$, compared to 22 percent for the prototype structure, while $e_{pb} = 0$, $e_{sb} = 0$ should have further reduced ductility and displacement by half that experienced at $e_{pb} = 0$ (Figures 3.12(a) and 3.13(b)). Instead, no further improvement was detected. Despite the lack of further improvement, for KB / KF = 3.0 and $e_{pb} = 0$ the ductility demand of the prototype is expected to be half that of the unbraced MRF structure, and Frames 1 through 5 are expected to remain near or below the elastic limit.

As a final illustration of the benefits obtained by redistributing the slip load between the braced frames, one may consider the plastic hinge formation within the structure. Figures 4.18 and 4.19 depict the hinge formation for the 'current design' approach and the refined $e_{pb} = 0$ design for the structure subjected to the Newmark-Blume-Kapur artificial earthquake and having KB / KF = 3.0. As shown in Figure 4.17, frames 4, 5, and 6 exhibit plastic hinging under the 'current design', while only frame 6 is subjected to hinging when $e_{pb} = 0$. In total, the 'current design' leads to 75 plastic hinges compared to 30 hinges for the $e_{pb} = 0$ case.

The results described above show that the tuning process employed reduces the ductility demand of the 'current design' distribution. At higher stiffness ratios, slip load redistribution is sufficient to reduce the ductility demand of the flexible side by half that of MRF, and further tuning with respect to stiffness is unnecessary.

4.8.7 Energy Requirements

Assuming that sufficient structural ductility is present, practical aseismic design of structures allows for large inelastic deformations of resisting members. Most of the energy causing these deformations is absorbed by the structure in the form of plastic displacements, with little contribution from the elastic strain potential of the elements. Adding friction braces to a structure diverts to the braces the excess energy, that would

otherwise cause plastic deformations, where it is absorbed and dissipated as heat.

Because of the assumed elastoplastic behavior of the beams and columns, the inelastic energy for an unbraced MRF structure may be calculated as the summation of the product of the moment capacity and accumulated plastic rotations of each of the resisting members. The energy absorbed by the friction braces is simply calculated as the summation of the product of the slip load of each brace and its slip displacement. In the case of the FDBF structures, if members yield the inelastic energy of these members adds to that of the braces. If no members yield, the total energy absorbed by the structure is represented by the summation of the brace energies.

Figures 4.20 and 4.21 depict the energy dissipated by the brace equipped prototype. The inelastic energy absorbed by the unbraced moment resisting frame is included, although it is not the intent of this report to demonstrate the capability of the FDBF to absorb more energy than the MRF, but rather, the goal is to compare the redistribution effects represented by the 'suggested design' ($e_{pb} = 0$) and 'alternative design' ($e_{pb} = 0$, $e_{sb} = 0$) to those of the 'current design'.

Figure 4.20 shows the inelastic energy dissipated for KB / KF = 1.5. The total energy dissipated by the 'current design' is 956.5 kN·m, whereas it is 1009 kN·m for the 'suggested design' and 1026 kN·m for the 'alternative design'. Figure 4.21 shows the inelastic energy absorbed by the structure when KB / KF is increased to 3.0. In this case, the energy absorbed by the 'current design' is 1650 kN·m, which is 1.73 times that of the same arrangement for KB / KF = 1.5. The 'suggested design' and 'alternative design' configurations dissipate approximately the same amount as they did when KB / KF = 1.5 (1080 kN·m and 1050 kN·m compared to 1009 kN·m and 1026 kN·m).

Ignoring the large discrepancy in the dissipation of the 'current design' configuration, several observations can be made from the behavior of the 'suggested design' and 'alternative design' structures. First, the notion of greater importance of the slip load distribution over that of the stiffness distribution as depicted by Figures 4.12 to

4.17 is further supported by Figures 4.20 and 4.21 since in each, the 'suggested design' ($e_{pb} = 0$) dissipates as much energy as the 'alternative design' ($e_{pb} = 0$, $e_{sb} = 0$). Second, given that the modified braces for both KB / KF = 1.5 and KB / KF = 3.0 dissipate similar amounts of energy, just as the displacements and ductility ratios were similar despite the doubling of KB / KF, this further suggests that there exists an optimum limit to KB / KF for each structure considered.

The question of large energy dissipation for the 'current design' distribution having KB / KF = 3.0 requires some clarification. Analysis of the computer output reveals that the energy dissipated by the braces in Frame 6 (flexible side) is similar for all brace slip load and stiffness distributions considered. Differences stem from the energy dissipation of braces on the stiff side (Frame 2). For KB / KF = 3.0, the 'current design' distribution demonstrates an increase in the frequency of plastic slips in the braces of Frame 2, although maximum slip displacements are similar to those obtained for $e_{pb} = 0$ and $e_{pb} = 0$, $e_{sb} = 0$. Therefore, braces in Frame 2 (stiff side) having the 'current design' distribution are dissipating more energy because they are experiencing more slips than other brace arrangements, and not because they are experiencing larger slip displacements.

Comparison of the energy dissipation for the multi-storey structure to that of the single storey models seems to yield conflicting results. Redistribution of the brace slip loads such that $e_{pb} = 0$ shows a significant increase in the absorption capacity of the single storey model (Figure 4.10), while that of the multi-storey model shows a minor increase when KB / KF = 1.5 and a significant decrease when KB / KF = 3.0 (Figures 4.20 and 4.21). Closer examination of the computer outputs reveals that the frames of the single storey models are undergoing larger plastic deformations under the 'current design' brace distribution than those of the multi-storey structure. Redistribution of the slip loads such that $e_{pb} = 0$ converts the hinging in the frames to slip displacements of the braces, thereby causing the friction braces to dissipate more energy. In the five storey structure, the frames

exhibit little plastic hinging when the braces are introduced according to the 'current design'. Redistribution of the slip loads reduces the plastic hinging in the frame members, or simply reduces the number of slip episodes experienced by the friction devices.

4.9 SUMMARY

The study conducted in this chapter evaluated the benefits of modifying the slip load and stiffness distribution of FDBF's already incorporated into an early version of a prototype structure for the Concordia University Library [10]. Two cases having a large eccentricity caused by a shift in the center of mass by $-0.35D_n$ along the Y-axis were studied, namely, KB / KF = 1.5 and KB / KF = 3.0.

Although Reference [3] recommends using KB / KF values larger than seven to reduce the response of highly eccentric structures ($e_s^* > 0.75$) below that of similar symmetric structures, this limit has been demonstrated to be unrealistic for real 3-D structures. For the structure considered, the practical limit was found to be KB / KF = 3.0.

Repeating the Phase I analysis of Chapter 3 for this lower value of KB / KF has confirmed that redistributing the slip load according to $e_{pb} = -e_s$ provides the best response for the structure, while $e_{pb} = 0$ is still an excellent design alternative, as it was for KB / KF = 10.

Analysis of the three dimensional structure with KB / KF = 3.0 shows that the single storey model adequately predicts improvements in response and ductility demand due to changes in slip load distribution for $e_{pf} = e_s$ and $e_s^* = 1.0$ (35 percent reduction for the single storey model versus 23 percent for the prototype structure). While displacements and rotations are unaffected by a redistribution of stiffness according to $e_{sb} = 0$ for either KB / KF = 1.5 or KB / KF = 3.0, ductility demands are further reduced for $e_{sb} = 0$ for KB / KF = 1.5 as expected from Chapter 3, but no improvement was recorded for KB / KF = 3.0. Slip load redistribution ($e_{pb} = 0$) for KB / KF = 3.0 is expected to

reduce the ductility demand of the 'current design' by 20 percent.

Comparison of the results of KB / KF = 1.5 to those of KB / KF = 3.0 show that there is only a 10 percent difference in response values, even though KB / KF has been doubled. This may indicate a more profound relationship between KB / KF and the structural response than that depicted in this study and in References [3] and [10]. More research is necessary to address this question.

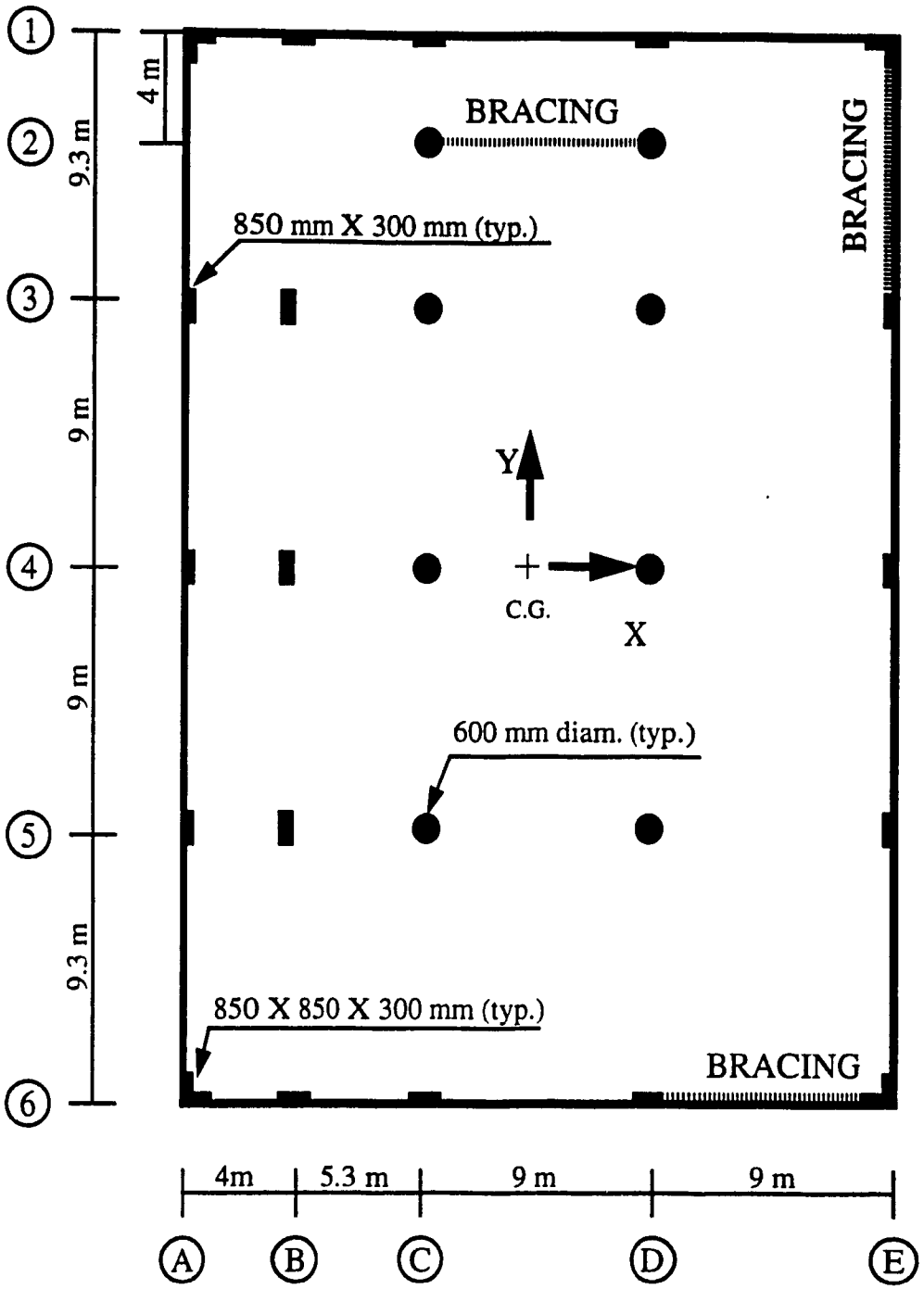

Figure 4.1. Floor plan of 5-storey prototype building.

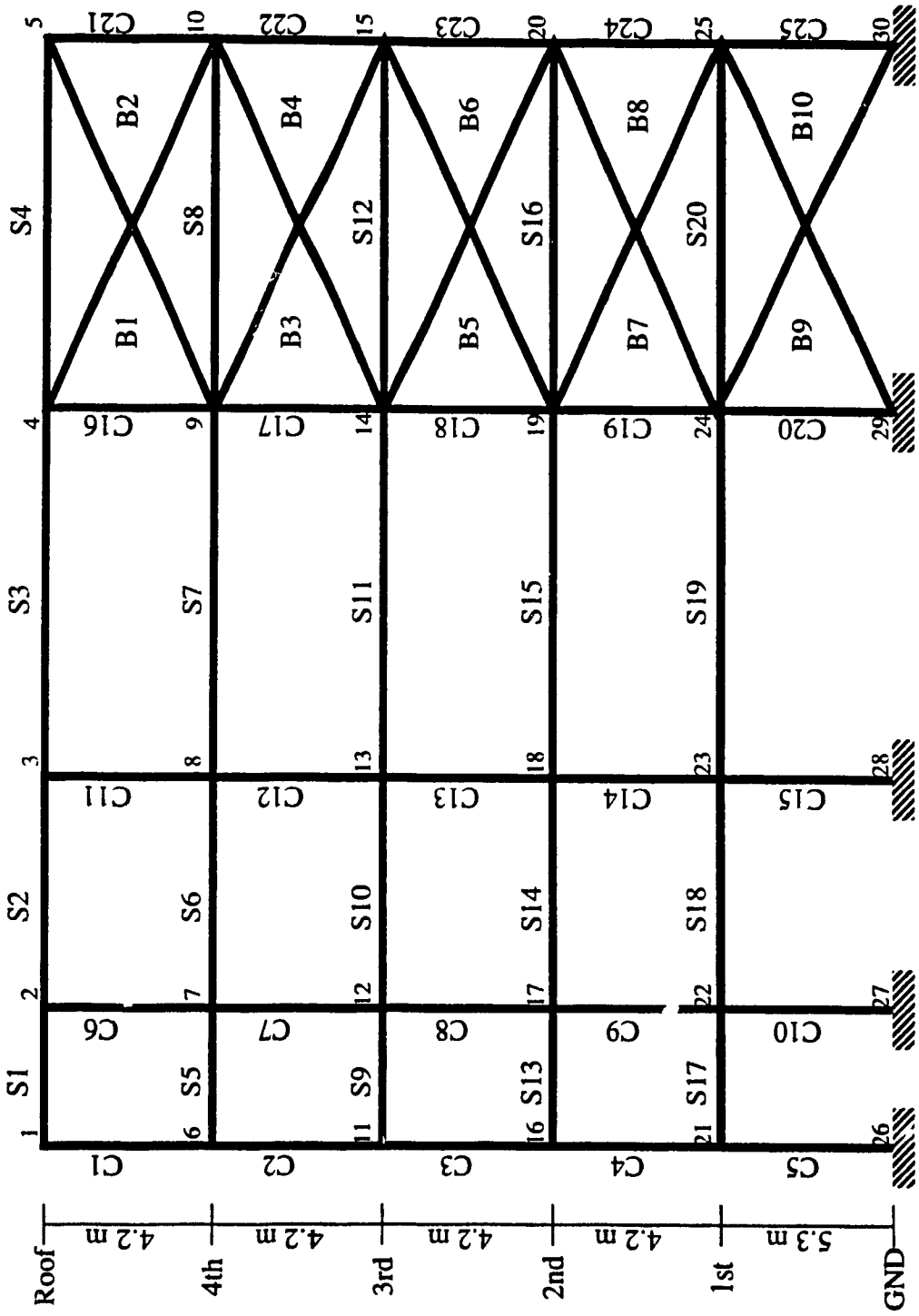

Figure 4.2. Elevation of frame 6.

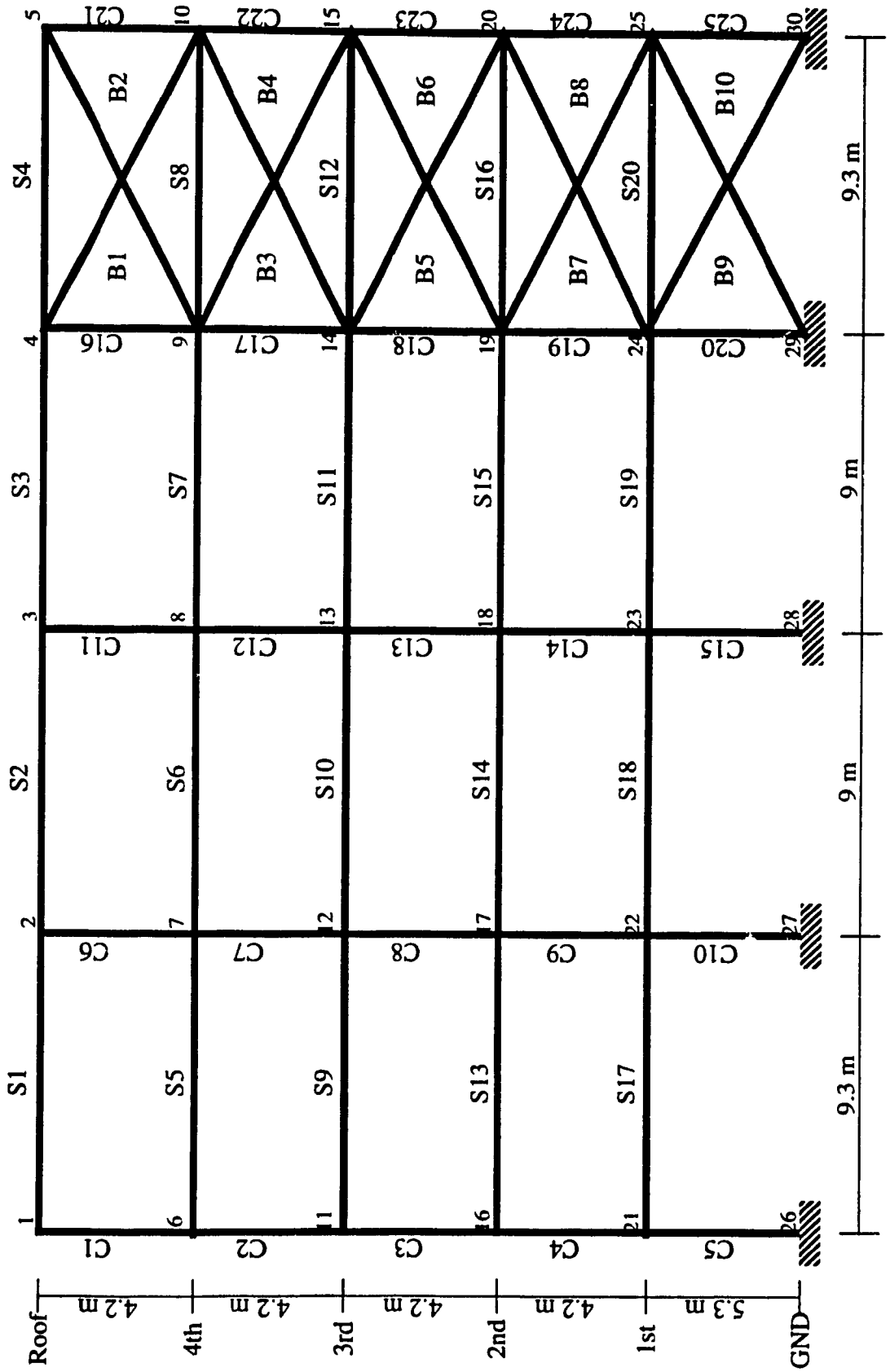

Figure 4.3. Elevation of frame E.

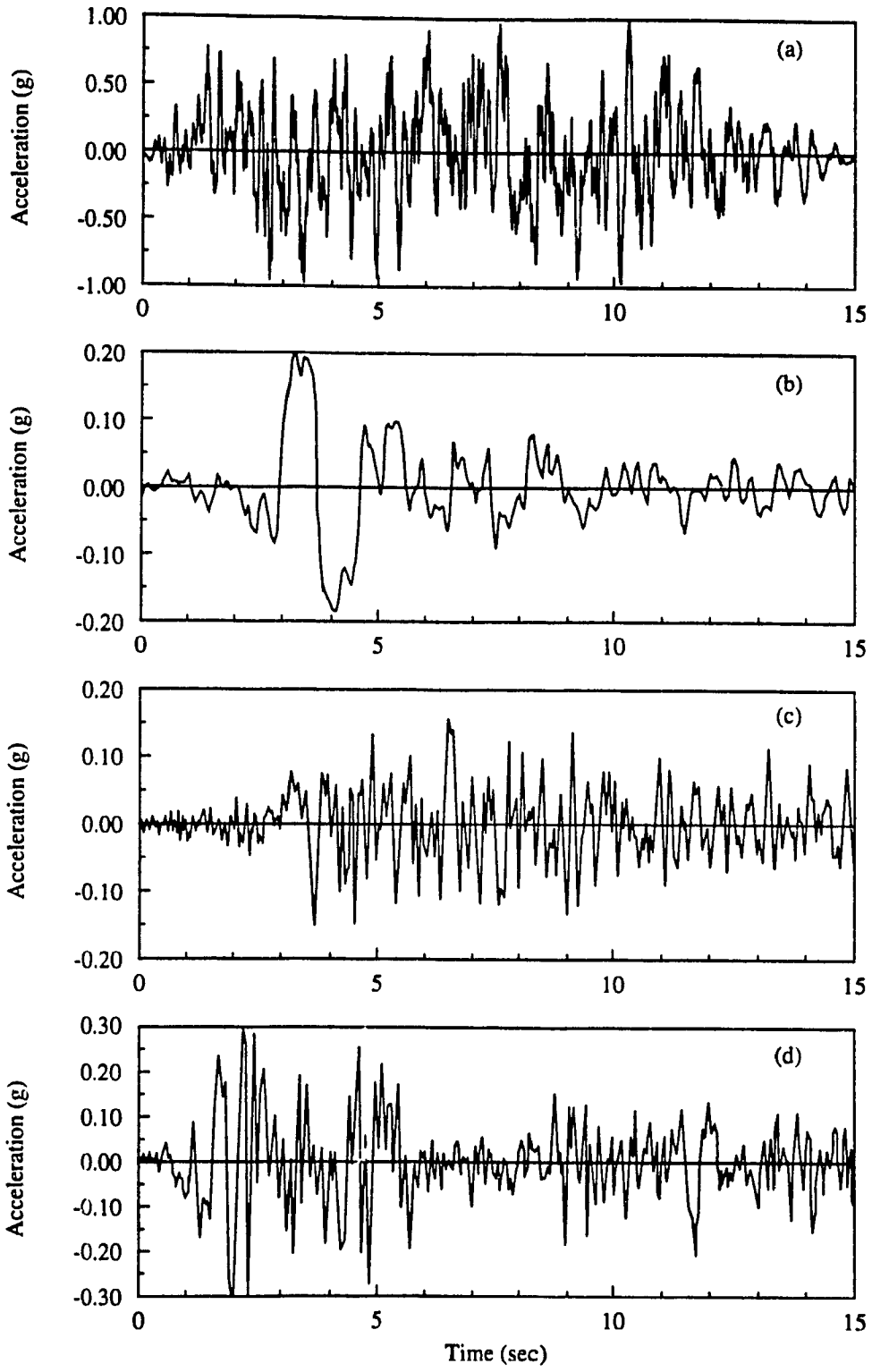

Figure 4.4. Acceleration time history for earthquake ensemble: a) Newmark-Blume-Kapur artificial excitation; b) 1977 Bucharest N-S; c) 1952 Taft S69E; d) 1940 El Centro N-S.

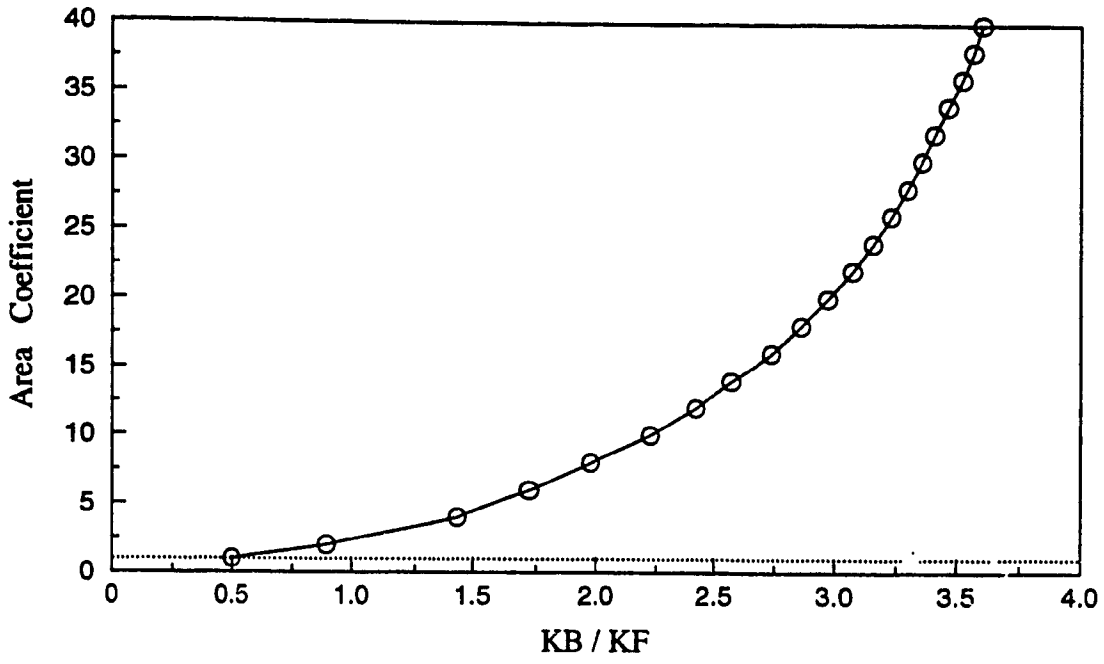

Figure 4.5. Variation of brace area required vs. stiffness ratio.

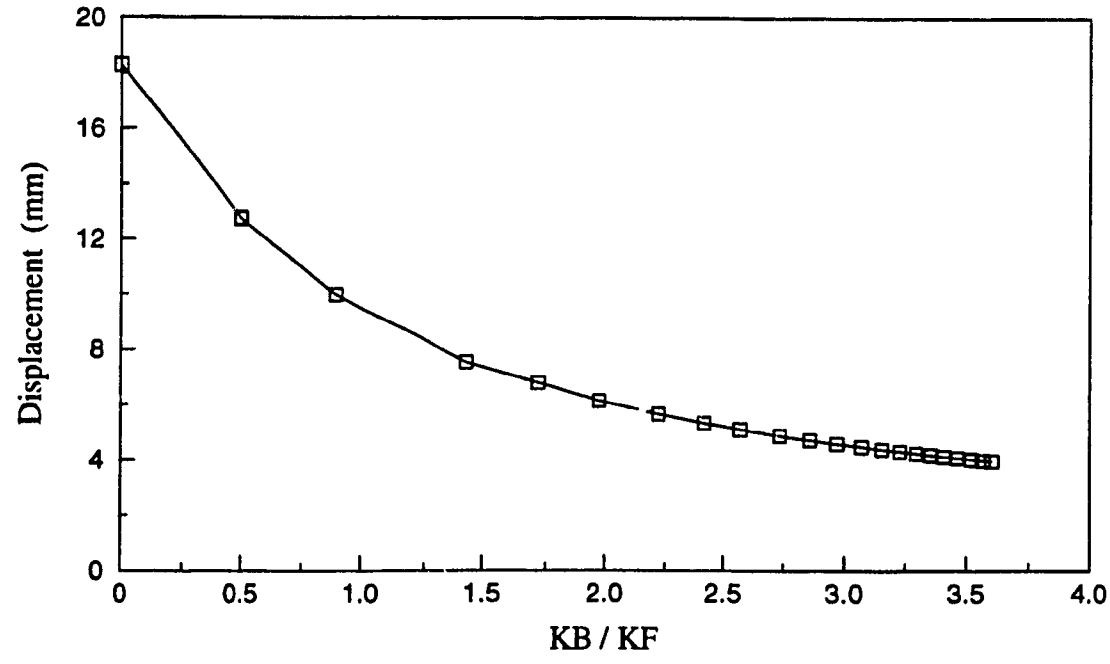

Figure 4.6. Response of structure under pseudo-static loading vs. KB / KF.

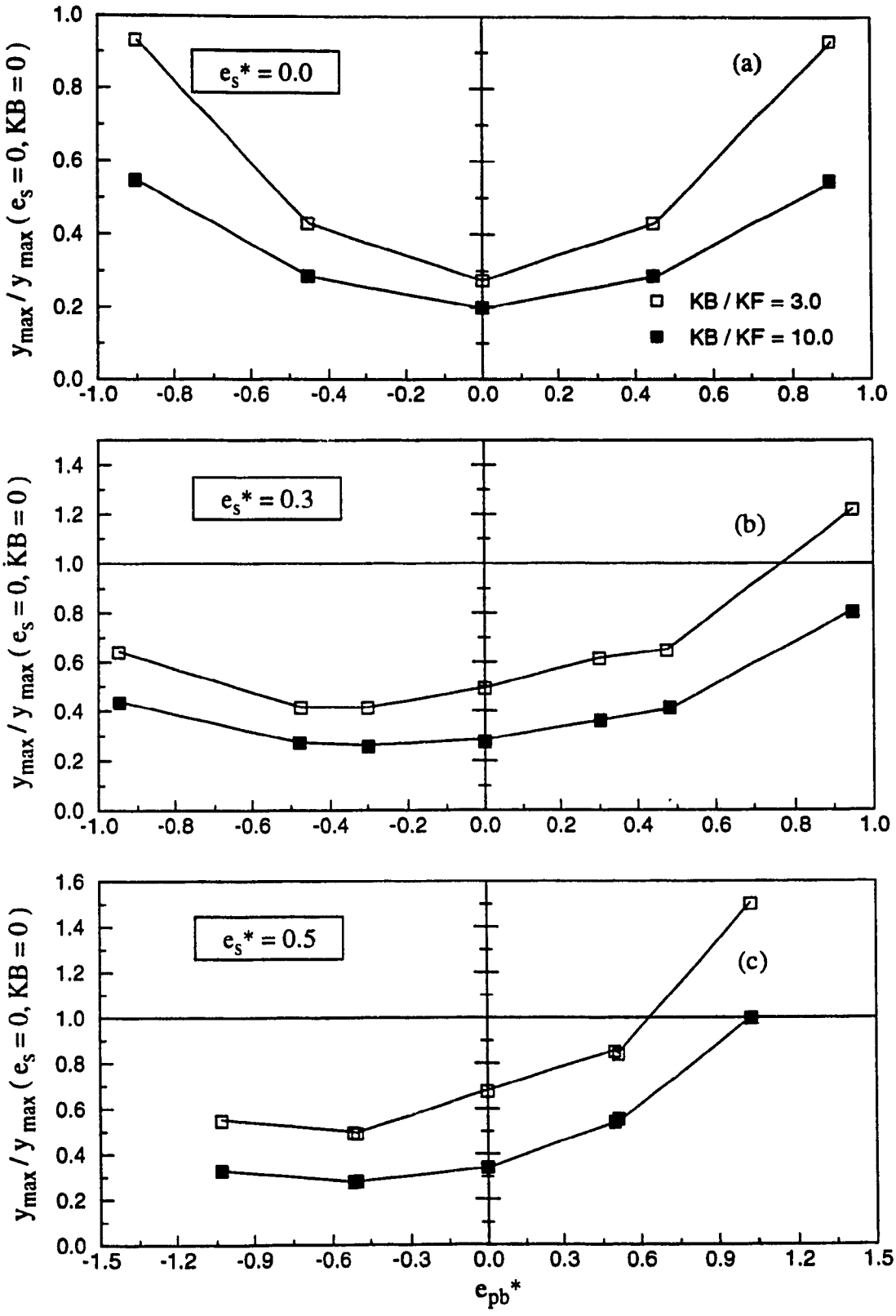

Figure 4.7. Response of stiffness eccentric model ($e_{pf} = e_s$) to variation in strength eccentricity e_{pb} of the braces.

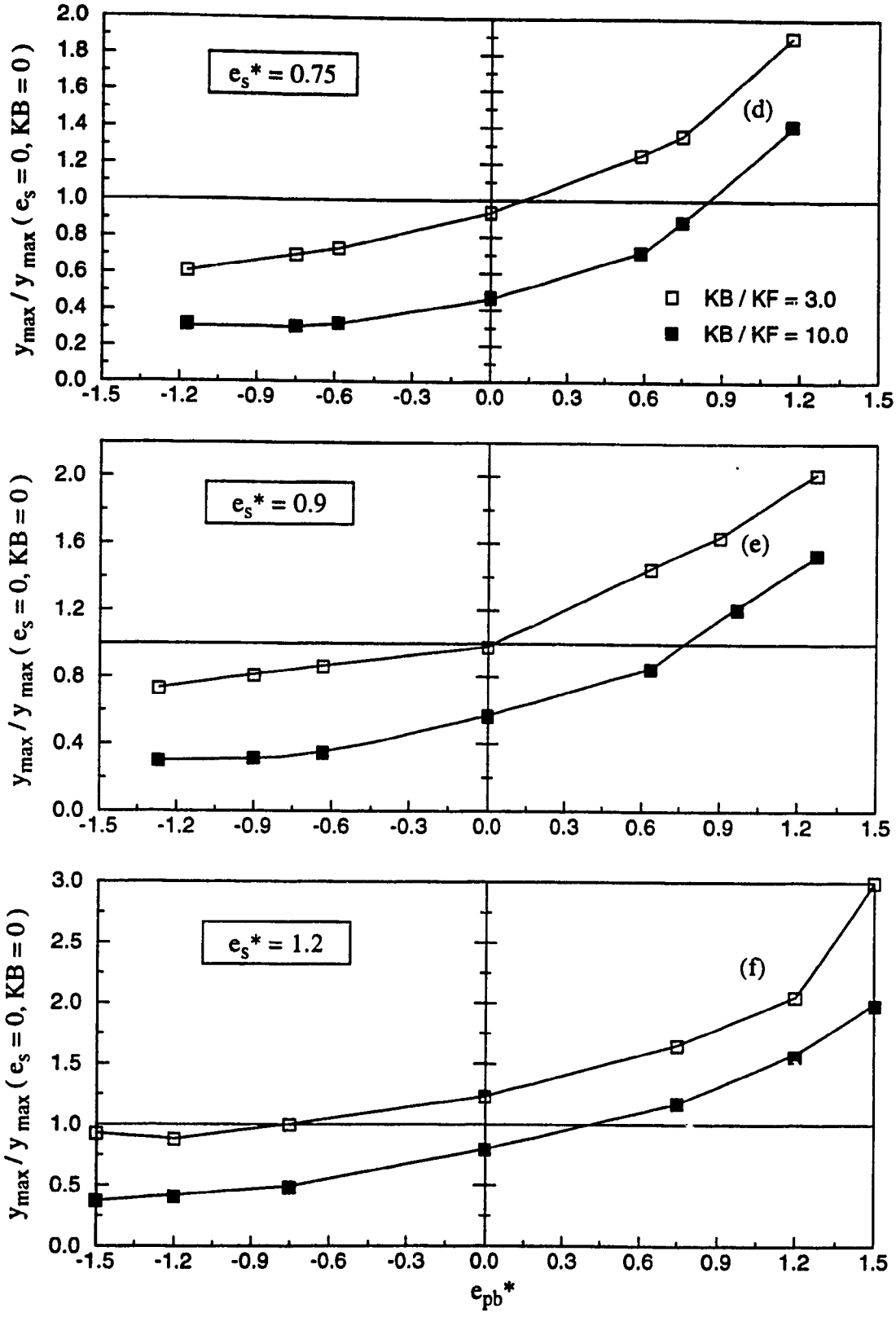

Figure 4.7 (Cont'd). Response of stiffness eccentric model ($e_{pf} = e_s$) to variation in strength eccentricity e_{pb} of the braces.

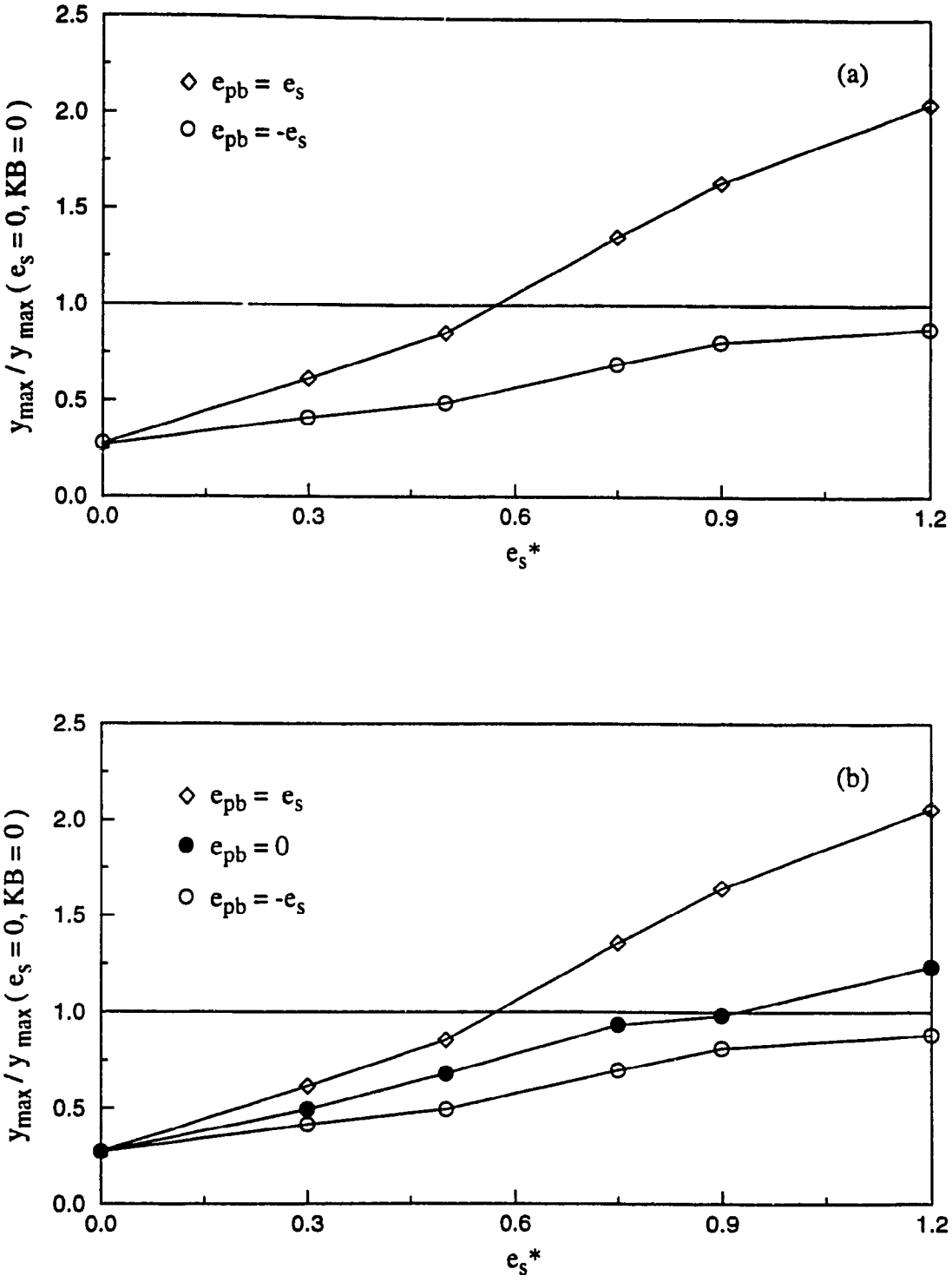

Figure 4.8. Comparison of response over stiffness eccentricity e_s^* for KB / KF = 3.0.
(a) Current design ($e_{pb} = e_s$) and optimum ($e_{pb} = -e_s$) slip load eccentricity.
(b) Includes suggested design ($e_{pb} = 0$).

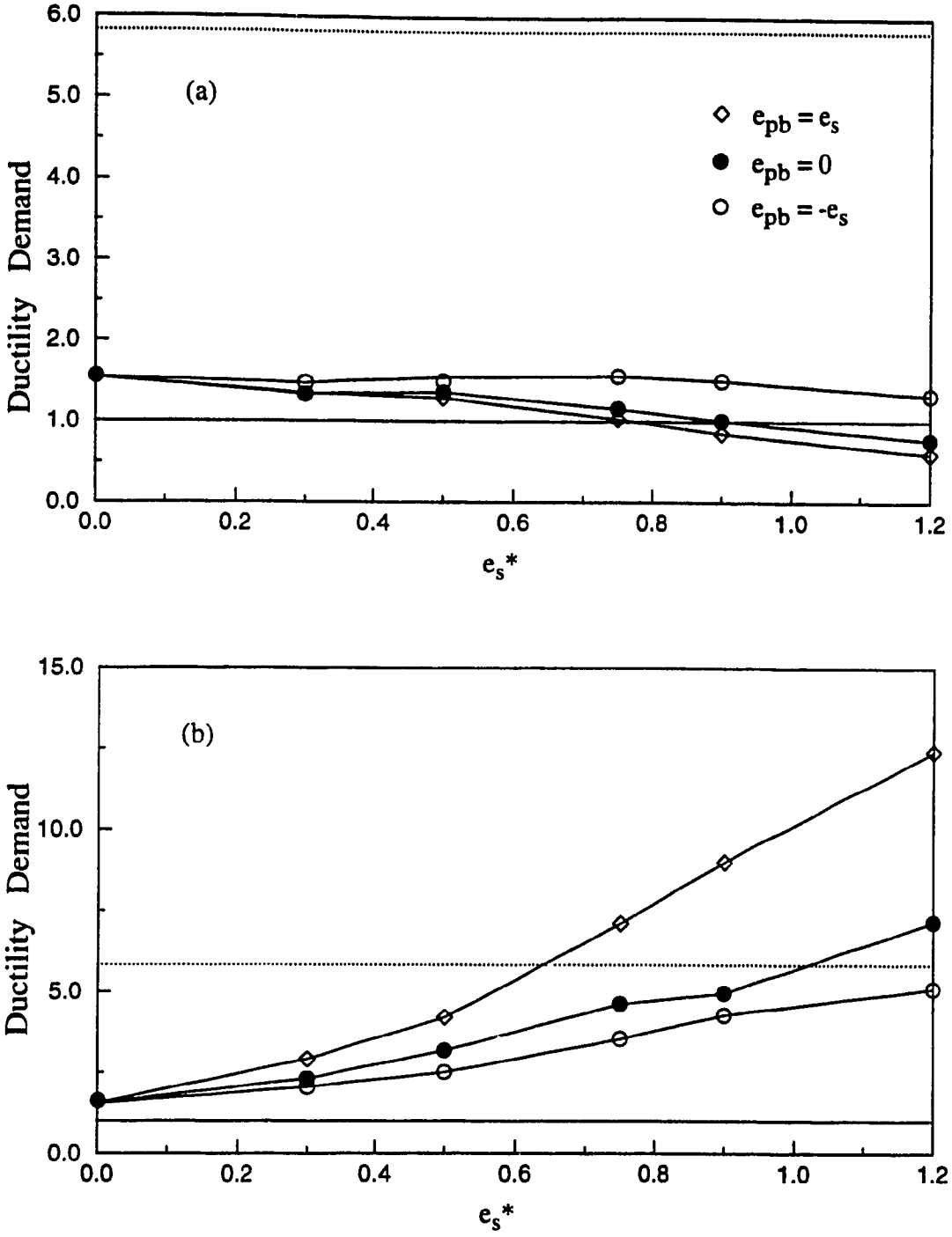

Figure 4.9. Effect of slip load eccentricity on ductility demand for strength eccentric model ($e_{pf} = e_s$) with KB / KF = 3.0. (a) Stiff side. (b) Flexible side.

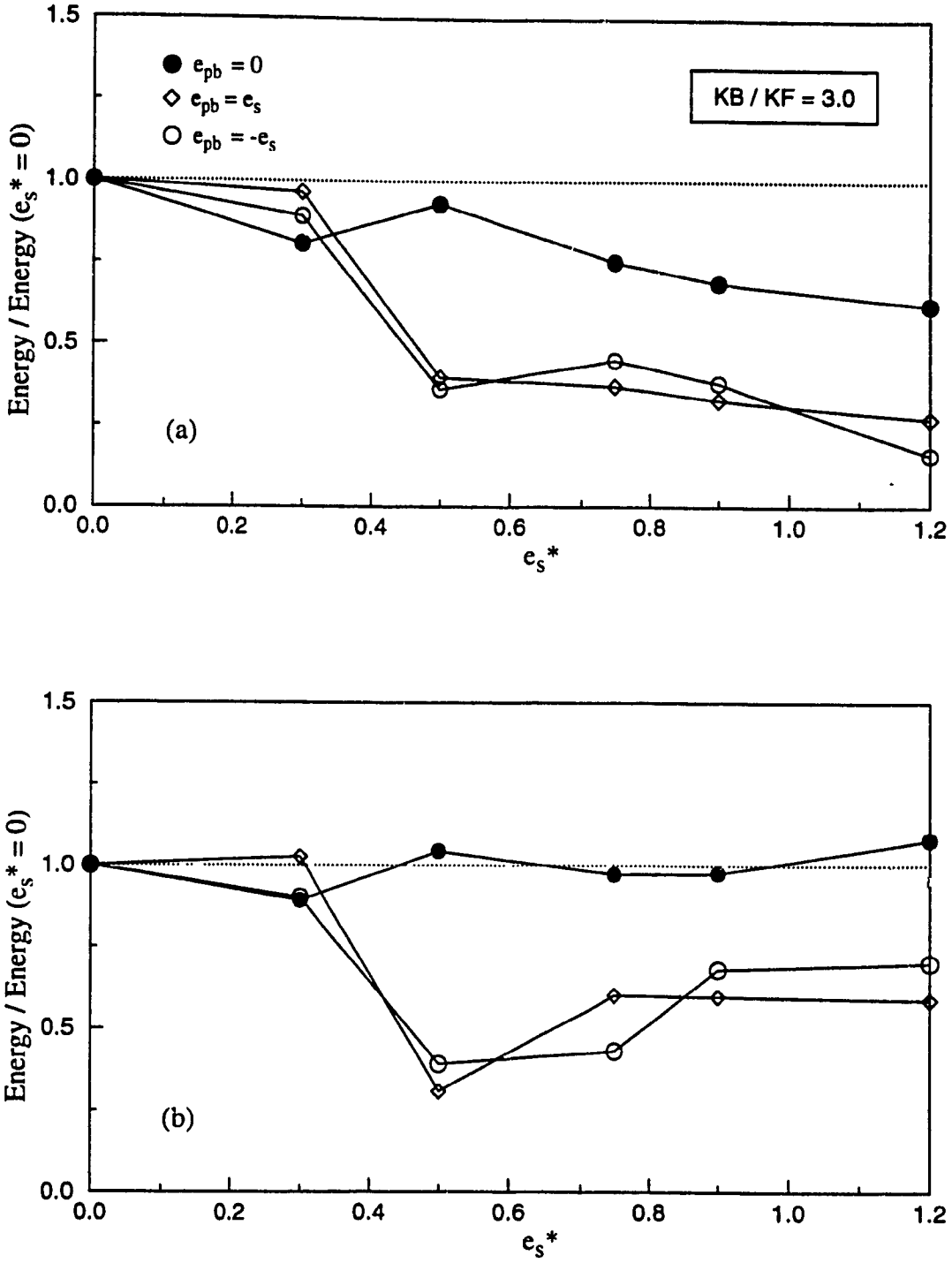

Figure 4.10. Energy dissipated by braces of 1-storey strength eccentric model ($e_{pf} = e_s$) according to current design ($e_{pb} = e_s$), suggested design ($e_{pb} = 0$), and optimum slip load eccentricity ($e_{pb} = -e_s$). (a) Romania excitation excluded. (b) Romania excitation included.

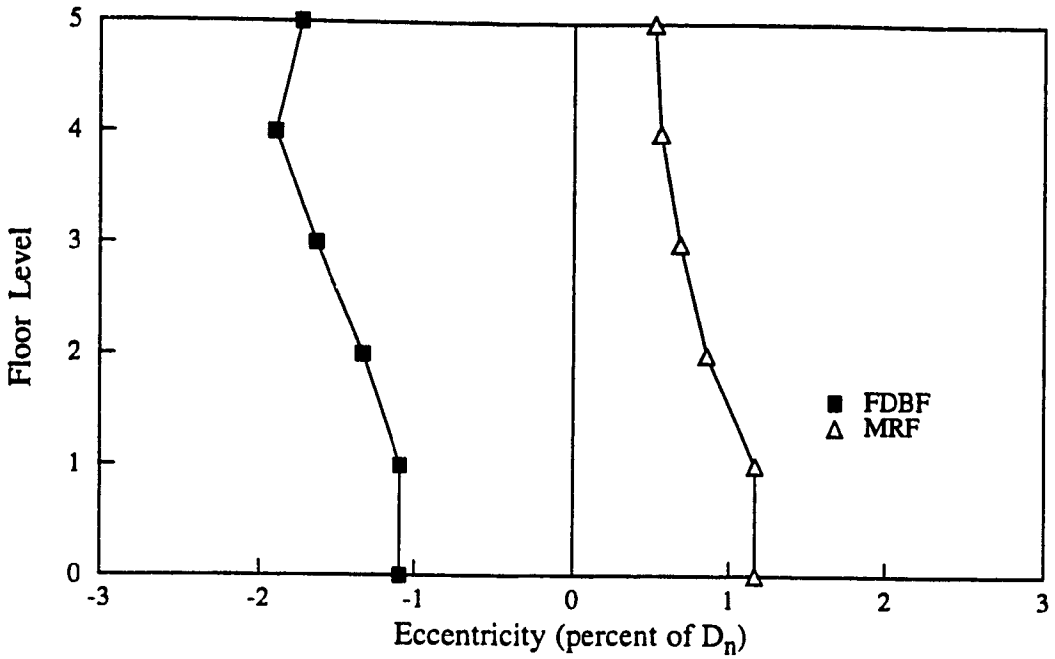

Figure 4.11. Eccentricity with height of building for X-direction excitations [10].

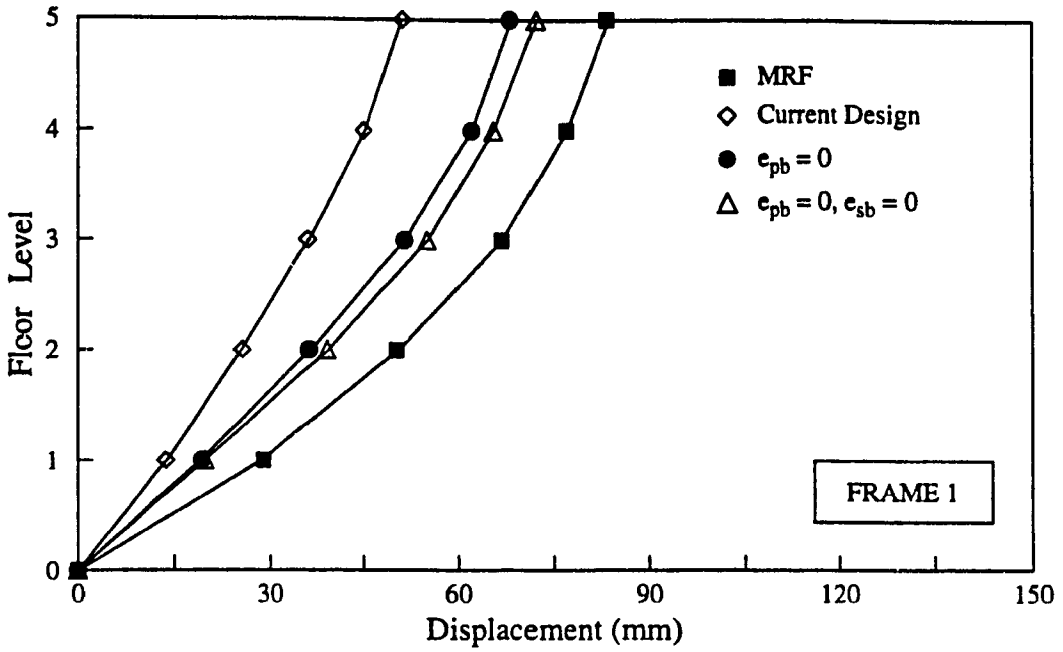

Figure 4.12a. Displacement of stiff side, earthquake ensemble in X-direction.
KB / KF = 1.5, CM @ -0.35 D_n, 0.36g.

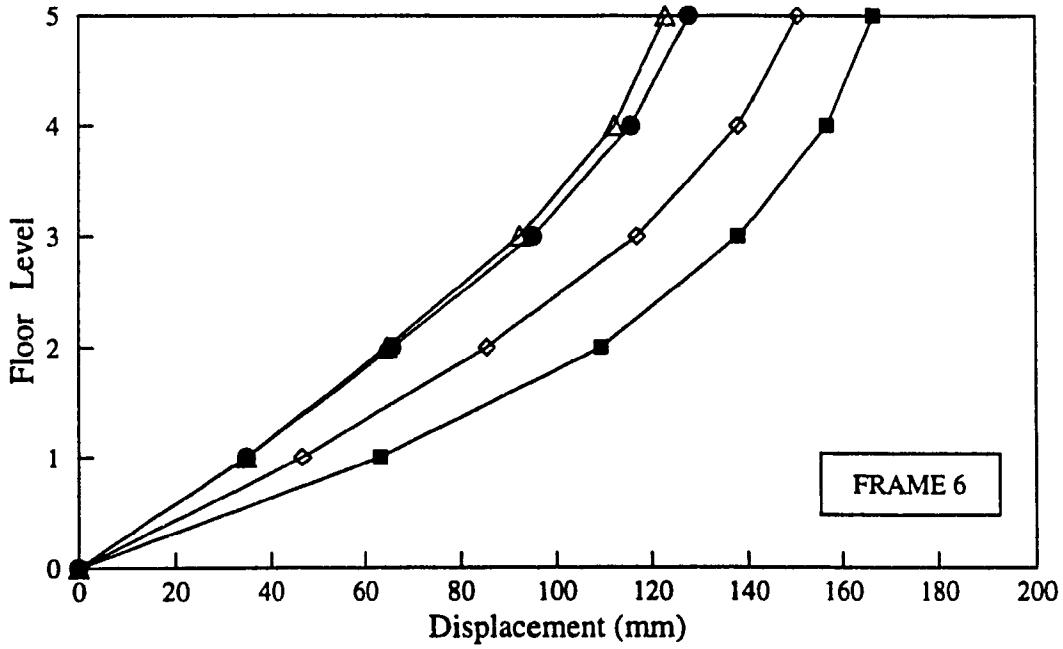

Figure 4.12b. Displacement of flexible side, earthquake ensemble in X-direction.
KB / KF = 1.5, CM @ -0.35 D_n, 0.36g.

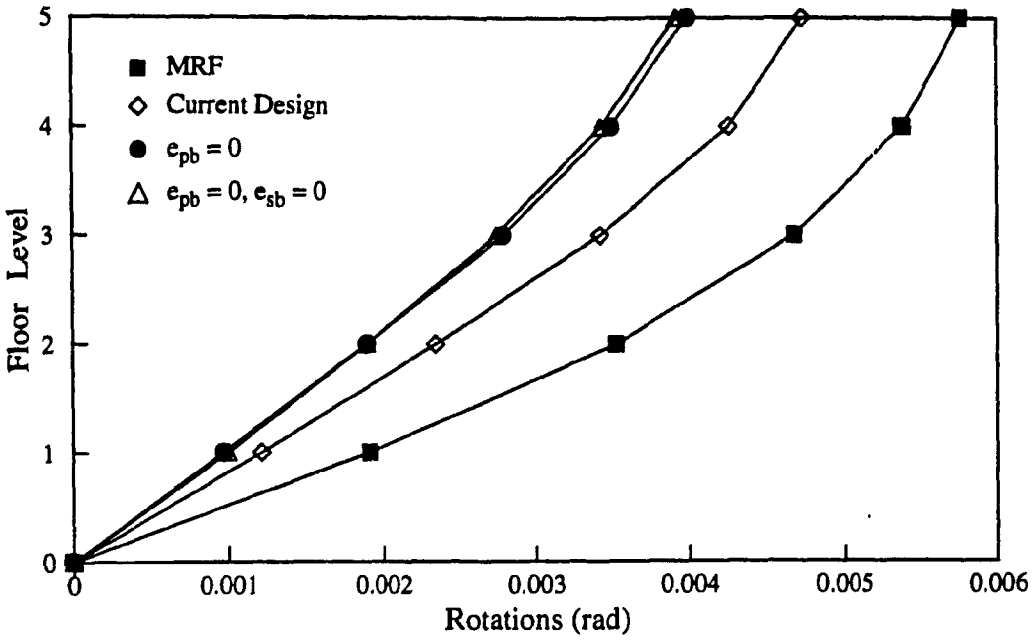

Figure 4.13. Rotation of floor decks for earthquake ensemble in X-direction.
KB / KF = 1.5, CM @ -0.35 D_n, 0.36g.

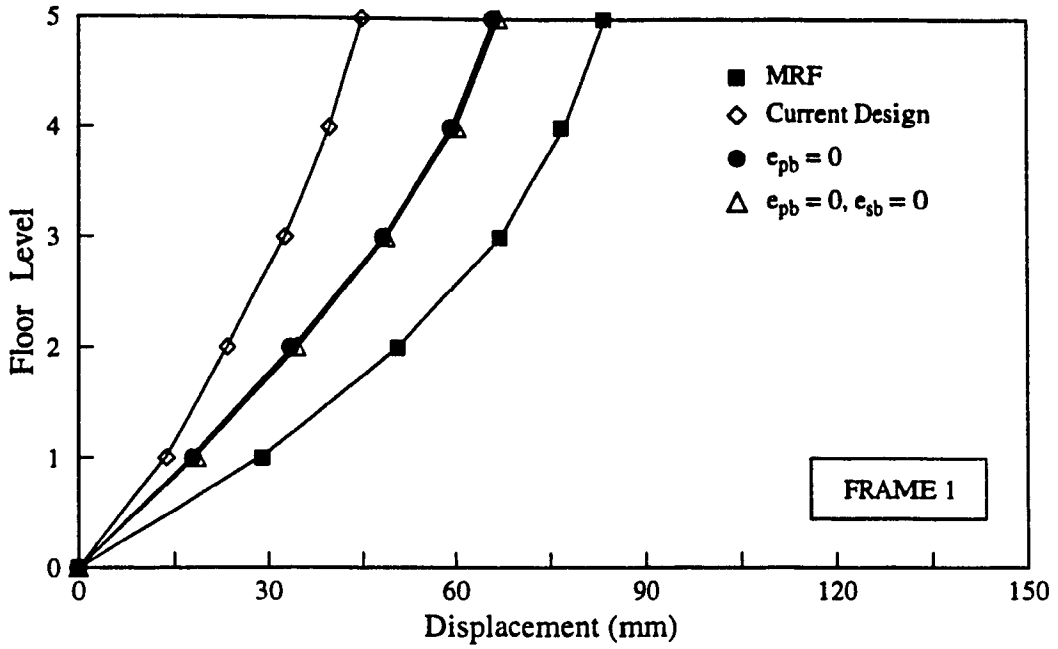

Figure 4.14a. Displacement of stiff side, earthquake ensemble in X-direction.
KB / KF = 3.0, CM @ -0.35 D_n, 0.36g.

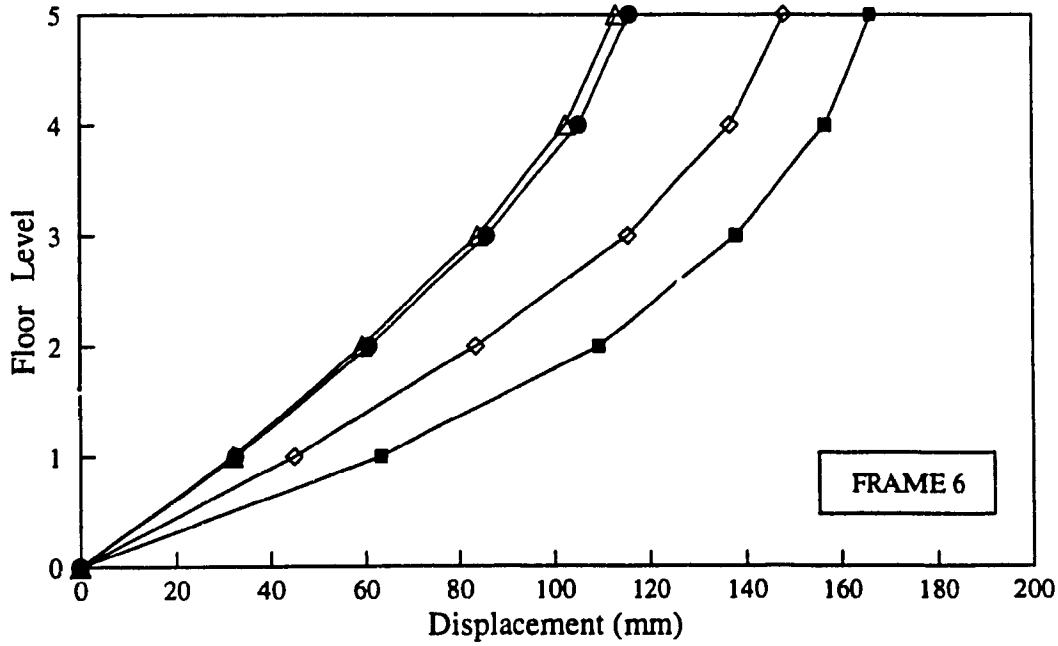

Figure 4.14b. Displacement of flexible side, earthquake ensemble in X-direction.
KB / KF = 3.0, CM @ -0.35 D_n, 0.36g.

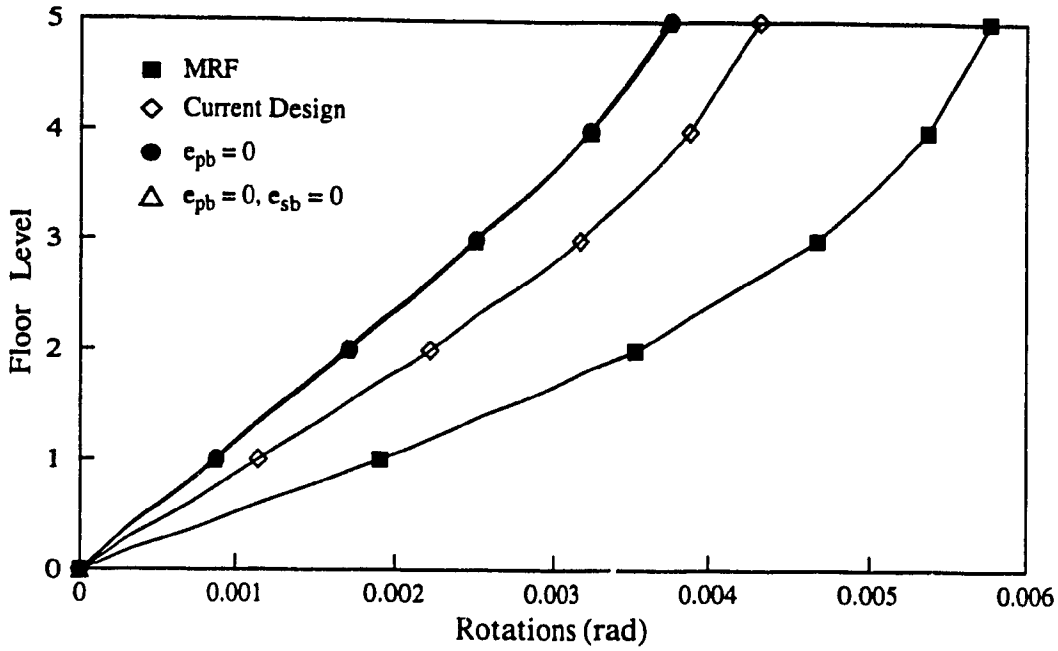

Figure 4.15. Rotation of floor decks for earthquake ensemble in X-direction.
KB / KF = 3.0, CM @ -0.35 D_n, 0.36g.

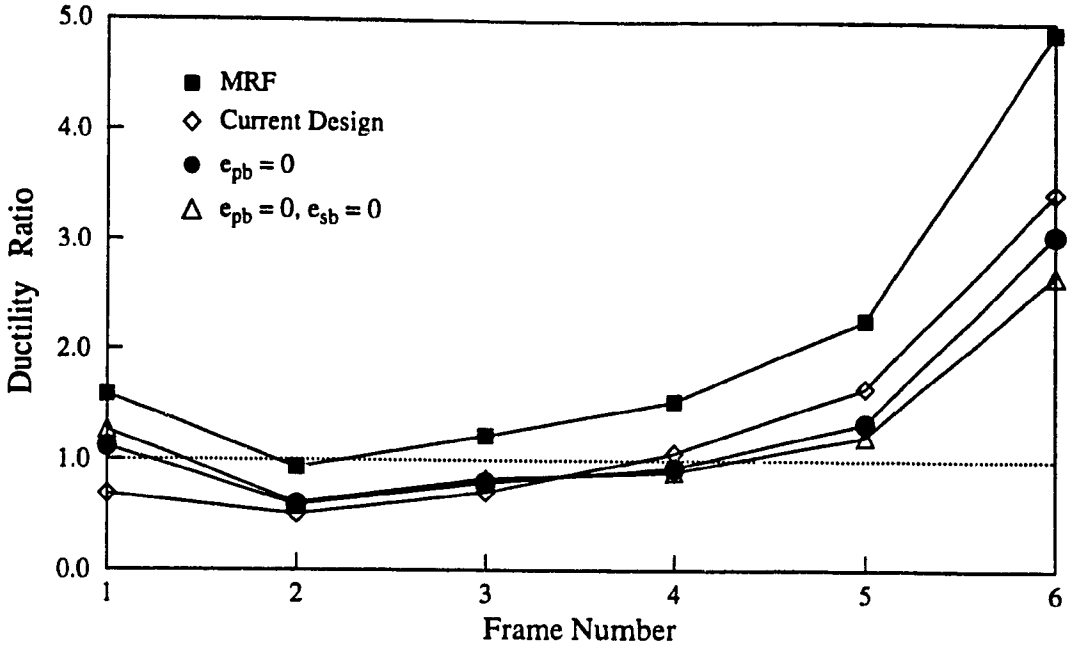

Figure 4.16a. Ductility demand for earthquake ensemble in X-direction.
KB / KF = 1.5, CM @ -0.35 D_n, 0.36g.

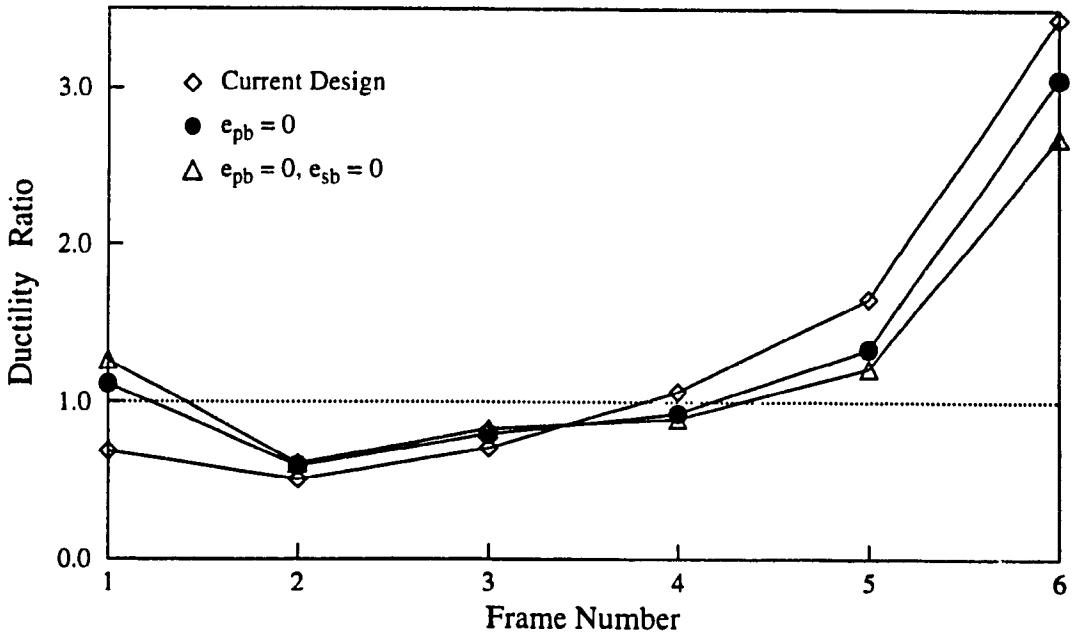

Figure 4.16b. Ductility demand for earthquake ensemble in X-direction (no MRF).
KB / KF = 1.5, CM @ -0.35 D_n, 0.36g.

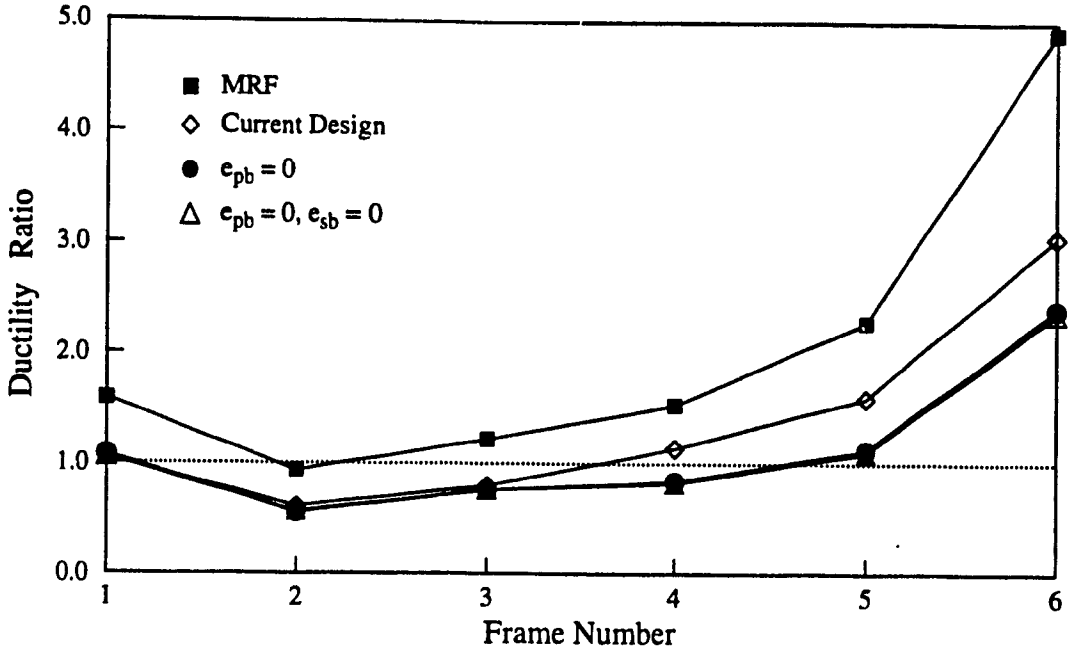

Figure 4.17a. Ductility demand for earthquake ensemble in X-direction.
KB / KF = 3.0, CM @ -0.35 D_n, 0.36g.

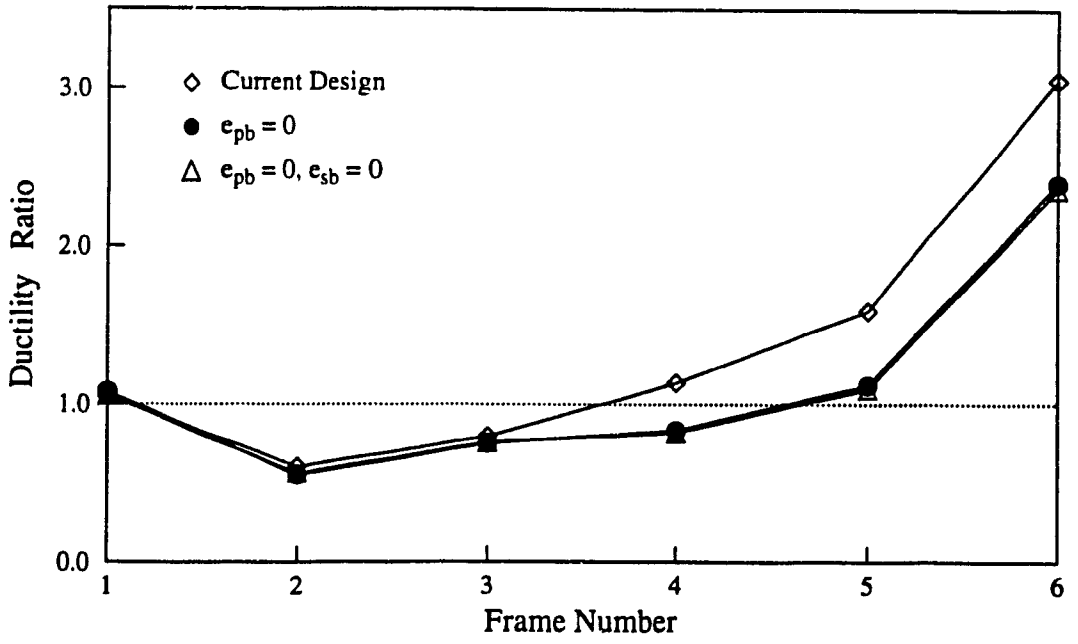

Figure 4.17b. Ductility demand for earthquake ensemble in X-direction (no MRF).
KB / KF = 3.0, CM @ -0.35 D_n, 0.36g.

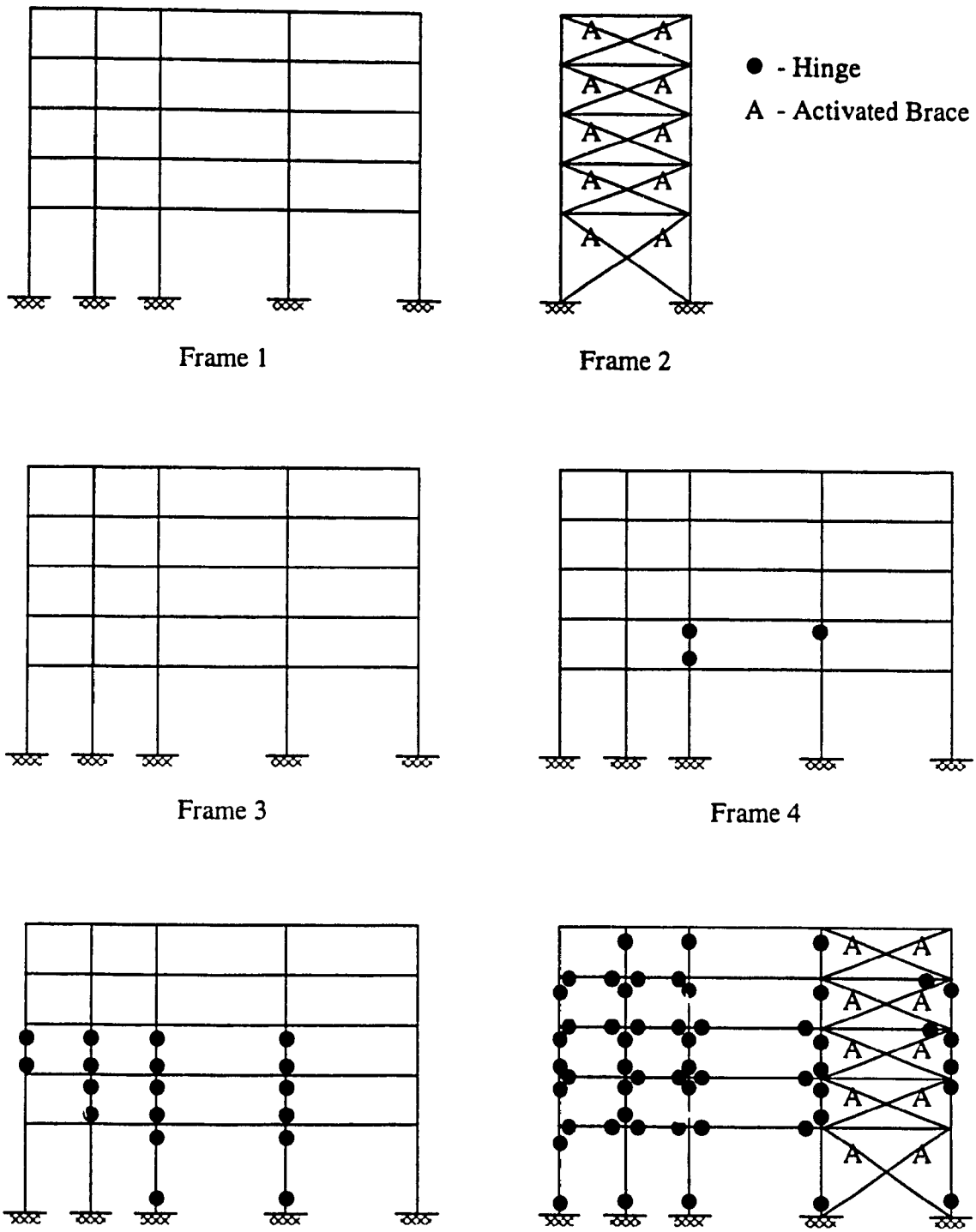

Figure 4.18. Damage to frames, Newmark-Blume-Kapur earthquake in X-direction. Current design, KB / KF = 3.0, CM @ -0.35 D_n, 0.36g.

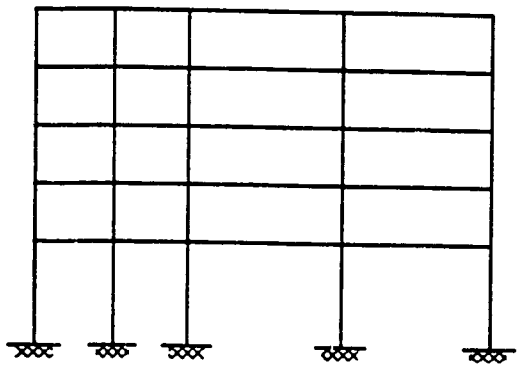

Frame 1

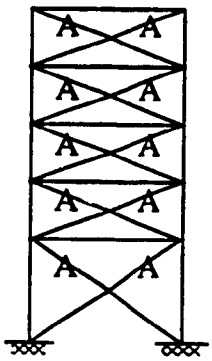

● - Hinge

A - Activated Brace

Frame 2

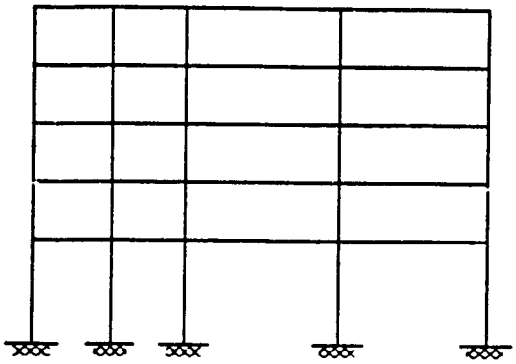

Frame 3

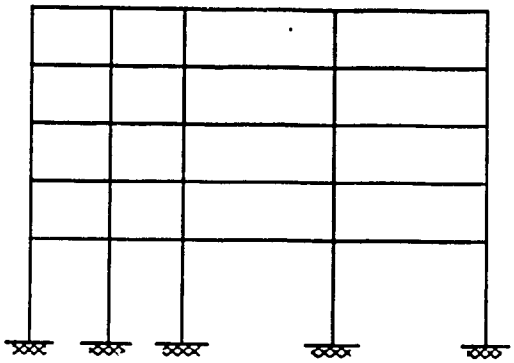

Frame 4

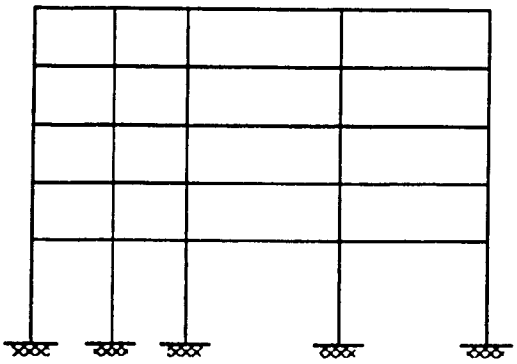

Frame 5

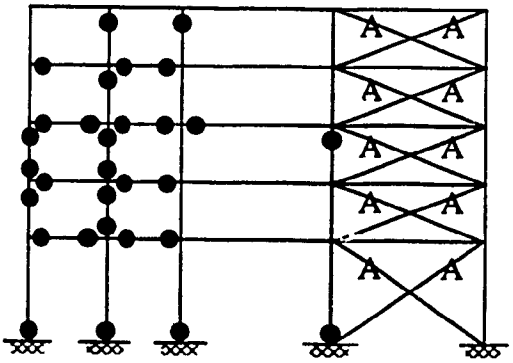

Frame 6

Figure 4.19. Damage to frames, Newmark-Blume-Kapur earthquake in X-direction.
e_{pb} = 0, KB / KF = 3.0, CM @ -0.35 D_n, 0.36g.

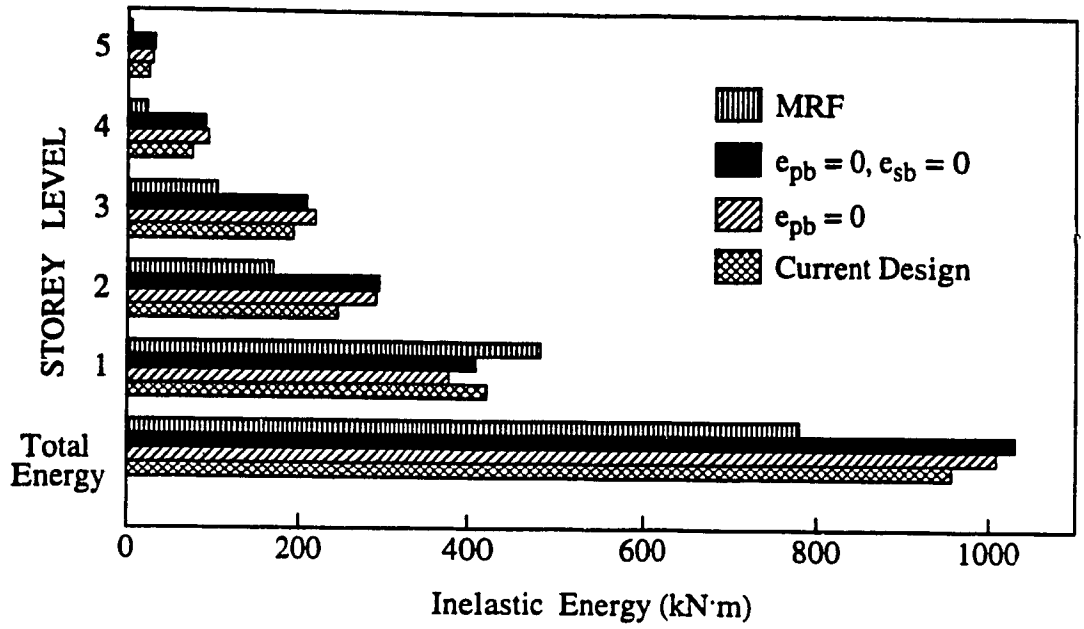

Figure 4.20. Energy absorption, earthquake ensemble in X-Direction.
KB / KF = 1.5, CM @ -0.35D_n, 0.36g.

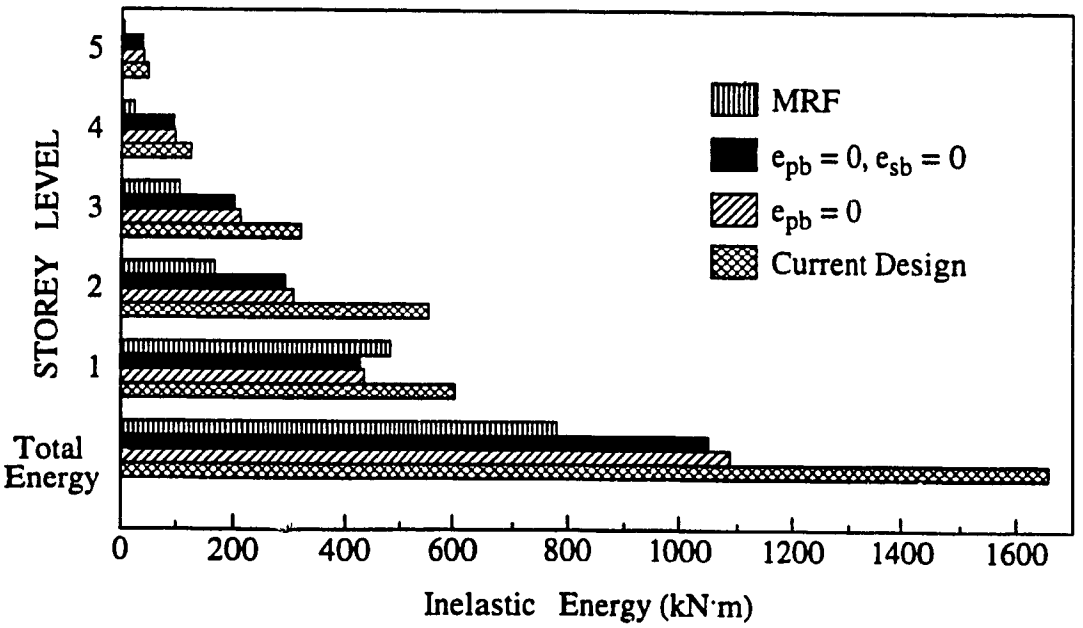

Figure 4.21. Energy absorption, earthquake ensemble in X-Direction.
KB / KF = 3.0, CM @ -0.35D_n, 0.36g.

CHAPTER 5

CONCLUSIONS

This work examined the possibility of refining the process currently employed in designing the friction braces of a FDBF to improve performance. The study consisted of three parts: first - a parametric study of a two dimensional, single storey model equipped with FDBF was conducted using the program DRAIN-2D to determine the optimum and also the most practical slip load distributions; second - using this slip load distribution, a parametric study was conducted on the same model to determine the importance of the stiffness distribution of the braces in the response of the model; third - a case study of a five storey reinforced concrete building equipped with the refined braces was analyzed using the program DRAIN-Tabs and the results were compared to the same building equipped with braces designed according to current practice.

In Chapter 2, a description of single storey models was presented along with the equations that govern the placement of the braces and resisting frames as well as the distribution of the stiffness, strength and slip loads.

In Chapter 3, the parametric study of the one storey structure revealed limitations in the mass eccentric models of previous studies. It was determined that a full range of slip load eccentricities ($-e_s < e_{pb} < e_s$) was only possible for structures having elastic stiffness eccentricity in the range $-0.5 < e_s < 0.5$. This caused the need for a shift to a stiffness eccentric model in order to carry out the analysis for larger eccentricities and comparisons were made with the mass eccentric models to validate the findings. Analysis of the responses obtained for various slip load distributions and elastic stiffness eccentricities showed that optimum responses are obtained when the slip load eccentricity is opposite that of the stiffness eccentricity (i.e. $e_{pb} = -e_s$), but that for practical design purposes distributing the slip load according to $e_{pb} = 0$ provides equally acceptable results. These two slip load distributions provided improvements of up to 70 percent and 40 percent,

respectively, over the model designed according to current practice, namely, $e_{pb} = e_s$.

Adopting the same analysis procedure for the determination of the stiffness distribution as that used for the slip load distribution revealed that distributing the brace stiffness according to $e_{sb} = -e_{sf} / 2$ gives the best results, although these represent an improvement of less than 10 percent over $e_{sb} = 0$. For the model having KB / KF = 10, these distributions suggest an improvement of approximately 50 percent over the current design procedure which maintains $e_{sb} = e_{sf}$. These results, however, are limited because of the magnitude of KB / KF = 10 employed.

It may be concluded that designing braces according to a practical slip load distribution of $e_{pb} = 0$ can significantly improve the expected performance of the FDBF. Comparison of the energy absorbed by the braces of the one storey model before and after refinement shows that the new design of $e_{pb} = 0$ should increase the participation of the braces by twice that of the current design methodology, namely, $e_{pb} = e_s$.

Chapter 4 incorporated the findings of Chapter 3 into a case study of a fictitious building corresponding to an early design of the Concordia University Library Complex which had been equipped with braces designed according to the current accepted approach. When using the NBCC pseudo-static design loads to determine the necessary brace areas to provide KB / KF = 10, it was noted that for this particular building, the KB / KF ratio could not realistically reach the magnitude of 10, and that a practical limit is represented by KB / KF = 3.0. A portion of the analysis of Chapter 3 was thus repeated to verify that the conclusions drawn on the basis of KB / KF = 10 are still valid for KB / KF = 3.0. Although the magnitude of the responses obtained were higher than for KB / KF = 10, the improvement of $e_{pb} = 0$ over that of $e_{pb} = e_s$ was virtually the same as that observed for KB / KF = 10. This shortened analysis also showed that the refined brace configuration should enable the braces to dissipate twice the energy of the old configuration while maintaining the ductility demand below that of the unbraced symmetric structure.

Eccentricity in the three dimensional structure considered was created with a plan shift of the center of mass by $-0.35D_n$ from its geometric centroid, thereby causing $e_s^* \approx 1.0$. The refined devices reduced flexible side response by 23 percent that of the current design. The suggested design approach of $e_{pb} = 0$ also improved ductility demand of the flexible side and expected floor rotations by 22 percent and 13 percent, respectively.

The alternate design of $e_{pb} = 0$ and $e_{sb} = 0$, which considered the redistribution of the brace stiffness, did not demonstrate any further improvements in response over that of the suggested design approach ($e_{pb} = 0$), as indicated in Chapter 3. Also, comparison of the results for KB / KF = 3.0 to those of KB / KF = 1.5 showed little improvement compared to the large increase in stiffness ratio, thereby corroborating the findings of a previous study which suggested that for this structure, providing KB / KF > 2.0 would be unnecessary.

It is concluded from this case study, that in the overall design of FDBF's, three considerations are of importance, namely, the optimum value of RB / RF, the optimum value of KB / KF, and the optimum distribution of slip load between the braces. For the latter, $e_{pb} = 0$ is the practical approach, while the optimum is given by $e_{pb} = -e_s$.

Suggested areas requiring further investigation include:

- For SDOF systems, a more detailed investigation is required of the energy dissipation mechanism in FDBF's since reduced energy dissipation accompanied reduced displacements and ductility demands when redistribution of slip loads was optimized.
- Following the large difference in performance for structures subjected to the Romania earthquake versus those subjected to the remainder of the ensemble, further study should include a selection of earthquakes with a variety of characteristics.
- For multi-degree of freedom systems, the results herein were confined to one 3-D structure. Different structures should be considered in future research.
- Whereas improvement in displacement performance with slip load redistribution was obtained, the degree of improvement predicted by the SDOF structure was not achieved.

This is most likely due to simplifying assumptions made when rendering the single storey models. Future research should consider including SDOF structures having structural properties which are better correlated to those of the 3-D structures considered.

REFERENCES

1. A. S. Pall and C. Marsh, 'Response of friction damped braced frames', *J. struct. div. ASCE.* 108, 1313-1323 (1982).
2. P. Baktash, 'Friction damped braced frames', *Ph.D. Thesis*, Concordia University, Montreal, Quebec, 1989.
3. O. A. Pekau and R. Guimond, 'Controlling Seismic Response of Eccentric Structures by Friction Dampers', *Earthquake Engineering and Structural Dynamics,* vol. 20, pp. 505-521 (1991).
4. R. K. Goel and A. K. Chopra, 'Inelastic seismic response of one-storey, asymmetric-plan systems', *Report No. EERC 90-14*, Earthquake Engineering Research Center, University of California, Berkeley, CA, 1990.
5. M. Bruneau and S. A. Mahin, 'Inelastic seismic response of structures with mass or stiffness eccentricities in plan', *Report No. EERC 87-12*, Earthquake Engineering Research Center, University of California, Berkeley, CA, 1987.
6. A. G. Ayala, O. Garcia, and J. A. Escobar, 'Evaluation of seismic design criteria for asymmetric buildings', *Proc. 10th world conf. earthquake eng.* Balkema, 5693-5698, (1992)
7. W. K. Tso and H. Ying, 'Additional seismic inelastic deformation caused by structural asymmetry', *Earthquake eng. struct. dyn.* 19, 243-258 (1990).
8. A. W. Sadek and W. K. Tso, 'Strength eccentricity concept for inelastic analysis of asymmetrical structures', *Eng. struct.* 11, 189-194 (1989).
9. Guendelman-Israel, R. and G. H. Powell, 'Drain-Tabs, A Computer Program for the Inelastic Earthquake Response of Three-Dimensional Buildings', *EERC 78,* Earthquake Engineering Research Center, University of California, Berkeley, CA, 1977.
10. R. Guimond, 'Accidental Eccentricity and Limiting the Effects of Design Eccentricity for Seismic Response of Buildings', *M. ENG. Thesis*, Concordia University, Montreal, Quebec, 1989, 188pp.
11. Associate Committee on the National Building Code, 'NBCC 1985', National Research Council of Canada, Ottawa 1985.
12. J. L. Humar, 'Design for Seismic Torsional Forces', *Canadian Journal of Civil Engineering,* vol. 11, pp. 150-163 (1984).
13. A. E. Kannan and G. M. Powell, 'Drain-2D, A General Purpose Computer Program for Dynamic Analysis of Inelastic Plane Structures', *Report No. EERC* 73-6, Earthquake Engineering Research Center, University of California, Berkeley, CA, 1973.
14. W. K. Tso, 'A Proposal to Improve the Static Torsional Provisions for the National Building Code of Canada', *Canadian Journal of Civil Engineering,* vol. 10, pp. 561-565 (1983).

15.Associate Committee on the National Building Code, 'NBCC 1990', National Research Council of Canada, Ottawa 1990.

16.A. Rutenberg and O. A. Pekau, 'Earthquake Response of Asymmetric Buildings: A Parametric Study', *Fourth Canadian Conference on Earthquake Engineering Proceedings,* pp. 271-281(1983).

17.A. Filiatrault and S. Cherry, 'Seismic Tests of Friction Damped Steel Frames', *Dynamic Response of Structures,* Proceedings of the Third Conference Organized by the Engineering Mechanics Division of the ASCE, UCLA, California, pp. 138-145 (1986).

18.A. Filiatrault and S. Cherry, 'Comparative Performance of Friction Damped Systems and Base Isolation Systems for Earthquake Retrofit and Aseismic Design', *Earthquake Engineering and Structural Dynamics,* vol. 16, pp. 389-416 (1988).

19.C. Uang and V. V. Bertero, 'Evaluation of seismic energy in structures', *Earthquake eng. struct. dyn.* 19, 77-90 (1990).

20.A. W. Sadek and W. K. Tso, 'Inelastic seismic response of simple eccentric structures', *Earthquake eng. struct. dyn.* 13, 255-269 (1985).

21.H. Kuwamura and T. V. Galambos, 'Earthquake load for structural reliability', *J. struct. eng.* 115, 1446-1462 (1989).

22.P. Fajfar, T. Vidic, and M. Fischinger, 'Seismic demand in medium- and long-period structures', *Earthquake eng. struct. dyn.* 18, 1133-1144 (1989).

23.V. W.-T. Cheung and W. K. Tso, 'Eccentricity in Irregular Multistorey Buildings', *Canadian Journal of Civil Engineering,* vol. 13, pp. 46-52 (1986).